

ATTACHMENT 3

CDI REPORT NO. 11-04NP, "STRESS EVALUATION OF NINE MILE POINT UNIT 2 STEAM DRYER USING ACM REV. 4.1 ACOUSTIC LOADS," REVISION 0 (NON-PROPRIETARY)

Certain information, considered proprietary by Continuum Dynamic, Incorporated, has been deleted from this Attachment. The deletions are identified by double square brackets.

CDI Report No. 11-04NP

Stress Evaluation of Nine Mile Point Unit 2 Steam Dryer
Using ACM Rev. 4.1 Acoustic Loads

Revision 0


Prepared by

Continuum Dynamics, Inc.
34 Lexington Avenue
Ewing, NJ 08618

Prepared under Purchase Order No. 7722326 for

Constellation Energy Group
Nine Mile Point Nuclear Station, LLC
P.O. Box 63
Lycoming, NY 13093

Prepared by



Alexander H. Boschitsch

Approved by



Alan J. Bilanin

May 2011

This report complies with Continuum Dynamics, Inc. Nuclear Quality Assurance Program currently in effect.

Executive Summary

The finite element model and analysis methodology, used to assess stresses induced by the flow of steam through the steam dryer at Nine Mile Point Unit 2 (NMP2), are described and applied to obtain stresses at CLTP conditions. The stress analysis is consistent with those carried out in the U.S. for prior dryer qualification to EPU conditions and the resulting stresses are assessed for compliance with the ASME B&PV Code 2007 [1], Section III, subsection NG, for the load combination corresponding to normal operation (the Level A Service Condition).

The stress analysis is carried out in the frequency domain, which confers a number of useful computational advantages over a time-accurate transient analysis including the ability to assess the effects of frequency scaling in the loads without the need for additional finite element calculations. The analysis develops a series of unit stress solutions corresponding to the application of a unit pressure at a MSL at specified frequency, f . Each unit solution is obtained by first calculating the associated acoustic pressure field using a separate analysis that solves the damped Helmholtz equation within the steam dryer [2]. This pressure field is then applied to a finite element structural model of the steam dryer and the harmonic stress response at frequency, f , is calculated using the commercial ANSYS 10.0 finite element analysis software. This stress response constitutes the unit solution and is stored as a file for subsequent processing. Once all unit solutions have been computed, the stress response for any combination of MSL pressure spectrums (obtained by Fast Fourier Transform of the pressure histories in the MSLs) is determined by a simple matrix multiplication of these spectrums with the unit solutions.

The acoustic loads for the results herein are prepared using an acoustic circuit model (ACM) that has recently been revised to version 4.1 [3]. This version reflects new biases and uncertainties obtained during re-benchmarking against available Quad Cities (QC) data carried out under the requirement that identical filtering methods be used on both QC data and new plant signal measurements. The benchmarking and associated biases and uncertainties are based on the QC2 data at the 790MWe power level and using 16 sensors. Also, the ACM acoustic load predictions are obtained using recently acquired main steam line strain gage measurements [4]. Other than the removal of known non-acoustic discrete frequencies (e.g., electrical noise at multiples of 60 Hz) and the application of coherence filtering (which was also invoked when processing the QC data) no other filtering methods are used. In particular, no noise subtraction using low power data is performed. Further details of the acoustic load processing procedure are given in [3].

It is required that the alternating stress ratios at EPU be above a target level of 2.0. Since flow-induced acoustic resonances are not anticipated in the steam dryer, the alternating stress ratios at EPU operation can be obtained by scaling the CLTP values by the steam flow velocity squared, $(U_{EPU}/U_{CLTP})^2 = 1.1756^2 = 1.382$. This corresponds to a target alternating stress ratio at CLTP of 2.76. When the loads are impressed on the existing dryer configuration several locations are found to have a predicted alternating stress ratio below this target level. As a result modifications to the dryer have been implemented to achieve EPU stress ratios above 2.0. These modifications are detailed in Section 5 which identifies four distinct groups of nodes that require modifications. Briefly, these groups consist of the following:

- (1) Nodes located on the weld connecting the lifting rod braces to the vane bank side plates. The end of each such weld has high stress. High stresses are addressed by a combination of localized reinforcement plates (the two upper-most braces) and increased weld size (lower-most brace).
- (2) Nodes on the weld lying on the inward edge of the middle hood reinforcement strip. The high stresses are alleviated by adding a 1/8th inch thick reinforcement plate onto the portion of the middle hood lying outboard of the closure plate.
- (3) The inner hood/hood support welds. The stresses are reduced by placing a total of four 15 lb masses on the centermost inner hoods.
- (4) All remaining nodes located on the bottom of the drain channels, ends of tie bars and the hood/hood support/base plate junctions which have alternating stress ratios slightly below the CLTP target stress ratio of 2.76.

In addition to these modifications to address individual high stress nodes, the closure plates are reinforced with ribs to eliminate adverse resonant responses encountered with the existing configuration that produced high stresses in the closure plate attachment welds.

In prior stress evaluations, sub-models were used [5] to obtain refined estimates of the linearized stresses at high stress locations. These models were also used to evaluate the effectiveness of proposed modifications such as increasing the weld size of the lifting rod brace and introducing a wrap-around weld at the bottom of the drain channel/skirt weld. In the current report no sub-model results are used. Instead [[

(3)]]

A stress evaluation of the entire post-reinforcement NMP2 steam dryer shows that at nominal CLTP operation (no frequency shift) the minimum alternating stress ratio (SR-a) anywhere on the steam dryer is SR-a=3.29. The loads used to obtain this value account for all the end-to-end biases and uncertainties in the loads model [4] and finite element analysis. To account for uncertainties in the modal frequency predictions of the finite element model, the stresses are also computed for loads that are shifted in the frequency domain by $\pm 2.5\%$, $\pm 5\%$, $\pm 7.5\%$ and $\pm 10\%$. The minimum alternating stress ratio encountered at any frequency shift is found to be SR-a=2.83 occurring at the -10% shift and occurring on outer hood/hood support/cover plate junction. The stress ratio due to maximum stresses (SR-P) is dominated by static loads and is SR-P=1.26 with all frequency shifts considered.

The assessment shows that with the modifications in place all locations meet the required stress margin EPU operation.

Table of Contents

Section	Page
Executive Summary	i
Table of Contents	iii
1. Introduction and Purpose	1
2. Methodology & Evaluation Procedures	4
2.1 Overview	4
2.2 [[..... ⁽³⁾]]	6
2.3 Computational Considerations	7
2.4 [[..... ⁽³⁾]]	9
2.5 Flaw Evaluation	10
3. Finite Element Model Description	18
3.1 Steam Dryer Geometry	18
3.2 Material Properties	21
3.3 Model Simplifications	21
3.4 Perforated Plate Model	22
3.5 Vane Bank Model	24
3.6 Water Inertia Effect on Submerged Panels	25
3.7 Structural Damping	25
3.8 Mesh Details and Element Types	25
3.9 Connections between Structural Components	25
3.10 Pressure Loading	37
4. Structural Analysis	40
4.1 Static Analysis	40
4.2 Harmonic Analysis	40
4.3 Post-Processing	46
4.4 Computation of Stress Ratios for Structural Assessment	46
4.5 [[..... ⁽³⁾]]	49
5. Proposed Modifications to Meet EPU Stress Margins	52
5.1 Lifting Rod Support Brackets (Group 1)	52
5.2 Middle Hood/Reinforcement Strip (Group 2)	59
5.3 Inner Hoods/Hood Support (Group 3)	61
5.4 Group 4 Locations	64
5.5 Modification of Closure Plates	65
5.6 Summary of Modifications	70
6. Results	71
6.1 General Stress Distribution and High Stress Locations	72
6.2 Load Combinations and Allowable Stress Intensities	86
6.3 Frequency Content and Filtering of the Stress Signals	110
7. Conclusions	120
8. References	121

1. Introduction and Purpose

Plans to qualify the Nine Mile Point nuclear plant for operation at Extended Power Uprate (EPU) operating condition require an assessment of the steam dryer stresses experienced under the increased loads. The steam dryer loads due to pressure fluctuations in the main steam lines (MSLs) are potentially damaging and the cyclic stresses from these loads can produce fatigue cracking if loads are sufficiently high. The industry has addressed this problem with physical modifications to the dryers, as well as a program to define steam dryer loads and their resulting stresses. The purpose of the stress analysis discussed here is to calculate the maximum and alternating stresses generated during Current Licensed Thermal Power (CLTP) and Extended Power Uprate (EPU) and to determine the margins that exist when compared to stresses that comply with the ASME Code (ASME B&PV Code, Section III, subsection NG).

The stress analysis of the modified NMP2 steam dryer establishes whether the existing and proposed modifications are adequate for sustaining structural integrity and preventing future weld cracking under planned EPU operating conditions. The load combination considered here corresponds to normal operation (the Level A Service Condition) and includes fluctuating pressure loads developed from NMP2 main steam line data, and weight. The fluctuating pressure loads, induced by the flowing steam, are predicted using a separate acoustic circuit analysis of the steam dome and main steam lines [6]. Level B service conditions, which include seismic loads, are not included in this evaluation.

The current stress evaluation of the NMP2 steam dryer is performed using acoustic loads generated using a revised Acoustic Circuit Model (ACM) Rev. 4.1 [2, 3]. The development of this revision was motivated primarily by a desire for consistent usage of noise filtering strategies during both model calibration against available data and application of the model to plants. Other than the removal of known non-acoustic discrete frequencies (e.g., electrical noise at multiples of 60 Hz) and the application of coherence filtering (which was also invoked when processing the Quad Cities data) no other filtering methods are used. In particular, no noise subtraction using low power data is performed. Further details of the ACM Rev. 4.1 calibration activity are provided in [3]. Its application to obtain NMP2 steam dryer acoustic loads is detailed in [4]. As described in [3] re-benchmarking the ACM against available Quad Cities data produced updated estimates of the acoustic speed and damping in the acoustics description and also revised biases and uncertainties due to changes in the model, coherence-based noise filtering and comparison method. The biases and uncertainties used for the present load estimates are based on the comparison with QC data at 790MWe using 16 sensors.

In order to qualify the NMP2 steam dryer for EPU operation it is required that the limiting alternating stress ratio at EPU be above a target level of 2.0. Since flow-induced acoustic resonances are not anticipated in the steam dryer, the alternating stress ratios at EPU operation can be obtained by scaling the CLTP values by the steam flow velocity squared, $(U_{EPU}/U_{CLTP})^2 = 1.1756^2 = 1.382$. This corresponds to a target alternating stress ratio at CLTP of 2.76. When the ACM Rev. 4.1 acoustic loads are impressed on the existing dryer configuration the predicted alternating stress ratios at several locations are below the target level. In Section 5, these locations are organized into four groups. Modifications to the dryer have been

implemented for each group to ensure that all locations meet or exceed the target stress ratio. Briefly, the groups and associated modifications consist of the following:

- Group 1: The lifting rod bracket/side plate welds. High membrane stresses are predicted on the end of the existing weld. For the upper and middle brackets the modification to alleviate these stresses consists of reinforcement plates welded to the vane bank side plate and brace. For the lower-most brackets a simple increase in the weld size from $\frac{1}{4}$ " to $\frac{1}{2}$ " suffices to reduce the stress to acceptable levels.
- Group 2: The middle hood reinforcement strip incurs a high stress due to vibration of the outboard section of the middle hood. The design to alleviate this stress consists of overlaying a $\frac{1}{8}$ " curved plate over the portion of the middle hood located between the existing reinforcement strip and the closure plate. This modification is shown to provide ample margin at EPU.
- Group 3: The inner hood/hood support welds that experience high stresses due to the inner hood vibrations. The stress alleviation method consists of placing a total of four 15 lb masses on the central inner hood panels (the two panels connecting to the central hood support) 18" below the top of the vane bank surface.
- Group 4: A collection of locations that are close to, but do not quite meet the target stress ratios. These locations comprise the following locations:
 - (a) *Middle hood/hood support welds.* These stress locations are similar to the ones on the inner hood/hood support welds and are alleviated in a similar manner by adding a total of four 10 lb masses to the central sections of the middle hoods.
 - (b) *Bottoms of the drain channel/skirt welds.* These welds are reinforced by thickening the length and wrapping the weld around the junction terminus and continuing it for 1" along the interior side.
 - (c) *Outer hood/hood support/cover plate junctions.* A stress relief cut-out hole optimized to minimize the alternating stresses is added to the support plate

In addition to modifications at these high stress locations, stiffening strips added to the closure plate are required to simultaneously increase the plate resonance frequency and lower stresses. Without these strips the closure plates experience a strong resonant response at about 128 Hz leading to high stresses in the closure plate attachment welds. Previously it had been attempted to reduce these stresses to acceptable levels by thickening the attachment welds. With the current load estimates however, such weld reinforcements do not provide sufficient stress reduction which has motivated the strip-based reinforcement concept. Adding the reinforcement ribs obviates the need for any increases in the closure plate attachment weld sizes. With these reinforcements in place the dryer meets the EPU target stress levels.

To ensure that the modifications do not inadvertently introduce new high stress locations, unit solutions of the complete dryer are recomputed over the 30-250 Hz frequency range with the modifications in place including the stiffened closure plate, the masses added to the inner and middle hoods, and the $\frac{1}{8}$ " thick reinforcement plate placed over the middle hood section

outboard of the closure plate. Below 30 Hz the original un-modified steam dryer unit solutions are used. This is acceptable since the dynamic response of the dryer below this frequency is small; it is also conservative since no credit is taken for the stress reductions realized by these modifications. Other reinforcements such as the modified channel/skirt weld are localized [[

(3)]]

This report describes the overall methodology used to obtain the unit solutions in the frequency domain and how to assemble them into a stress response for a given combination of pressure signals in the MSLs (Section 2). This is followed by details of the NMP2 steam dryer finite element model including the elements used and overall resolution, treatment of connections between elements, the hydrodynamic model, the implementation of structural damping and key idealizations/assumptions inherent to the model (Section 3). Post-processing procedures are also reviewed including the computation of maximum and alternating stress intensities, identification of high stress locations, adjustments to stress intensities at welds and evaluation of stress ratios used to establish compliance with the ASME Code in Section 4. Section 4 also [[

(3)]]

The modifications necessary to meet the target stress ratios are provided in Section 5 followed by the results in terms of stress intensity distributions and stress ratios together with PSDs of the dominant stress components in Section 6.

The stress evaluation of the modified steam dryer in Section 6 shows that the limiting alternating stress ratio on the dryer at CLTP is $SR-a=2.83$ which corresponds to $SR-a=2.05$ at EPU. The limiting peak stress ratio due to maximum membrane and bending stresses including static contributions is $SR-P=1.26$. These values show that with the modifications in place all locations meet the required stress margin EPU operation.

2. Methodology & Evaluation Procedures

2.1 Overview

Based on previous analysis undertaken at Quad Cities Units 1 and 2, the steam dryer can experience strong acoustic loads due to the fluctuating pressures in the MSLs connected to the steam dome containing the dryer. C.D.I. has developed an acoustic circuit model (ACM) that, given a collection of strain gage measurements [7] of the fluctuating pressures in the MSLs, predicts the acoustic pressure field anywhere inside the steam dome and on the steam dryer [2, 4, 6, 8]. The ACM is formulated in frequency space and contains two major components that are directly relevant to the ensuing stress analysis of concern here. [[

⁽³⁾]]

[[

⁽³⁾]]

[[

⁽³⁾]]

2.2 [[
[[

⁽³⁾]]

⁽³⁾]]

[[

(3)]]

2.3 Computational Considerations

Focusing on the structural computational aspects of the overall approach, there are a number of numerical and computational considerations requiring attention. The first concerns the transfer of the acoustic forces onto the structure, particularly the spatial and frequency resolutions. The ANSYS finite element program inputs general distributed pressure differences using a table format. This consists of regular 3D rectangular (i.e., block) $n_x \times n_y \times n_z$ mesh where n_α is the number of mesh points in the i -th Cartesian direction and the pressure difference is provided at each mesh point (see Section 3.10). These tables are generated separately using a program that reads the loads provided from the ACM software, distributes these loads onto the finite element mesh using a combination of interpolation procedures on the surface and simple diffusion schemes off the surface (off-surface loads are required by ANSYS to ensure proper interpolation of forces), and written to ASCII files for input to ANSYS. A separate load file is written at each frequency for the real and imaginary component of the complex force.

The acoustic field is stored at 5 Hz intervals from 0 to 250 Hz. While a 5 Hz resolution is sufficient to capture frequency dependence of the acoustic field (i.e., the pressure at a point varies gradually with frequency), it is too coarse for representing the structural response especially at low frequencies. For 1% critical structural damping, one can show that the frequency spacing needed to resolve a damped resonant peak at natural frequency, f_n , to within 5% accuracy is $\Delta f = 0.0064 \times f_n$. Thus for $f_n = 10$ Hz where the lowest structural response modes occur, a frequency interval of 0.064 Hz or less is required. In our calculations we require that 5% maximum error be maintained over the range from $f_n = 5$ Hz to 250 Hz resulting in a finest frequency interval of 0.0321 Hz at the low frequency end (this adequately resolves all structural modes up to 250 Hz). Since there are no structural modes between 0 to 5 Hz, a 0.5 Hz spacing is used over this range with minimal (less than 5%) error. The unit load, $\hat{f}_n(\omega, \mathbf{R})$, at any frequency, ω_k , is obtained by linear interpolation of the acoustic solutions at the two nearest frequencies, ω_i and ω_{i+1} , spaced 5 Hz apart. Linear interpolation is sufficient since the pressure load varies slowly over the 5 Hz range (linear interpolation of the structural response would not be acceptable over this range since it varies much more rapidly over the same interval). Details regarding the frequency resolution have been provided in [10].

Solution Management

[[

(3)]]

[[

(3)]]

Structural Damping

In harmonic analysis one has a broader selection of damping models than in transient simulations. A damping factor, z , of 1% critical damping is used in the structural analysis. In transient simulations, this damping can only be enforced exactly at two frequencies (where the damping model is “pinned”). Between these two frequencies the damping factor can be considerably smaller, for example 0.5% or less depending on the pinning frequencies. Outside the pinning frequencies, damping is higher. With harmonic analysis it is straightforward to enforce very close to 1% damping over the entire frequency range. In this damping model, the damping matrix, \mathbf{D} , is set to

$$\mathbf{D} = \frac{2z}{\omega} \mathbf{K} \quad (7)$$

where \mathbf{K} is the stiffness matrix and ω the forcing frequency. When comparing the response obtained with this model against that for a constant damping ratio, the maximum difference at any frequency is less than 0.5%, which is far smaller than the 100% or higher response variation obtained when using the pinned model required in transient simulation.

Load Frequency Rescaling

One way to evaluate the sensitivity of the stress results to approximations in the structural modeling and applied loads is to rescale the frequency content of the applied loads. In this procedure the nominal frequencies, ω_k , are shifted to $(1+\lambda)\omega_k$, where the frequency shift, λ , ranges between $\pm 10\%$, and the response recomputed for the shifted loads. The objective of the frequency shifting can be explained by way of example. Suppose that in the actual dryer a strong structural-acoustic coupling exists at a particular frequency, ω^* . This means that the following conditions hold simultaneously: (i) the acoustic signal contains a significant signal at ω^* ; (ii) the structural model contains a resonant mode of natural frequency, ω_n , that is near ω^* ; and (iii) the associated structural mode shape is strongly coupled to the acoustic load (i.e., integrating the product of the mode shape and the surface pressure over the steam dryer surface produces a significant modal force). Suppose now that because of discretization errors and modeling idealizations that the predicted resonance frequency differs from ω^* by a small amount (e.g., 1.5%). Then condition (ii) will be violated and the response amplitude therefore significantly diminished. By shifting the load frequencies one re-establishes condition (ii) when $(1+\lambda)\omega^*$ is

near ω_n . The other two requirements also hold and a strong structural acoustic interaction is restored.

[[

(3)]]

Evaluation of Maximum and Alternating Stress Intensities

Once the unit solutions have been obtained, the most intensive computational steps in the generation of stress intensities are: (i) the FFTs to evaluate stress time histories from (5); and (ii) the calculation of alternating stress intensities. [[

(3)]]

The high computational penalty incurred in calculating the alternating stress intensities is due to the fact that this calculation involves comparing the stress tensors at every pair of points in the stress history. This comparison is necessary since in general the principal stress directions can vary during the response, thus for N samples in the stress history, there will be $(N-1)N/2$ such pairs or, for $N=64K$ (the number required to accurately resolve the spectrum up to 250 Hz in 0.01 Hz intervals), 2.1×10^9 calculations per node each requiring the determination of the roots to a cubic polynomial. [[

(3)]]

2.4 [[
[[

(3)]]

(3)]]

[[

(3)]]

2.5 Flaw Evaluation

As part of the steam dryer stress assessment for EPU operation an evaluation of existing flaws discovered in the outer hood/hood support/base plate junctions is required to establish whether or not flaw propagation will occur at EPU conditions. If growth of the existing indications cannot be readily ruled out then a modification to the existing locations is required. Performing the flaw evaluation and designing the stress relief cutout required the combined use of several analysis methods which are summarized here. The flaw growth assessment is

performed jointly by CDI and Structural Integrity Associates (SIA). CDI provided a high resolution sub-model that includes details of the local welds together with the perimeter loads and inertial and body forces as described above. CDI also conducted supporting calculations to estimate the RMS stresses and determine whether the behavior at these locations is symptomatic of load- or displacement-controlled stresses. Finally a modified sub-model of this location with a circular cutout in the hood support was developed as a contingency repair in the event that arresting of further crack growth at EPU operation cannot be assured under the current (unmodified) configuration. The sizing and placement of the circular cut-out is described in [5] and [[

(3)]]]. With these results, SIA conducted the flaw evaluation using a combination of analytical methods and finite element modeling using crack elements as described in [14].

Load- or Displacement-Controlled Stresses

The detailed flaw evaluation requires an assessment of whether the stress at the crack is primarily load- or displacement-controlled as this distinction warrants different criteria for establishing crack growth. In a load-controlled configuration the applied load essentially remains constant as the structure displaces. In a displacement-controlled configuration the forces experienced by the load are relieved as the structure displaces.

The distinction can be explained by way of example and reference to Figure 1 which depicts a structure similar to the hood support. The structure contains a flaw as shown and the right hand edge is either: (i) loaded with a constant force or (ii) required to move by a specified displacement. The former case would arise if the edge is directly loaded; the second situation arises when the hood response is dominated by the response of adjacent structures. Suppose that the displacement at the location indicated is monitored as the flaw length is increased. In a load-controlled configuration – case (i) - the monitored displacement is expected to increase as the flaw grows. Conversely in the displacement-controlled setting the monitored displacement will only be weakly affected by the flaw length and will either remain approximately the same or decrease with increasing flaw size.

For the outer hood/hood support/cover plate junction it is noted that the 1/4" outer hood support connects to the much thicker (1/2") outer hoods on the left edge and to the massive outer vane banks on the right edge. Since the outer hoods connect directly to the vane banks it can be surmised that acoustic forcing of the outer hoods will produce motions in the combined outer hood + vane bank assembly. Because of the comparatively stiff outer hoods and massive vane banks (compared to the hood support), the motions of this assembly is anticipated to be only weakly affected by a flaw at this junction.

To verify this behavior for a complex structure such as the dryer where multiple load paths exist, a practical means of establishing whether the forces transmitted to the hood support plates are displacement-limited is required. To this end the global finite element model is used and elements along the hood/hood support weld line progressively disconnected to simulate flaws of different lengths. Thus one begins with the fully connected model and evaluates the displacements at selected locations on the hood support and connected components when subjected to the ACM Rev. 4.1 acoustic loads. These locations are chosen to lie between 3-9

inches away from the high stress location as shown in Figure 2. The lowest finite element in the hood support that is adjacent to the outer hood/hood support weld is then disconnected. The nearest middle hood/hood support is similarly disconnected and the displacements at the same locations recalculated. Next this process is repeated by disconnecting the two lowest finite elements along the weld (i.e., the one disconnected previously and the one immediately above it also adjacent to the weld) and re-evaluating the displacements; then disconnecting the three lowest elements, etc. The displacements are then plotted as a function of disconnection length to see whether the displacements generally increase with disconnection length which is indicative of load-controlled behavior, or whether the displacements remain constant or reduce with disconnection length which implies displacement-controlled response. These plots are presented in Figure 3. From these plots the response at the outer hood/hood support/cover plate is consistent with displacement-controlled behavior as all displacements tend to reduce with crack length or plateau to constant values.

At the middle hood/hood support/base plate junction, the displacement amplitudes all decrease gradually or plateau except for the middle hoods themselves whose amplitudes continue to grow. This is indicative of a vibration mode that continues to grow as the restraint provided by the hood support is reduced. For the hood support itself however, where the dominant stress occur, the displacements at 2A and 2B are generally level or diminishing with crack length (see Figure 3) indicating that the hood support stress is also displacement-controlled.

The stress at the flaw tip is also recorded as a function of crack length to corroborate whether or not the stress is displacement-controlled. Generally, one would expect to observe a reduction in this stress as the crack is extended. This observation is indeed borne out as shown in Figure 4. This plot records the maximum unit solution stress at the flaw tip as a function of displacement length where the maximum is taken over all frequencies and MSL forcings.

Finally, it is noted that the displacement-controlled stress behavior at all hood/hood support/base plate junctions is supported by field observations at explained at length in [14]. Essentially, for a load-controlled stress state the observed flaws would have grown to considerably longer lengths. Instead, the flaws which are believed to have been initiated by residual stresses, have grown to approximately 2" on the outer hood supports and 0.5" at the middle and some inner hood supports and stopped. This is fully consistent with a displacement-controlled stress situation and also corroborates the analysis conducted in [14] which predicts crack growth to approximately 2" during the first operational cycle and subsequent arrest of the crack as the crack tip stress field diminishes. While the evaluation in [14] focuses on the outer hood support, this evaluation constitutes the bounding flaw assessment for all (outer, middle and inner) hood support junctions given that the highest junction stresses occur on the outer hood supports and all locations evidence displacement-controlled stress behavior near the flaws.

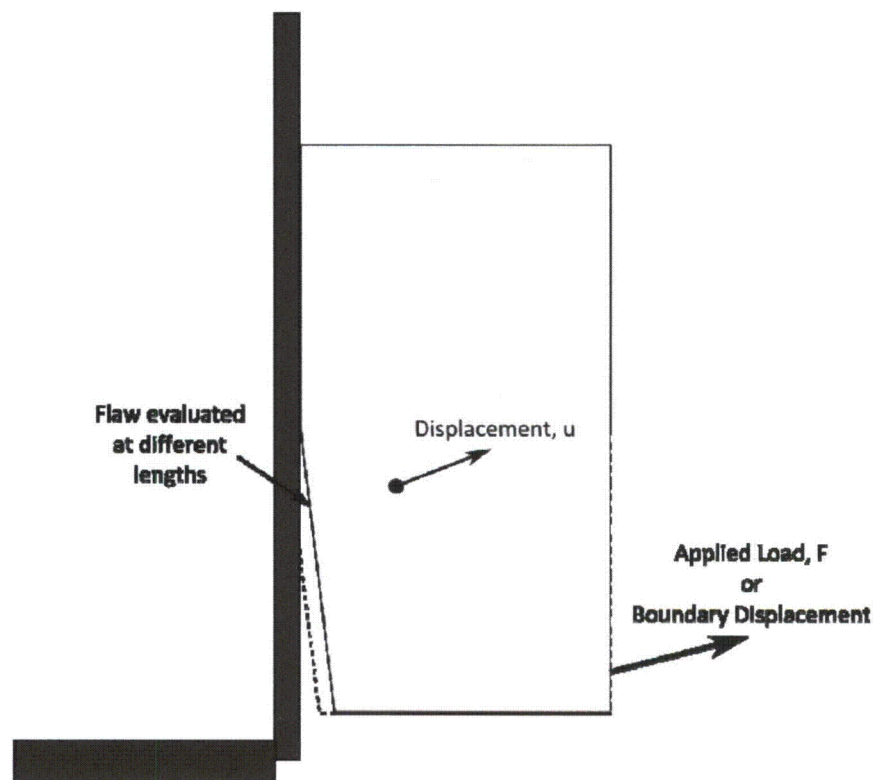


Figure 1. Conceptual arrangement of hood support geometry for the determining whether the limiting stresses are load- or displacement-controlled.

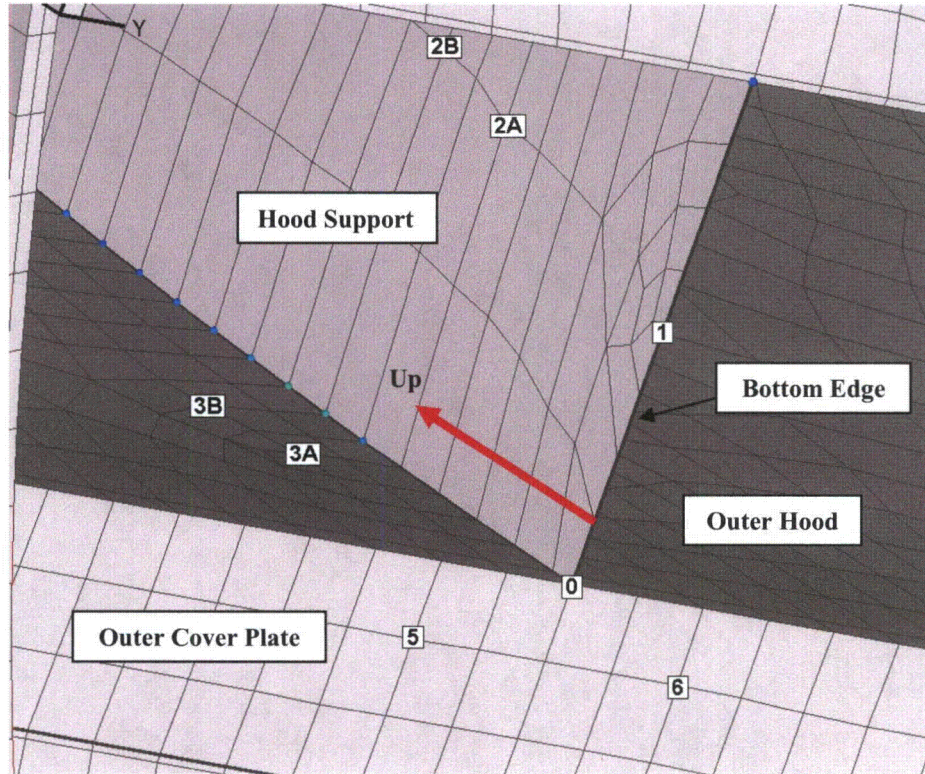


Figure 2. Depiction from below of locations near the outer hood/hood support/cover plate high stress point where displacements are recorded. Location 0 lies at the high stress location. Location 1 lies on the bottom edge of the hood support whereas locations 2A and 2B lie approximately 9" and 13" respectively above location 1. Locations 3A and 3B reside on the outer hood at approximately the same heights as 2A and 2B; Locations 4A and 4B are similarly placed on the outer hood and are located behind the hood support and thus obscured by the hood support in this view. Finally locations 5 and 6 are on the outer cover plate. Precise values are given in Table 1. Analogous locations are erected about the middle hood/hood support junction.

Table 1. Coordinates of Locations 0-6 in Figure 2.

Index	node	x	y	z
0	95267	-102.75	28.39	0
1	14954	-94.875	28.39	0
2A	14789	-93.7966	28.39	10.0558
2B	14840	-93.7159	28.39	13.6998
3A	79184	-102.624	23.9483	9.44825
3B	78999	-102.495	23.689	13.4162
4A	77836	-102.617	33.8335	9.70184
4B	77835	-102.48	34.3628	13.8147
5	48374	-105.543	24.76	0
6	48388	-106.358	32.0303	0

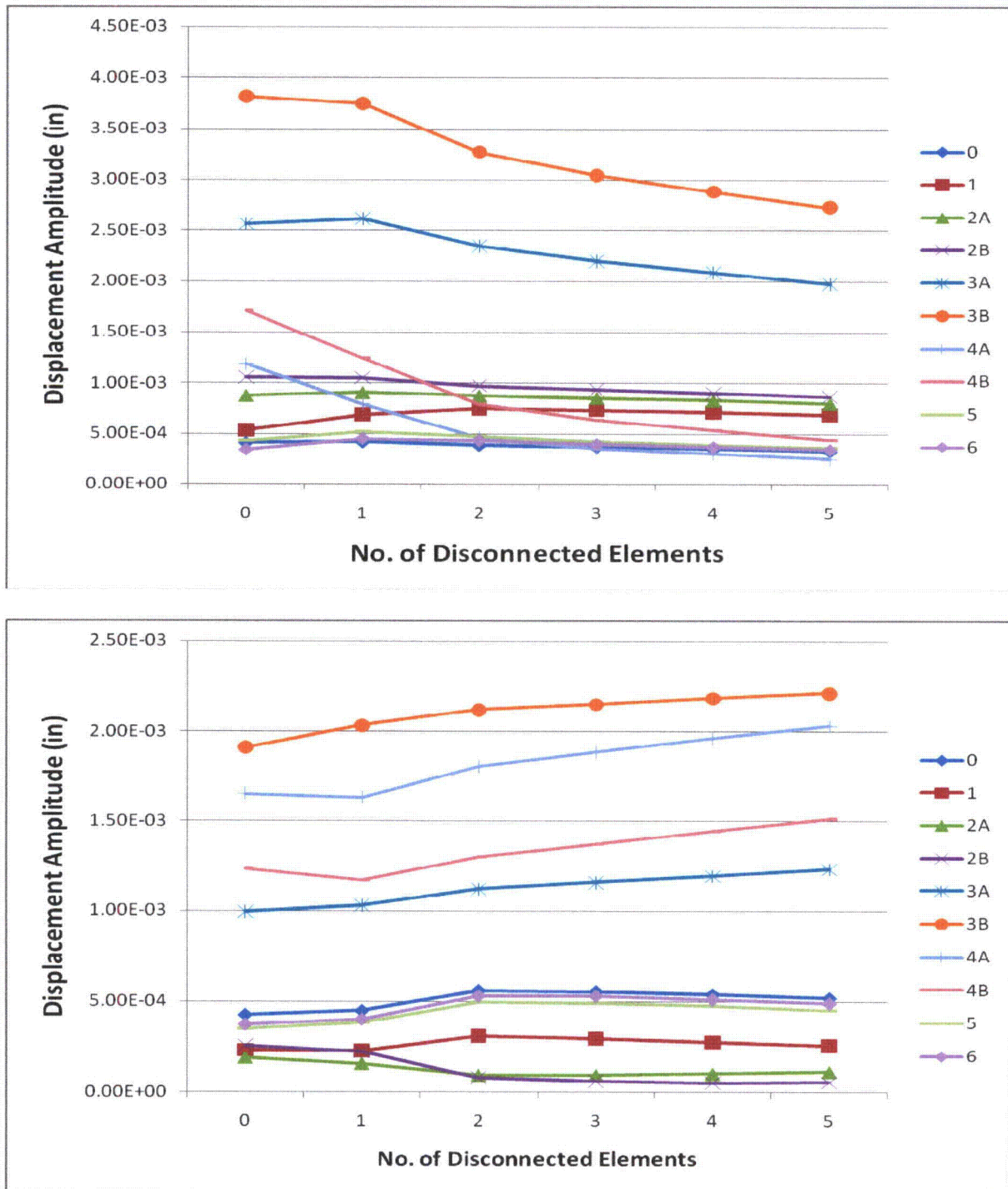


Figure 3. Variation of displacement amplitudes at the locations depicted in Figure 2 as a function of the number of disconnected elements along the hood/hood support weld line. Top – outer hood; bottom – middle hood.

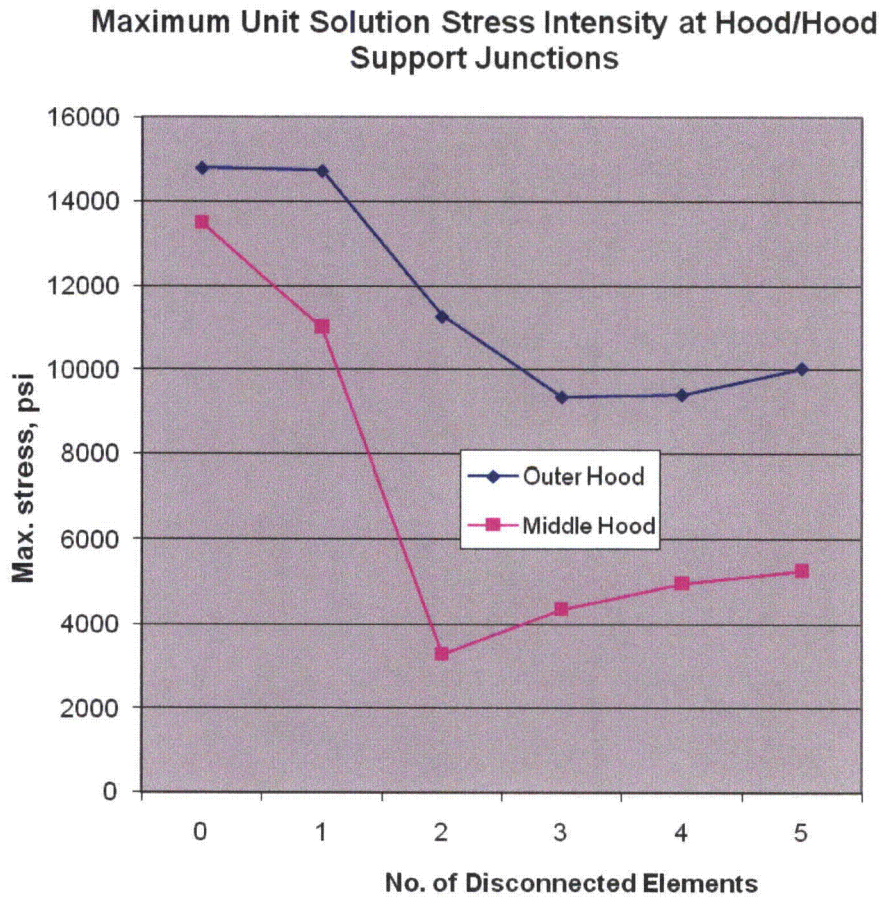


Figure 4. Variation of the maximum unit solution stress at the tip of the disconnection line as a function of the number of disconnected elements. The maximum of the stress intensity is taken over all MSL loadings and frequencies.

Sizing and Positioning the Stress Relief Cut-Out Hole

If the flaw evaluation shows insufficient margin a means of reducing the stress is needed. The option considered here is the insertion of a semi-circular stress relief cutout hole. The cut-out hole is optimized by adjusting the position and radius of the hole to minimize the overall stress ratio. The optimization process is carried out using a shell-based sub-model to expedite the overall design process. [[

(3)]]

3. Finite Element Model Description

A description of the ANSYS model of the nine Mile Point Unit 2 steam dryer follows.

3.1 Steam Dryer Geometry

A geometric representation of the Nine Mile Point Unit 2 steam dryer was developed from available drawings (provided by Constellation Energy Group and included in the design record file, DRF-C-279C) within the Workbench module of ANSYS. The completed model is shown in Figure 5. This model includes on-site modifications to the Nine Mile Point Unit 2 steam dryer. These are as follows.

On-Site Modifications

- (i) The top tie rods are replaced with thicker ones.
- (ii) Inner side plates are replaced with thicker ones.
- (iii) Middle hoods are reinforced with additional strips.
- (iv) Lifting rods are reinforced with additional gussets.
- (v) Per FDDR KG1-0265 the support conditions are adjusted to ensure that the dryer is supported 100% on the seismic blocks.

These additional modifications have been incorporated into the NMP2 steam dryer model and are reflected in the results presented in this report. The affected areas are shown in Figure 6.

Modifications Planned for EPU Operation

In [15] several modifications were proposed to meet target EPU stress margins using a previous acoustic loads model (ACM Rev. 4.0) without noise subtraction. These modifications are now superseded here by the ones below and detailed in Section 5 that are obtained by on the basis of acoustic loads processed using the ACM Rev. 4.1 analysis. These planned modifications include:

- (vi) Reinforcement strips are added to the closure plates.
- (vii) Reinforcements to the upper-most and middle lifting rod braces are made in the form of additional strengthening plates.
- (viii) Increase the attachment weld size of the lower-most lifting rod brace from 1/4" to 1/2".
- (ix) A 1/8th in curved plate is placed over the middle hood section lying outboard of the closure plate.
- (x) Four 15 lb masses are added to the central inner hood panels.
- (xi) Stress relief cut-outs are added to the outer hood/hood support/base plate junctions to alleviate local stresses.
- (xii) A wrap-around weld is added to the bottom of the drain channel/skirt weld.
- (xiii) Four 10 lb masses are added to the central middle hood panels.

All of the modifications summarized here and detailed in Section 5 are implemented in the results produced in Section 6.

Reference Frame

The spatial coordinates used herein to describe the geometry and identify limiting stress locations are expressed in a reference frame whose origin is located at the intersection of the steam dryer centerline and the plane containing the base plates (this plane also contains the top of the upper support ring and the bottom edges of the hoods). The y-axis is parallel to the hoods, the x-axis is normal to the hoods pointing from MSL C/D to MSL A/B, and the z-axis is vertical, positive up.

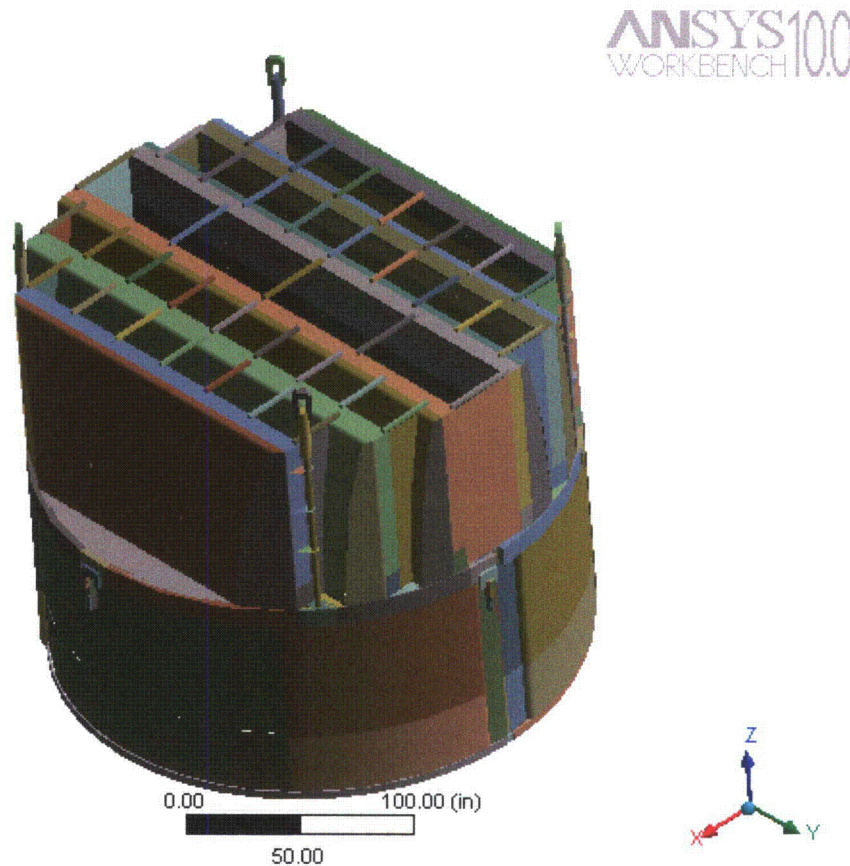


Figure 5. Overall geometry of the Nine Mile Point Unit 2 steam dryer model.

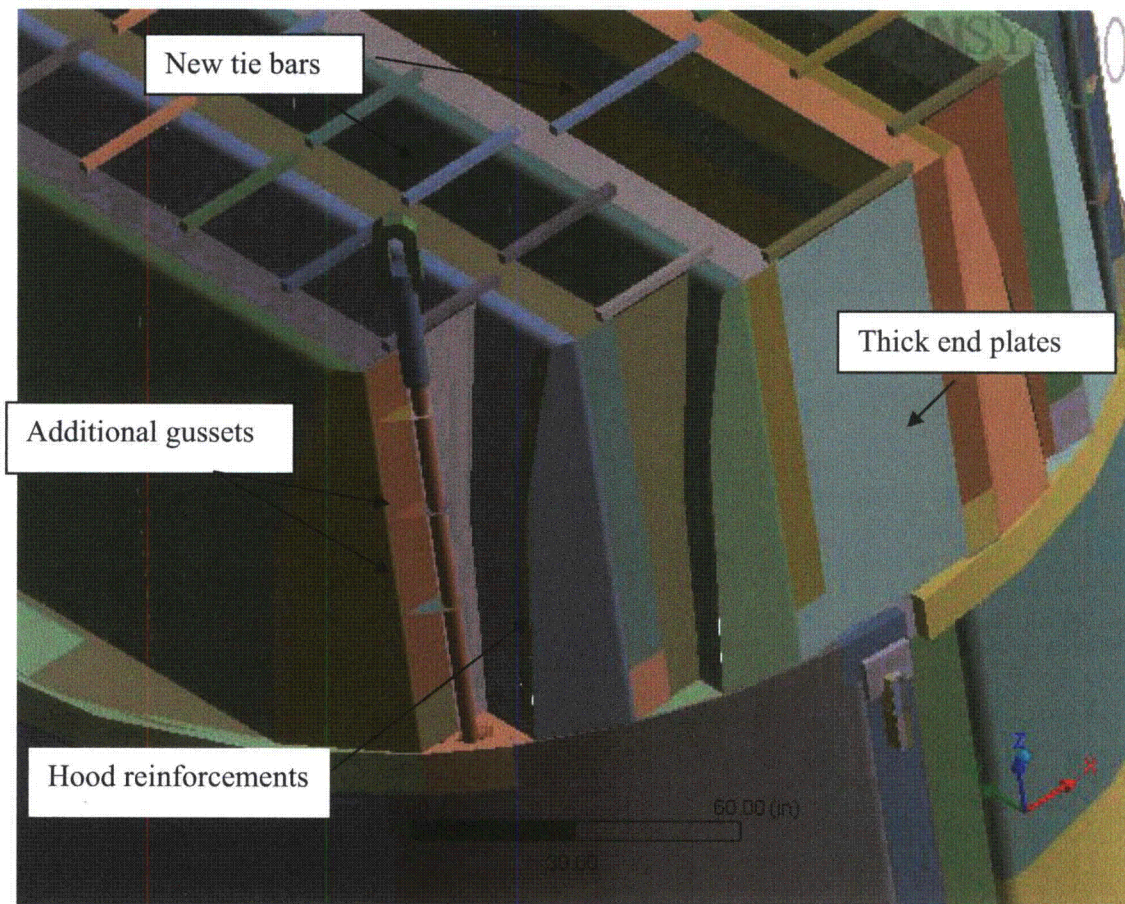


Figure 6. Existing on-site modifications accounted for in the model and associated geometrical details.

3.2 Material Properties

The steam dryer is constructed from Type 304 stainless steel and has an operating temperature of 550°F. Properties used in the analysis are summarized below in Table 2.

Table 2. Material properties.

	Young's Modulus (10^6 psi)	Density (lbm/in ³)	Poisson Ratio
stainless steel	25.55	0.284	0.3
structural steel with added water inertia effect	25.55	0.856	0.3

The structural steel modulus is taken from Appendix A of the ASME Code for Type 304 Stainless Steel at an operating temperature 550°F. The effective properties of perforated plates and submerged parts are discussed in Sections 3.4 and 3.6. Note that the increased effective density for submerged components is only used in the harmonic analysis. When calculating the stress distribution due to the static dead weight load, the unmodified density of steel (0.284 lbm/in³) is used throughout.

Inspections of the NMP Unit 2 dryer have revealed IGSCC cracks in the upper support ring (USR) and skirt. A separate analysis of these cracks [16] has been performed to determine whether: (i) they will propagate further into the structure and (ii) their influence upon structural response frequencies and modes must be explicitly accounted for. To establish (i) the stress calculated in the global stress analysis is used in conjunction with the crack geometry to calculate the stress intensity factor which is then compared to the threshold stress intensity. For the USR and skirt cracks the highest stress intensity factors are 1.47 ksi-in^{0.5} and 2.75 ksi-in^{0.5} respectively; both values are below the threshold value (3 ksi-in^{0.5}) implying that fatigue crack growth will not occur.

To determine (ii) the change in modal response frequencies due to the presence of a flaw is predicted by analytical means (in the case of the USR) or using finite element analysis (for the skirt). In each case, the flaw size used in these calculations is increased to ensure conservative estimates (for example, in the case of the skirt flaws extending up to ½ the panel width are considered). For the USR, the change in modal frequencies due to the presence of the cracks is less than 0.5%. For the skirt, using a conservative estimate for the crack to panel width of 0.3 (the measured value is less than 0.17) the change in modal frequency is also less than 0.5%. In both cases such small changes in modal frequencies are considered negligible and are readily accounted for when performing frequency shifting.

3.3 Model Simplifications

The following simplifications were made to achieve reasonable model size while maintaining good modeling fidelity for key structural properties:

- Perforated plates were approximated as continuous plates using modified elastic properties designed to match the static and modal behaviors of the perforated plates. The

perforated plate structural modeling is summarized in Section 3.4 and Appendix C of [17].

- The drying vanes were replaced by point masses attached to the corresponding trough bottom plates and vane bank top covers (Figure 8). The bounding perforated plates, vane bank end plates, and vane bank top covers were explicitly modeled (see Section 3.5).
- The added mass properties of the lower part of the skirt below the reactor water level were obtained using a separate hydrodynamic analysis (see Section 3.6).
- [[
(3)]]
- Four steam dryer support brackets that are located on the reactor vessel and spaced at 90° intervals were explicitly modeled (see Section 3.9).
- Most welds were replaced by node-to-node connections; interconnected parts share common nodes along the welds. In other locations the constraint equations between nodal degrees of freedom were introduced as described in Section 3.9.

3.4 Perforated Plate Model

The perforated plates were modeled as solid plates with adjusted elastic and dynamic properties. Properties of the perforated plates were assigned according to the type and size of perforation. Based on [18], for an equilateral square pattern with given hole size and spacing, the effective moduli of elasticity were found.

The adjusted properties for the perforated plates are shown in Table 3 as ratios to material properties of structural steel, provided in Table 2. Locations of perforated plates are classified by steam entry / exit vane bank side and vertical position.

Tests were carried out to verify that this representation of perforated plates by continuous ones with modified elastic properties preserves the modal properties of the structure. These tests are summarized in Appendix C of [17] and compare the predicted first modal frequency for a cantilevered perforated plate against an experimentally measured value. The prediction was obtained for 40% and 13% open area plates (these are representative of the largest and lowest open area ratios of the perforated plates at NMP2, as seen in Table 3) using the analytical formula for a cantilevered plate and the modified Young's modulus and Poisson's ratio given by O'Donnell [18]. The measured and predicted frequencies are in close agreement, differing by less than 3%.

[[

(3)]]

[[

⁽³⁾]]

[[

⁽³⁾]]

Figure 7. [[

⁽³⁾]]

Table 3. Material properties of perforated plates.

[[

⁽³⁾]]

3.5 Vane Bank Model

The vane bank assemblies consist of many vertical angled plates that are computationally expensive to model explicitly, since a prohibitive number of elements would be required. These parts have significant weight which is transmitted through the surrounding structure, so it is important to capture their gross inertial properties. Here the vane banks are modeled as a collection of point masses located at the center of mass for each vane bank section (Figure 4). The following masses were used for the vane bank sections, based on data found on provided drawings:

inner banks, 1618 lbm, 4 sections per bank;
middle banks, 1485 lbm, total 4 sections per bank; and
outer banks, 1550 lbm, 3 sections per bank.

These masses were applied to the base plates and vane top covers using the standard ANSYS point mass modeling option, element MASS21. ANSYS automatically distributes the point mass inertial loads to the nodes of the selected structure. The distribution algorithm minimizes the sum of the squares of the nodal inertial forces, while ensuring that the net forces and moments are conserved. Vane banks are not exposed to main steam lines directly, but rather shielded by the hoods.

The collective stiffness of the vane banks is expected to be small compared to the surrounding support structure and is neglected in the model. In the static case it is reasonable to expect that this constitutes a conservative approach, since neglecting the stiffness of the vane banks implies that the entire weight is transmitted through the adjacent vane bank walls and supports. In the dynamic case the vane banks exhibit only a weak response since (i) they have large inertia so that the characteristic acoustically-induced forces divided by the vane masses and inertias yield small amplitude motions, velocities and accelerations; and (ii) they are shielded from acoustic loads by the hoods, which transfer dynamic loads to the rest of the structure. Thus, compared to the hoods, less motion is anticipated on the vane banks so that

approximating their inertial properties with equivalent point masses is justified. Nevertheless, the bounding parts, such as perforated plates, side panels, and top covers, are retained in the model. Errors associated with the point mass representation of the vane banks are compensated for by frequency shifting of the applied loads.

3.6 Water Inertia Effect on Submerged Panels

Water inertia was modeled by an increase in density of the submerged structure to account for the added hydrodynamic mass. This added mass was found by a separate hydrodynamic analysis (included in DRF-C-279C supporting this report) to be 0.143 lbm/in^2 on the submerged skirt area. This is modeled by effectively increasing the material density for the submerged portions of the skirt. Since the skirt is 0.25 inches thick, the added mass is equivalent to a density increase by 0.572 lbm/in^3 . This added water mass was included in the ANSYS model by appropriately modifying the density of the submerged structural elements when computing harmonic response. For the static stresses, the unmodified density of steel is used throughout.

3.7 Structural Damping

Structural damping was defined as 1% of critical damping for all frequencies. This damping is consistent with guidance given on pg. 10 of NRC RG-1.20 [22].

3.8 Mesh Details and Element Types

Shell elements were employed to model the skirt, hoods, perforated plates, side and end plates, trough bottom plates, reinforcements, base plates and cover plates. Specifically, the four-node, Shell Element SHELL63, was selected to model these structural components. This element models bending and membrane stresses, but omits transverse shear. The use of shell elements is appropriate for most of the structure where the characteristic thickness is small compared to the other plate dimensions. For thicker structures, such as the upper and lower support rings, solid brick elements were used to provide the full 3D stress. The elements SURF154 are used to assure proper application of pressure loading to the structure. Mesh details and element types are shown in Table 4 and Table 5.

The mesh is generated automatically by ANSYS with refinement near edges. The maximum allowable mesh spacing is specified by the user. Here a 2.5 inch maximum allowable spacing is specified with refinement up to 1.5 inch in the following areas: drain pipes, tie rods, the curved portions of the drain channels and the hoods. Details of the finite element mesh are shown in Figure 9. Numerical experiments carried out using the ANSYS code applied to simple analytically tractable plate structures with dimensions and mesh spacings similar to the ones used for the steam dryer, confirm that the natural frequencies are accurately recovered (less than 1% errors for the first modes). These errors are compensated for by the use of frequency shifting.

3.9 Connections between Structural Components

Most connections between parts are modeled as node-to-node connections. This is the correct manner (i.e., within the finite element framework) of joining elements away from discontinuities. At joints between shells, this approach omits the additional stiffness provided by the extra weld material. Also, locally 3D effects are more pronounced. The latter effect is accounted for using weld factors. The deviation in stiffness due to weld material is negligible, since weld dimensions are on the order of the shell thickness. The consequences upon modal

frequencies and amplitude are, to first order, proportional to t/L where t is the thickness and L a characteristic shell length. The errors committed by ignoring additional weld stiffness are thus small and readily compensated for by performing frequency shifts.

When joining shell and solid elements, however, the problem arises of properly constraining the rotations, since shell element nodes contain both displacement and rotational degrees of freedom at every node whereas solid elements model only the translations. A node-to-node connection would effectively appear to the shell element as a simply supported, rather than (the correct) cantilevered restraint and significantly alter the dynamic response of the shell structure.

To address this problem, constraint equations are used to properly connect adjacent shell- and solid-element modeled structures. Basically, all such constraints express the deflection (and rotation for shell elements) of a node, \mathbf{R}_1 , on one structural component in terms of the deflections/rotations of the corresponding point, \mathbf{P}_2 , on the other connected component. Specifically, the element containing \mathbf{P}_2 is identified and the deformations at \mathbf{P}_2 determined by interpolation between the element nodes. The following types of shell-solid element connections are used in the steam dryer model including the following:

1. Connections of shell faces to solid faces (Figure 10a). While only displacement degrees of freedom are explicitly constrained, this approach also implicitly constrains the rotational degrees of freedom when multiple shell nodes on a sufficiently dense grid are connected to the same solid face.
2. Connections of shell edges to solids (e.g., connection of the bottom of closure plates with the upper ring). Since solid elements do not have rotational degrees of freedom, the coupling approach consisted of having the shell penetrate into the solid by one shell thickness and then constraining both the embedded shell element nodes (inside the solid) and the ones located on the surface of the solid structure (see Figure 10b). Numerical tests involving simple structures showed that this approach and penetration depth reproduce both the deflections and stresses of the same structure modeled using only solid elements or ANSYS' bonded contact technology. Continuity of rotations and displacements is achieved.

The use of constraint conditions rather than the bonded contacts advocated by ANSYS for connecting independently meshed structural components confers better accuracy and useful numerical advantages to the structural analysis of the steam dryer including better conditioned and smaller matrices. The smaller size results from the fact that equations and degrees of freedom are eliminated rather than augmented (in Lagrange multiplier-based methods) by additional degrees of freedom. Also, the implementation of contact elements relies on the use of very high stiffness elements (in penalty function-based implementations) or results in indefinite matrices (Lagrange multiplier implementations) with poorer convergence behavior compared to positive definite matrices.

The steam dryer rests on four support blocks which resist vertical and lateral displacement. The support blocks contact the seismic blocks welded to the USR so that 100% of the dryer weight is transmitted through the seismic blocks per the FDDR KG1-265. Because the contact region between the blocks and steam dryer is small, the seismic blocks are considered free to

rotate about the radial axis. Specifically nodal constraints (zero relative displacement) are imposed over the contact area between the seismic blocks and the support blocks. Two nodes on each support block are fixed as indicated in Figure 11. One node is at the center of the support block surface facing the vessel and the other node is 0.5" offset inside the block towards the steam dryer, half way to the nearest upper support ring node. This arrangement approximates the nonlinear contact condition where the ring can tip about the block.

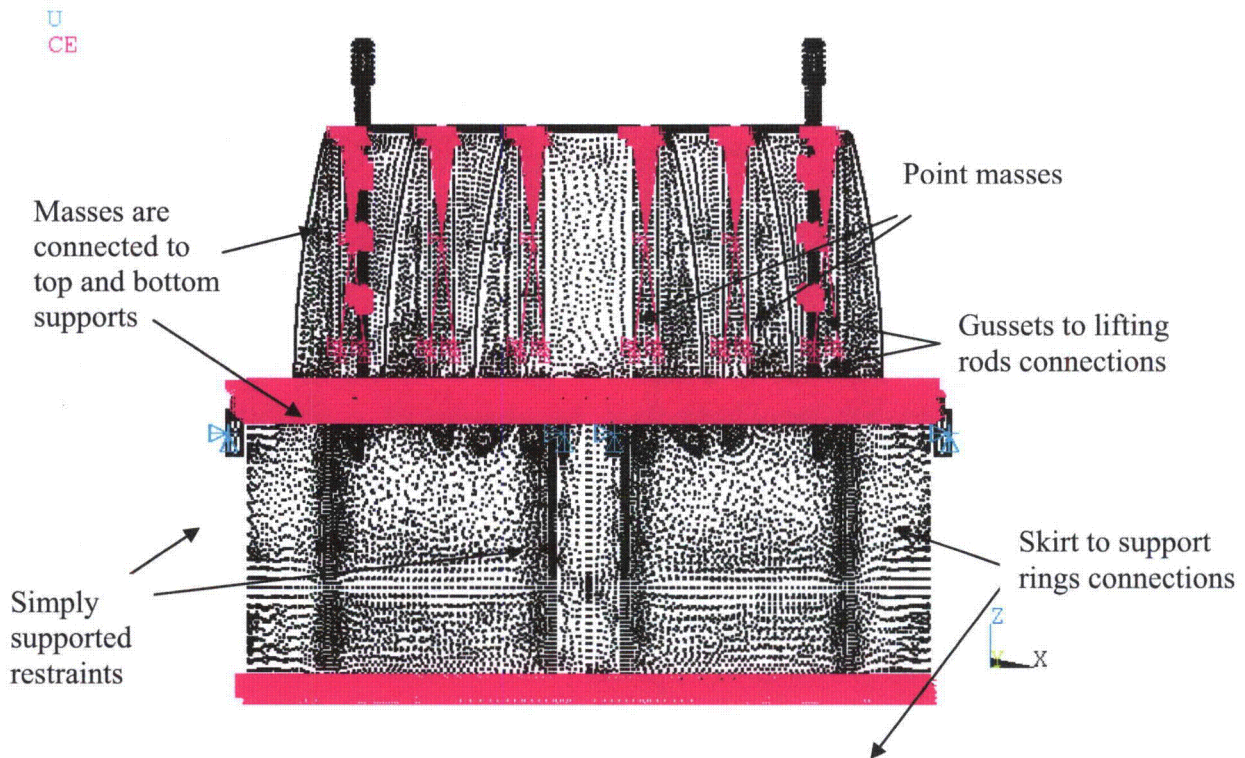


Figure 8. Point masses representing the vanes. The pink shading represents where constraint equations between nodes are applied (generally between solid and shell elements, point masses and nodes and $[[^{(3)}]]$).

Table 4. FE Model Summary.

Description	Quantity
Total Nodes ¹	159,793
Total Elements	124,496

1. Not including additional damper nodes and elements.

Table 5. Listing of Element Types.

Generic Element Type Name	Element Name	ANSYS Name
20-Node Quadratic Hexahedron	SOLID186	20-Node Hexahedral Structural Solid
10-Node Quadratic Tetrahedron	SOLID187	10-Node Tetrahedral Structural Solid
4-Node Elastic Shell	SHELL63	4-Node Elastic Shell
Mass Element	MASS21	Structural Mass
Pressure Surface Definition	SURF154	3D Structural Surface Effect
Damper element	COMBIN14	Spring-Damper

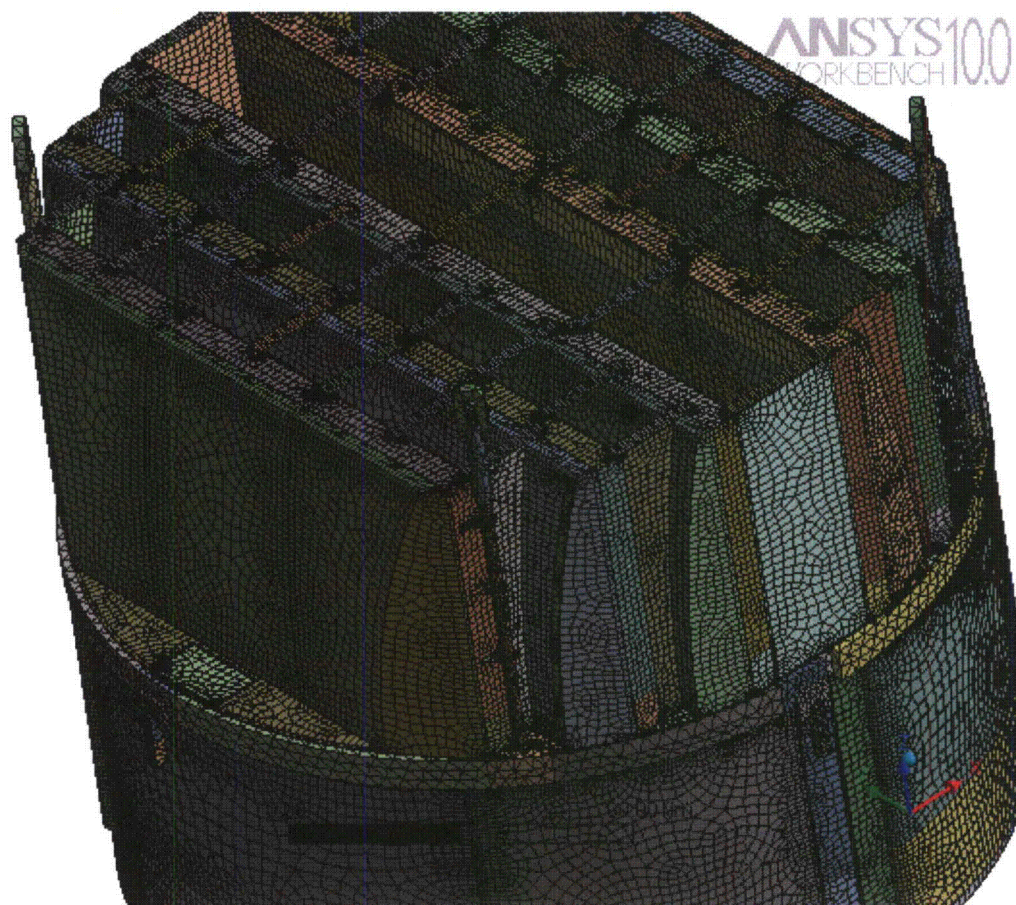


Figure 9a. Mesh overview.

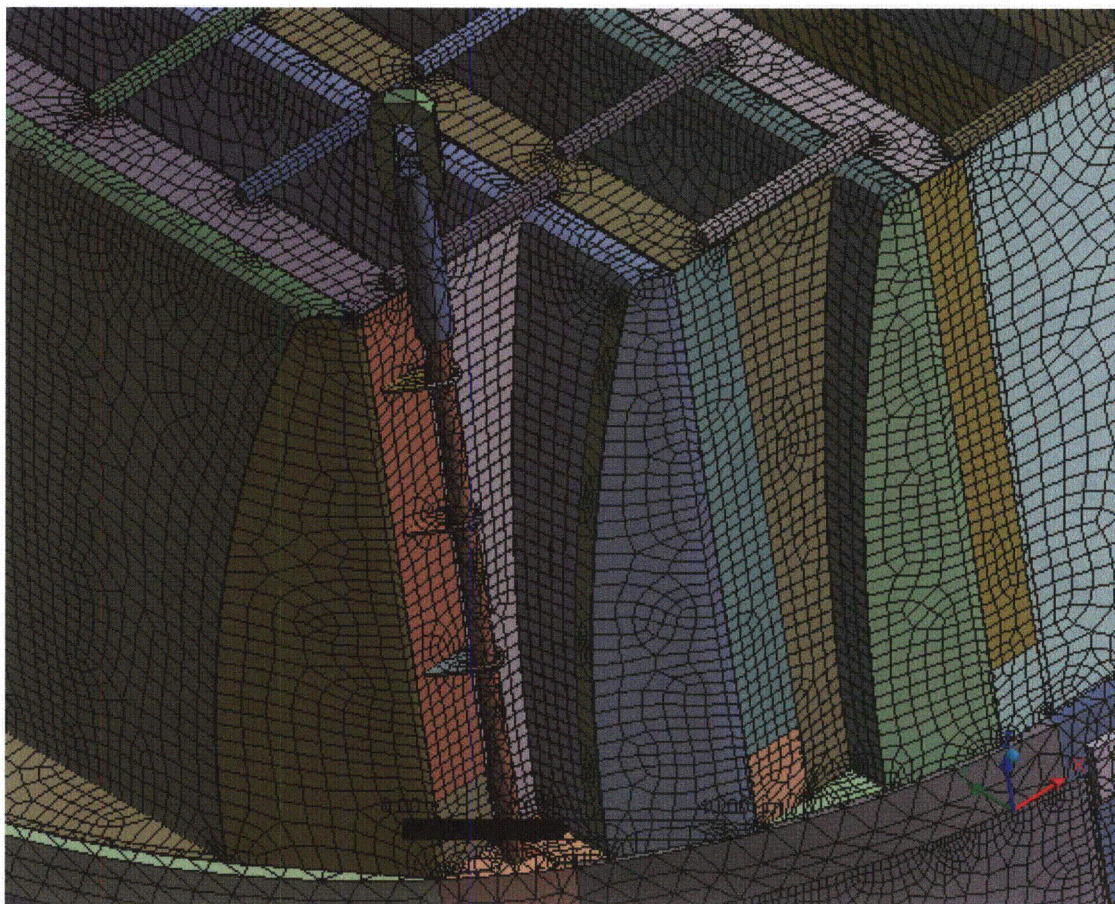


Figure 9b. Close up of mesh showing on-site modifications.



Figure 9c. Close up of mesh showing drain pipes and hood supports.

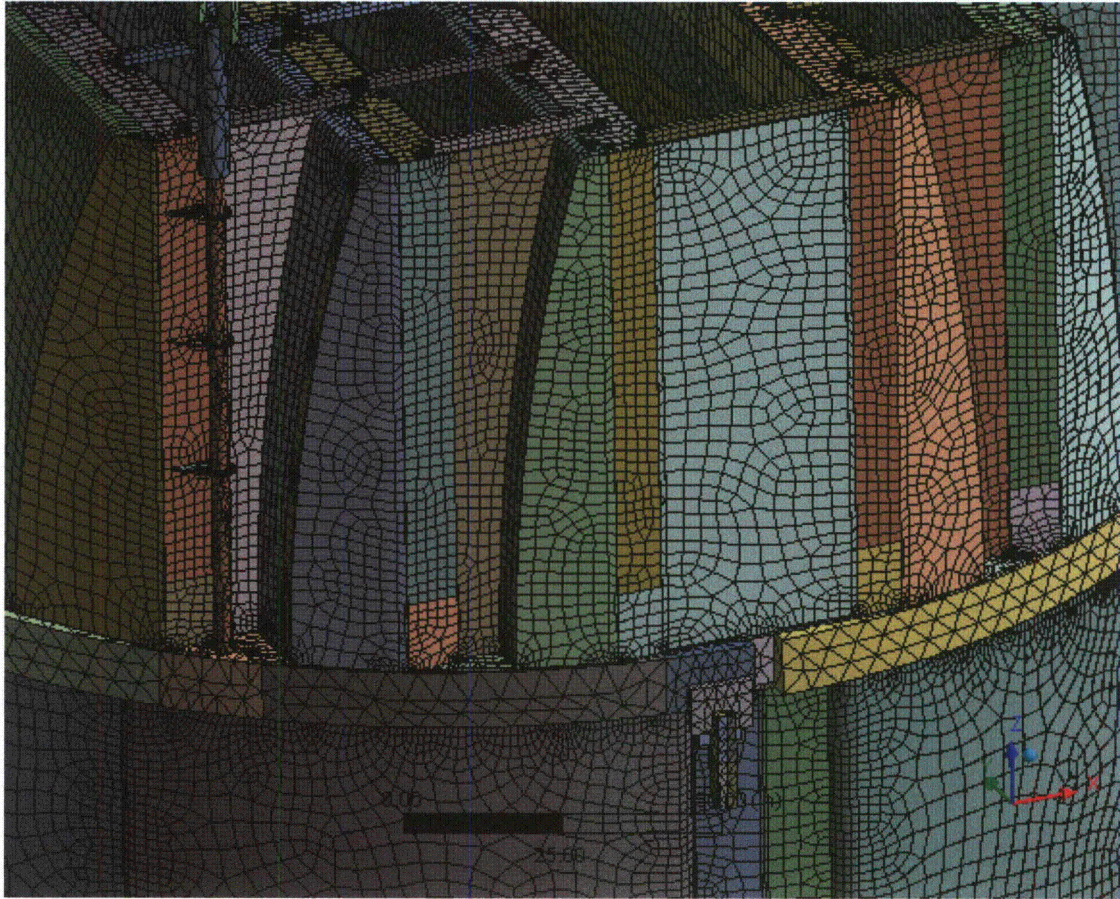


Figure 9d. Close up of mesh showing node-to-node connections between various plates.

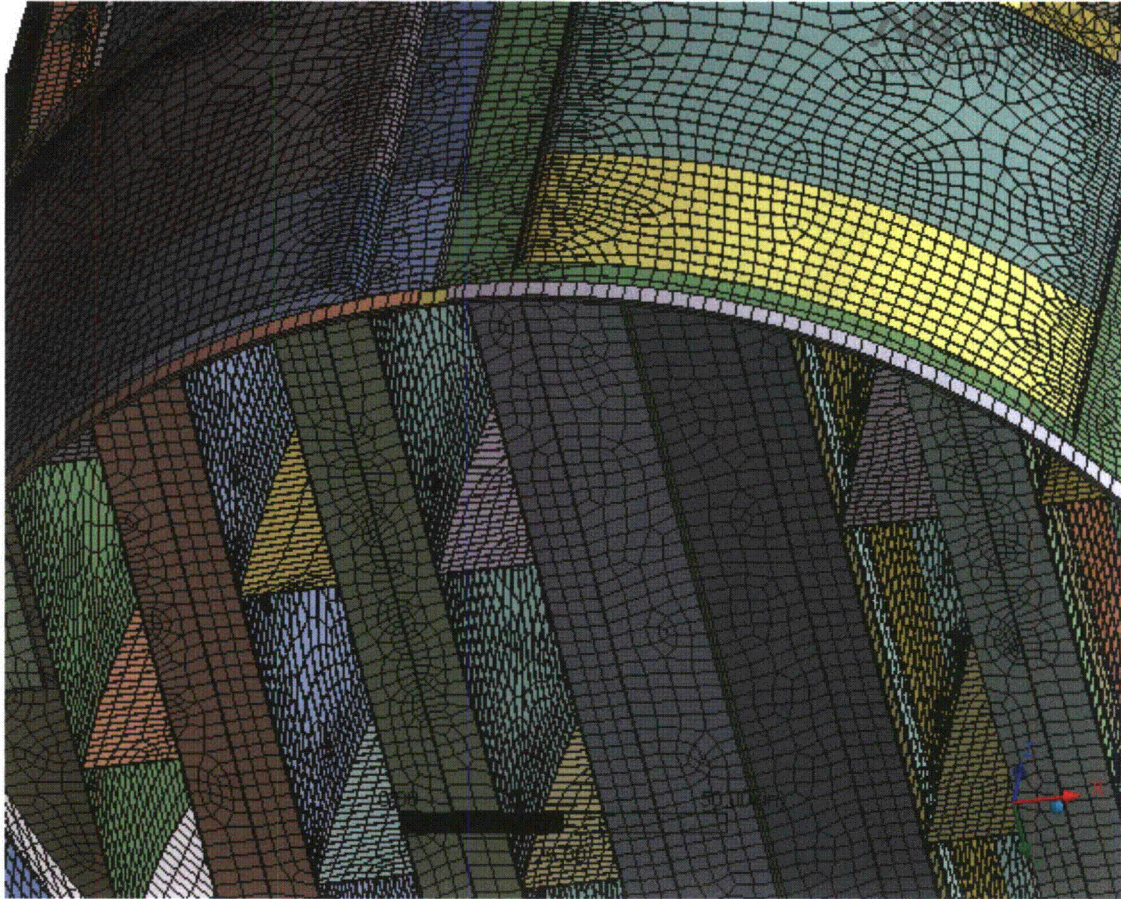


Figure 9e. Close up of mesh showing node-to-node connections between the skirt and drain channels; hood supports and hoods; and other parts.

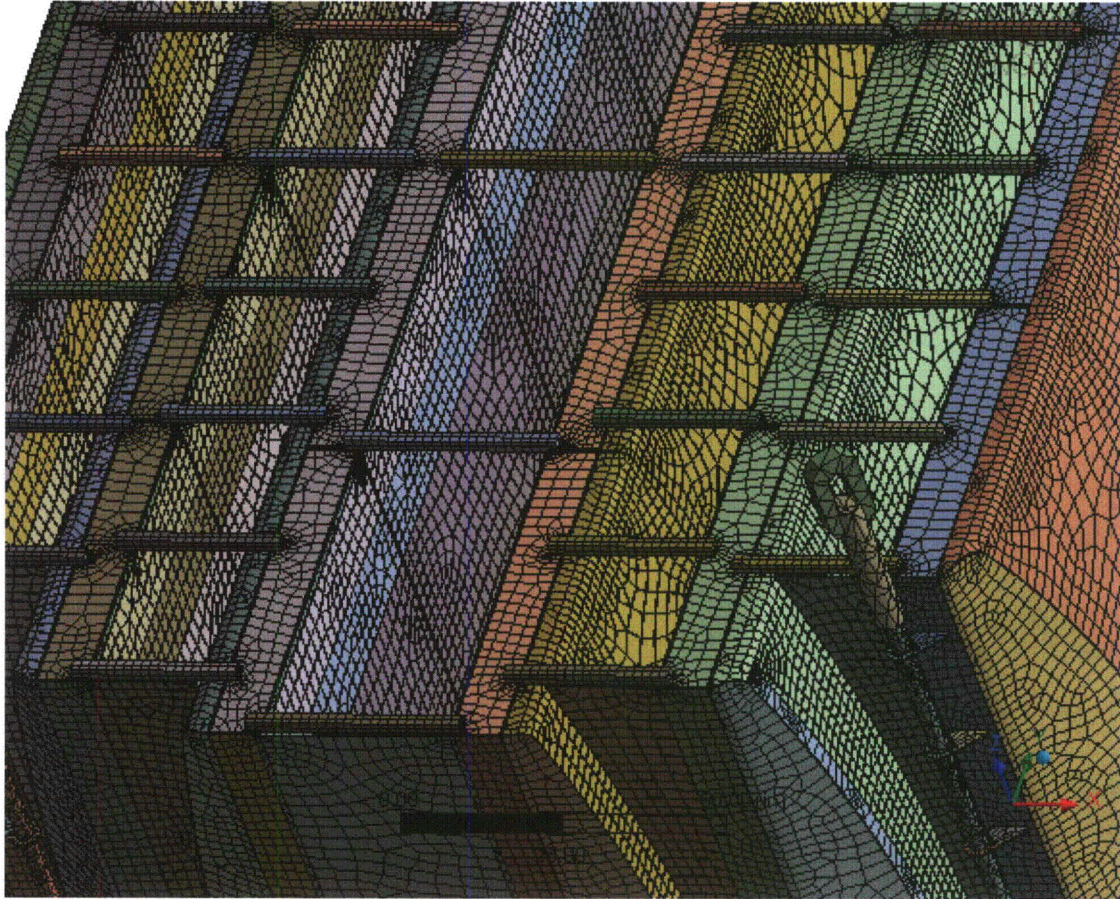


Figure 9f. Close up view of tie bars.

Shell nodes DOF are related to solid element shape functions

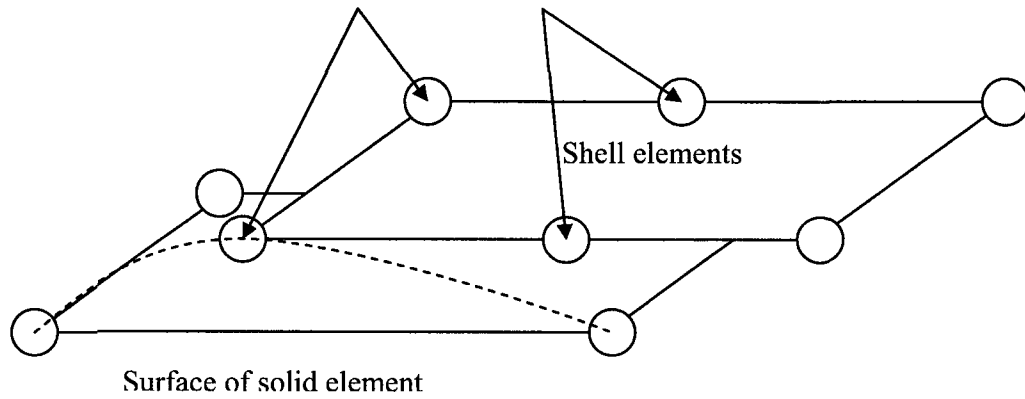


Figure 10a. Face-to-face shell to solid connection.

Shell nodes DOF are related to solid element shape functions

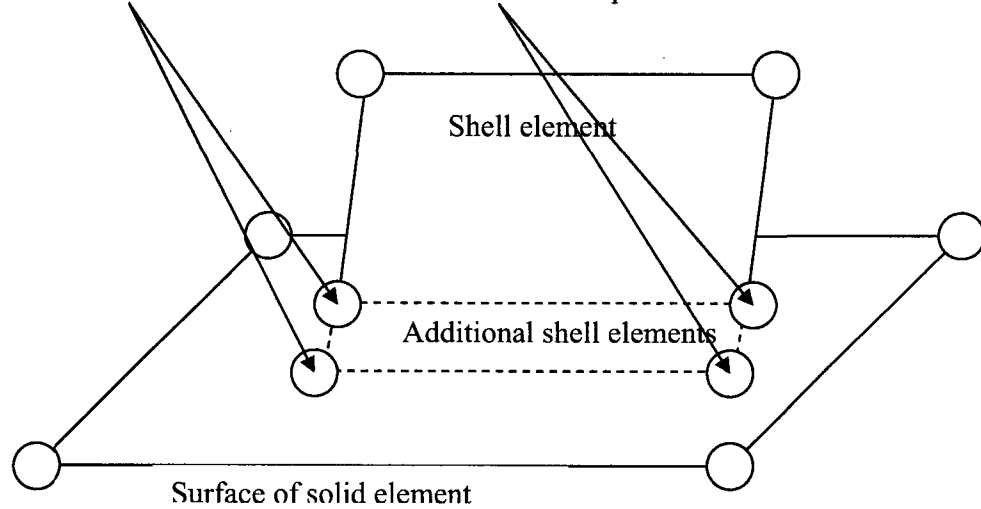


Figure 10b. Shell edge-to-solid face connection.

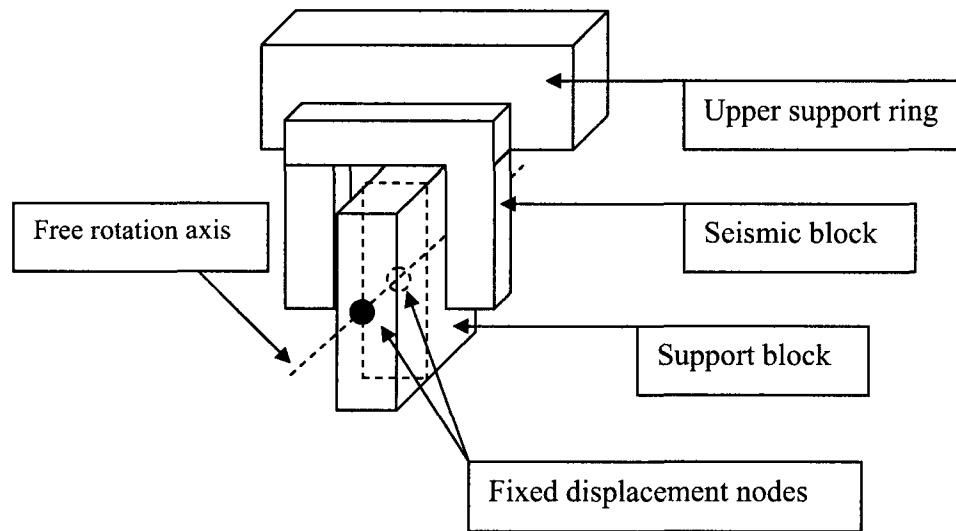


Figure 11. Boundary conditions. Inside node is half way between outer surface of support block and upper support ring.

3.10 Pressure Loading

The harmonic loads are produced by the pressures acting on the exposed surfaces of the steam dryer. At every frequency and for each MSL, the pressure distribution corresponding to a unit pressure at the MSL inlet is represented on a three-inch grid lattice grid (i.e., a mesh whose lines are aligned with the x-, y- and z-directions) that is superimposed over the steam dryer surface. This grid is compatible with the 'Table' format used by ANSYS to 'paint' general pressure distributions upon structural surfaces. The pressures are obtained from the Helmholtz solver routine in the acoustic analysis [2].

In general, the lattice nodes do not lie on the surface, so that to obtain the pressure differences at the surface it is necessary to interpolate the pressure differences stored at the lattice nodes. This is done using simple linear interpolation between the 8 forming nodes of the lattice cell containing the surface point of interest. Inspection of the resulting pressures at selected nodes shows that these pressures vary in a well-behaved manner between the nodes with prescribed pressures. Graphical depictions of the resulting pressures and comparisons between the peak pressures in the original nodal histories and those in the final surface load distributions produced in ANSYS, all confirm that the load data are interpolated accurately and transferred correctly to ANSYS.

The harmonic pressure loads are only applied to surfaces above the water level, as indicated in Figure 12. In addition to the pressure load, the static loading induced by the weight of the steam dryer is analyzed separately. The resulting static and harmonic stresses are linearly combined to obtain total values which are then processed to calculate maximum and alternating stress intensities for assessment in Section 5.

[[

⁽³⁾]] This is useful since revisions in the loads model do not necessitate recalculation of the unit stresses.

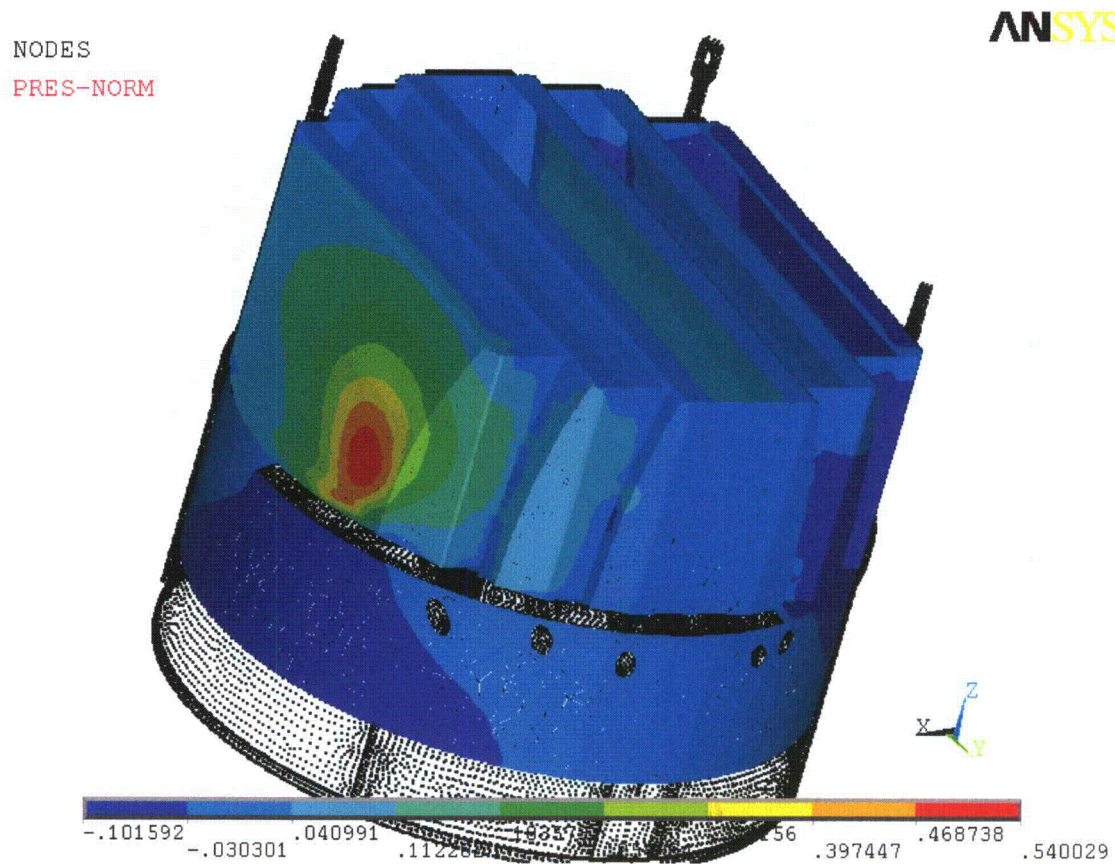


Figure 12a. Real part of unit pressure loading MSL A (in psid) on the steam dryer at 50.1 Hz. No loading is applied to the submerged surface and lifting rods.

NODES
PRES-NORM

ANSYS

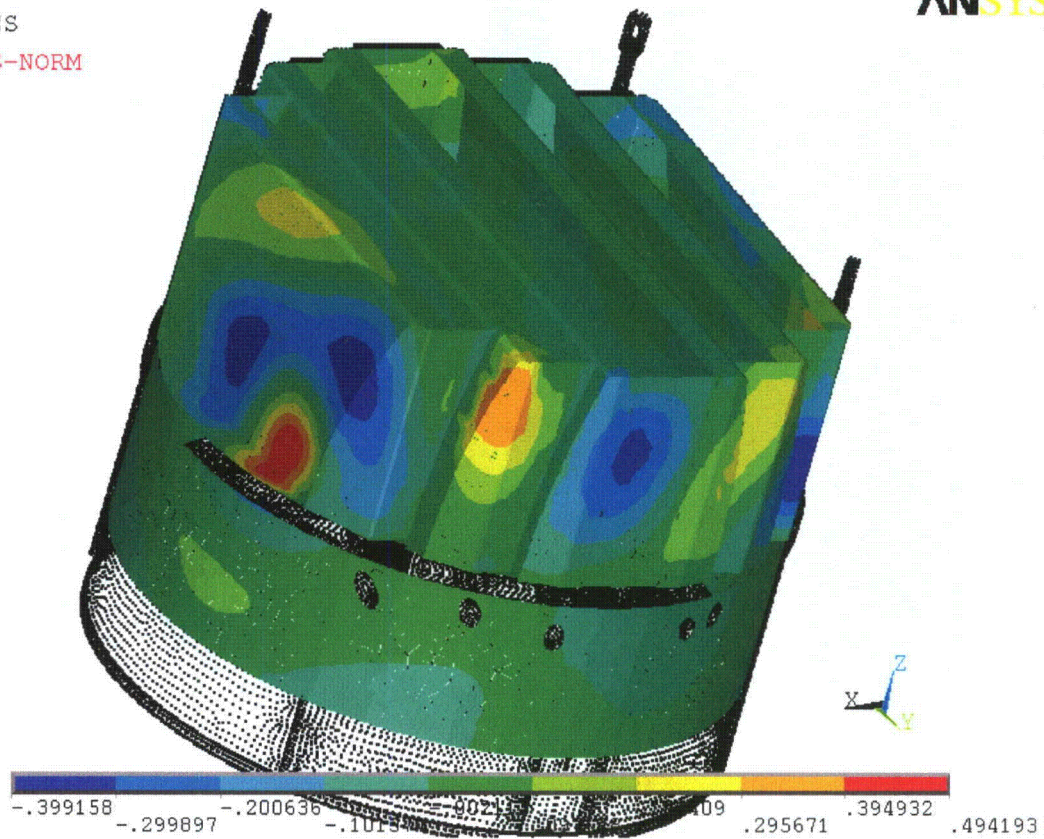


Figure 12b. Real part of unit pressure loading MSL A (in psid) on the steam dryer at 200.45 Hz. No loading is applied to the submerged surface and lifting rods.

4. Structural Analysis

The solution is decomposed into static and harmonic parts, where the static solution produces the stress field induced by the supported structure subjected to its own weight and the harmonic solution accounts for the harmonic stress field due to the unit pressure of given frequency in one of the main steam lines. All solutions are linearly combined, with amplitudes provided by signal measurements in each steam line, to obtain the final displacement and stress time histories. This decomposition facilitates the prescription of the added mass model accounting for hydrodynamic interaction and allows one to compare the stress contributions arising from static and harmonic loads separately. Proper evaluation of the maximum membrane and membrane+bending stresses requires that the static loads due to weight be accounted for. Hence both static and harmonic analyses are carried out.

4.1 Static Analysis

The results of the static analysis are shown in Figure 13. The locations with highest stress include the inner vane bank connection to inner base plate near support brackets with stress intensity 9,598 psi. There are four locations with artificial stress singularity, which are excluded from the analysis. The static stresses one node away are used at these locations as more realistic estimate of local stress. These locations are at the connections of the inner end plate to the inner base plate at the ends of the cut-out, as shown in Figure 13c.

4.2 Harmonic Analysis

The harmonic pressure loads were applied to the structural model at all surface nodes described in Section 3.10. Typical stress intensity distributions over the structure are shown in Figure 14. Stresses were calculated for each frequency, and results from static and harmonic calculations were combined.

To evaluate maximum stresses, the stress harmonics including the static component are transformed into a time history using FFT, and the maximum and alternating stress intensities for the response, evaluated. According to ASME B&PV Code, Section III, Subsection NG-3216.2 the following procedure was established to calculate alternating stresses. For every node, the stress difference tensors, $\sigma'_{nm} = \sigma_n - \sigma_m$, are considered for all possible pairs of the stresses σ_n and σ_m at different time levels, t_n and t_m . Note that all possible pairs require consideration since there are no "obvious" extrema in the stress responses. However, in order to contain computational cost, extensive screening of the pairs takes place (see Section 2.3) so that pairs known to produce alternating stress intensities less than 250 psi are rejected. For each remaining stress difference tensor, the principal stresses S_1, S_2, S_3 are computed and the maximum absolute value among principal stress differences, $S_{nm} = \max\{|S_1 - S_2|, |S_1 - S_3|, |S_2 - S_3|\}$, obtained. The alternating stress at the node is then one-half the maximum value of S_{nm} taken over all combinations (n,m), i.e., $S_{alt} = \frac{1}{2} \max_{n,m} \{S_{nm}\}$. This alternating stress is compared against allowable values, depending on the node location with respect to welds.

ANSYS

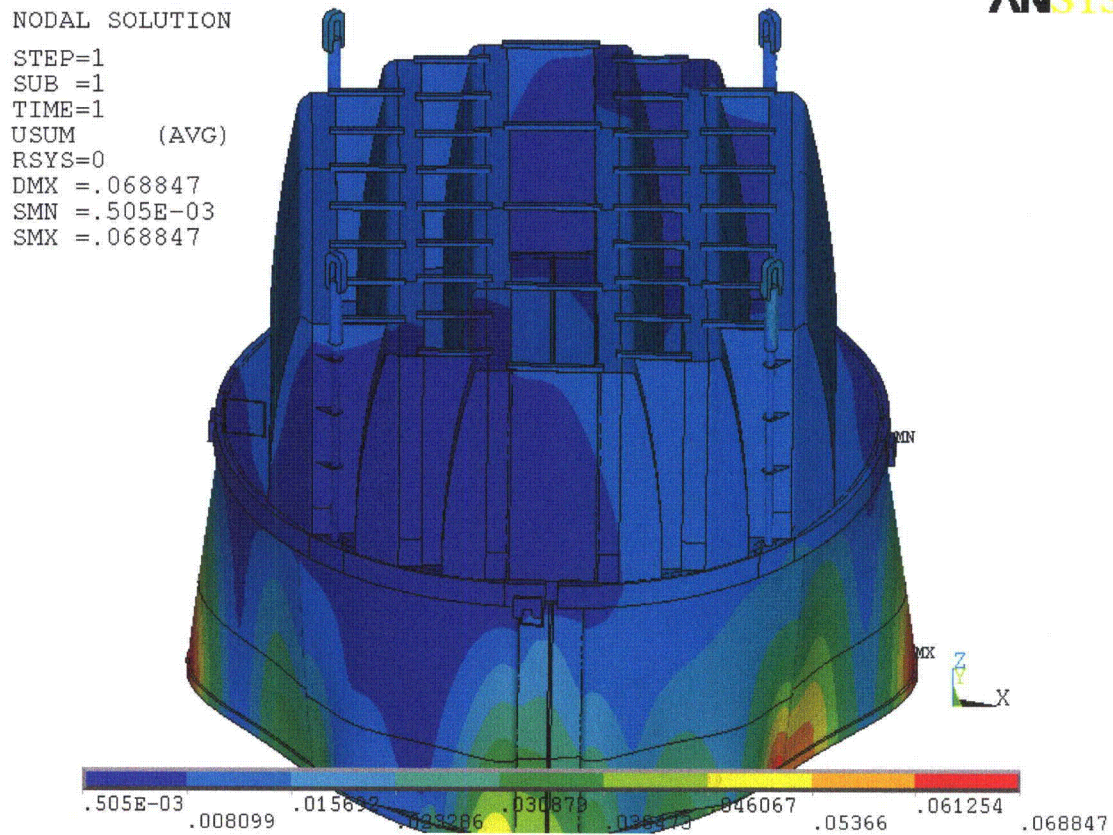


Figure 13a. Overview of static calculations showing displacements (in inches). Maximum displacement (DMX) is 0.069". Note that displacements are amplified for visualization.

ANSYS

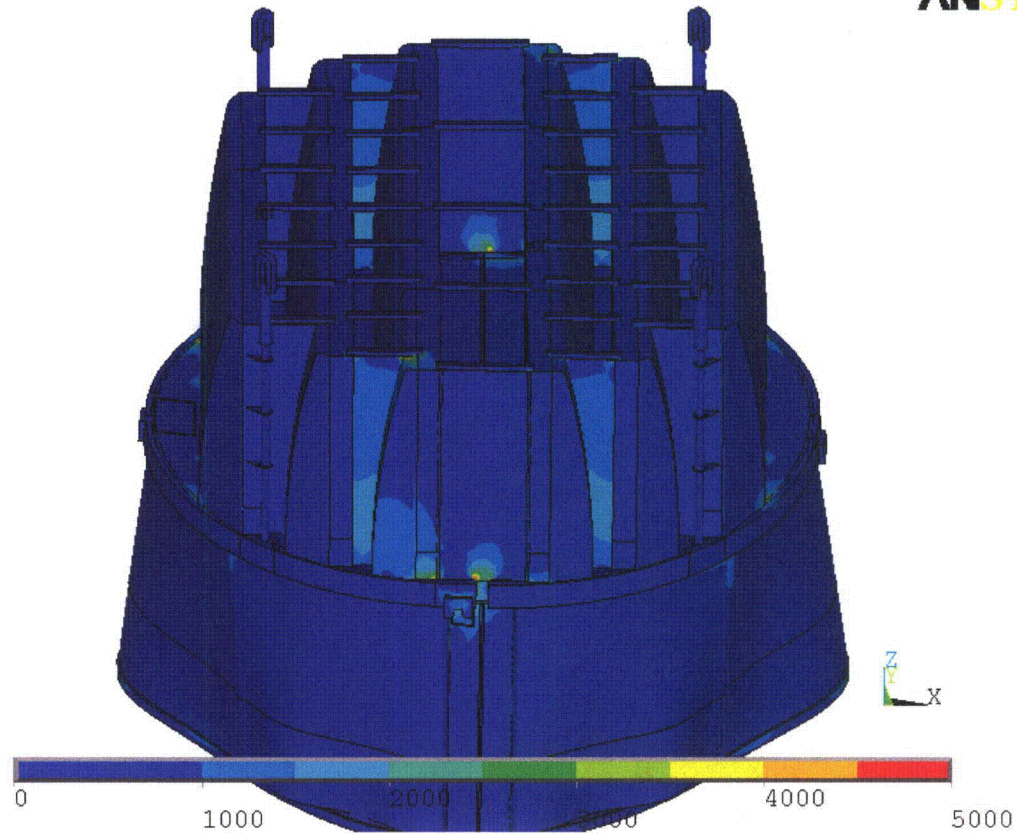


Figure 13b. Overview of static calculations showing stress intensities (in psi). Maximum stress intensity (SMX) is 9,598 psi. Note that displacements are amplified for visualization

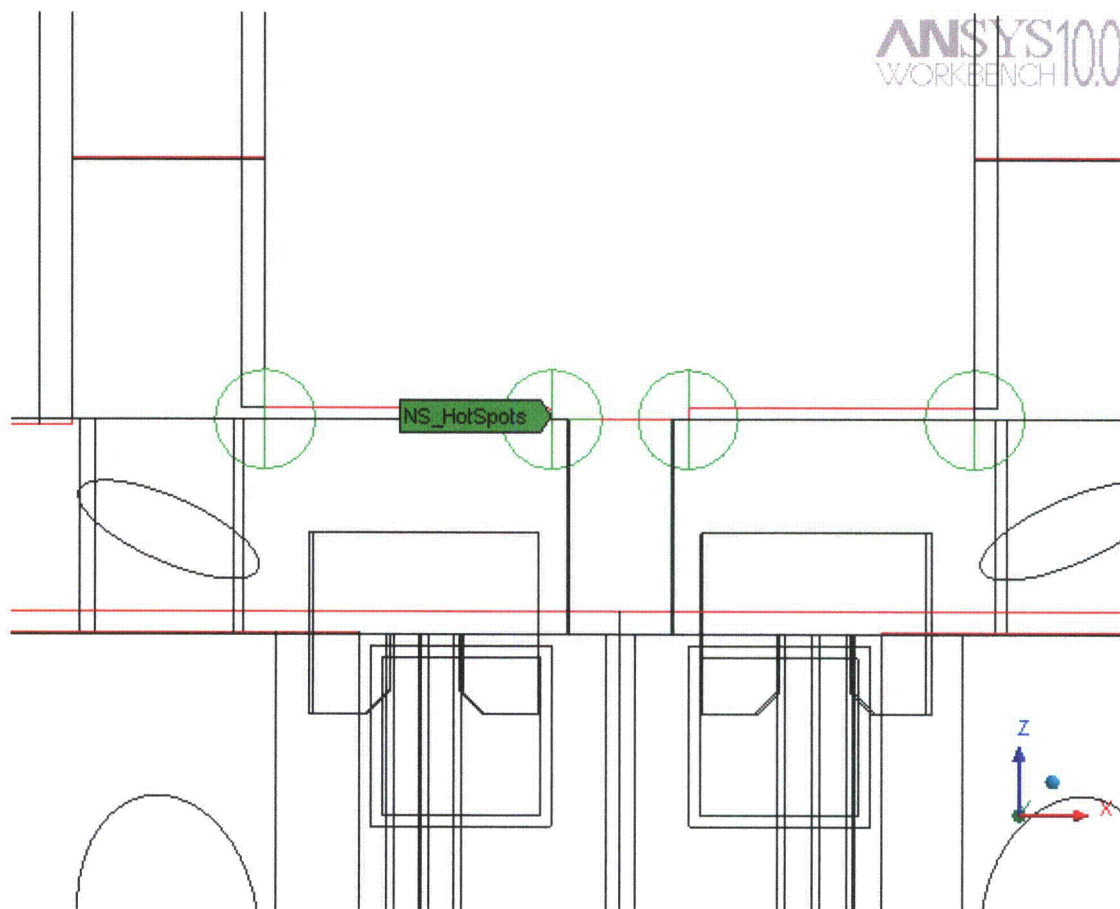


Figure 13c. Stress singularities. Model is shown in wireframe mode for clarity.

ANSYS

NODAL SOLUTION

STEP=1185

SUB =1

FREQ=50.418

REAL ONLY

SINT (AVG)

DMX =.195193

SMN =.081579

SMX =11642

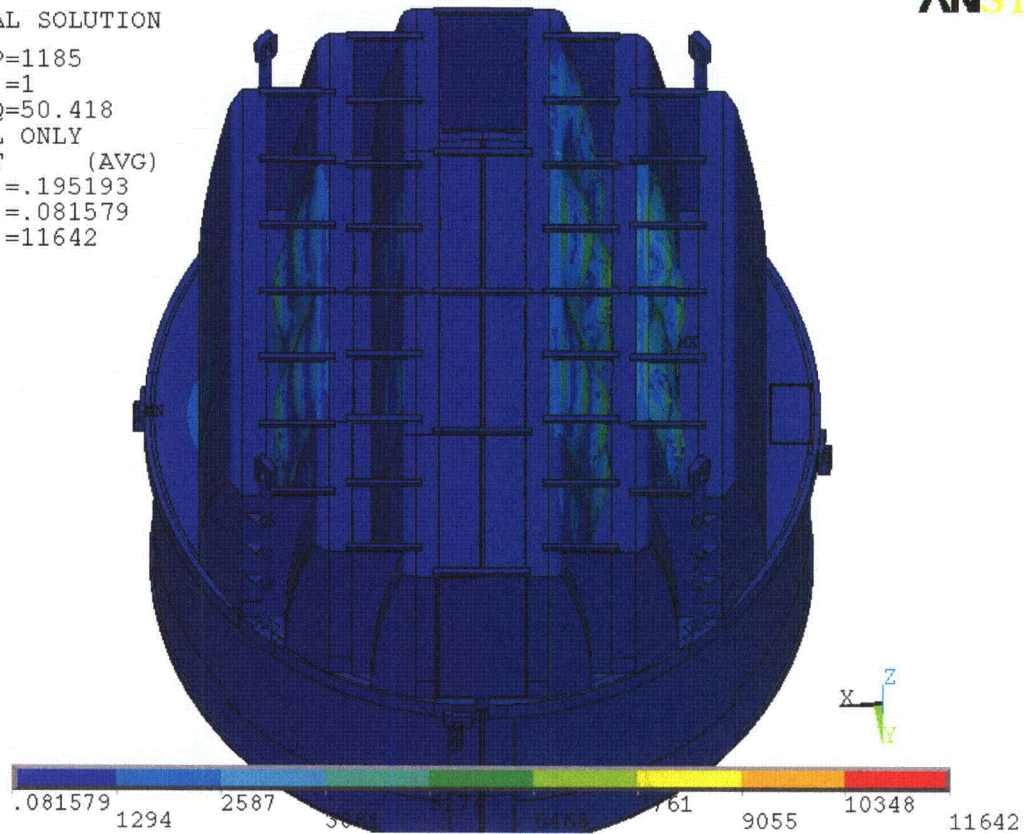


Figure 14a. Overview of harmonic calculations showing real part of stress intensities (in psi) along with displacements. Unit loading MSL A at 50.1 Hz (oriented to show high stress locations at the hoods).

ANSYS

NODAL SOLUTION
STEP=305
SUB =1
FREQ=200.446
REAL ONLY
SINT (AVG)
DMX =.021716
SMN =.177944
SMX =5801

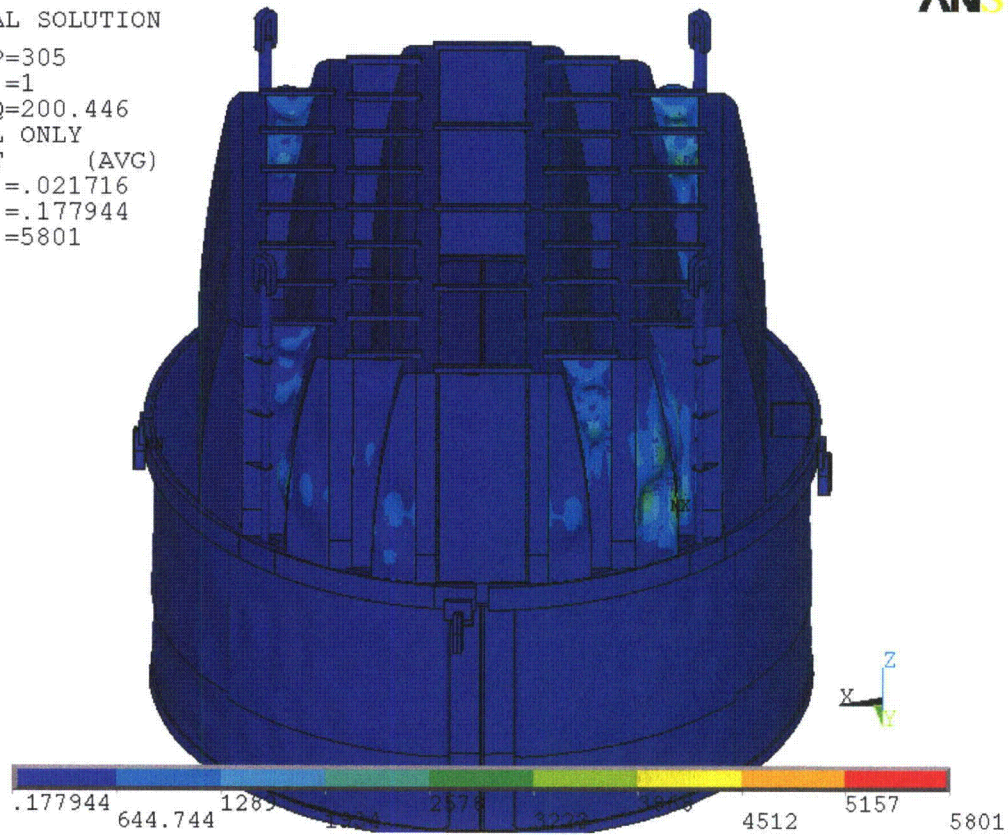


Figure 14b. Overview of harmonic calculations showing real part of stress intensities (in psi) along with displacements. Unit loading MSL A at 200.5 Hz.

4.3 Post-Processing

The static and transient stresses computed at every node with ANSYS were exported into files for subsequent post-processing. These files were then read into separate customized software to compute the maximum and alternating stresses at every node. The maximum stress was defined for each node as the largest stress intensity occurring during the time history. Alternating stresses were calculated according to the ASME standard described above. For shell elements the maximum stresses were calculated separately at the mid-plane, where only membrane stress is present, and at top/bottom of the shell, where bending stresses are also present.

For nodes that are shared between several structural components or lie on junctions, the maximum and alternating stress intensities are calculated as follows. First, the nodal stress tensor is computed separately for each individual component by averaging over all finite elements meeting at the node and belonging to the same structural component. The time histories of these stress tensors are then processed to deduce the maximum and alternating stress intensities for each structural component. Finally for nodes shared across multiple components the highest of the component-wise maximum and alternating stresses is recorded as the "nodal" stress. This approach prevents averaging of stresses across components and thus yields conservative estimates for nodal stresses at the weld locations where several components are joined together.

The maximum stresses are compared against allowable values which depend upon the stress type (membrane, membrane+bending, alternating – P_m , P_m+P_b , S_{alt}) and location (at a weld or away from welds). These allowables are specified in the following section. For solid elements the most conservative allowable for membrane stress, P_m , is used, although bending stresses are nearly always present also. The structure is then assessed in terms of stress ratios formed by dividing allowables by the computed stresses at every node. Stress ratios less than unity imply that the associated maximum and/or alternating stress intensities exceed the allowable levels. Post-processing tools calculate the stress ratios, identifying the nodes with low stress ratios and generating files formatted for input to the 3D graphics program, TecPlot, which provides more general and sophisticated plotting options than currently available in ANSYS.

4.4 Computation of Stress Ratios for Structural Assessment

The ASME B&PV Code, Section III, subsection NG provides different allowable stresses for different load combinations and plant conditions. The stress levels of interest in this analysis are for the normal operating condition, which is the Level A service condition. The load combination for this condition is:

$$\text{Normal Operating Load Combination} = \text{Weight} + \text{Pressure} + \text{Thermal}$$

The weight and fluctuating pressure contributions have been calculated in this analysis and are included in the stress results. The static pressure differences and thermal expansion stresses are small, since the entire steam dryer is suspended inside the reactor vessel and all surfaces are exposed to the same conditions. Seismic loads only occur in Level B and C cases, and are not considered in this analysis.

Allowable Stress Intensities

The ASME B&PV Code, Section III, subsection NG shows the following (Table 6) for the maximum allowable stress intensity (S_m) and alternating stress intensity (S_a) for the Level A service condition. The allowable stress intensity values for type 304 stainless steel at operating temperature 550°F are taken from Table I-1.2 and Fig. I-9.2.2 of Appendix I of Section III, in the ASME B&PV Code. The calculation for different stress categories is performed in accordance with Fig. NG-3221-1 of Division I, Section III, subsection NG. The allowable value for alternating stress is taken from curve C of Fig. I-9.2.2 in Appendix I in Section III of the ASME B&PV Code.

Table 6. Maximum Allowable Stress Intensity and Alternating Stress Intensity for all areas other than welds. The notation P_m represents membrane stress; P_b represents stress due to bending; Q represents secondary stresses (from thermal effects and gross structural discontinuities, for example); and F represents additional stress increments (due to local structural discontinuities, for example).

Type	Notation	Service Limit	Allowable Value (ksi)
<i>Maximum Stress Allowables:</i>			
General Membrane	P_m	S_m	16.9
Membrane + Bending	$P_m + P_b$	$1.5 S_m$	25.35
Primary + Secondary	$P_m + P_b + Q$	$3.0 S_m$	50.7
<i>Alternating Stress Allowable:</i>			
Peak = Primary + Secondary + F	S_{alt}	S_a	13.6

When evaluating welds, either the calculated or allowable stress was adjusted, to account for stress concentration factor and weld quality. Specifically:

- For maximum allowable stress intensity, the allowable value is decreased by multiplying its value in Table 6 by 0.55.
- For alternating stress intensity, the calculated weld stress intensity is multiplied by a weld stress intensity (fatigue) factor of 1.8 for a fillet weld and 1.4 for a full penetration weld, before comparison to the S_a value given above.

The weld factors of 0.55 and 1.4 (full penetration weld) or 1.8 (fillet weld) were selected based on the observable quality of the shop welds and liquid penetrant NDE testing of all welds (excluding tack and intermittent welds, which were subject to 5X visual inspection) during fabrication. These factors are consistent with fatigue strength reduction factors recommended by the Welding Research Council, [23], and stress concentration factors at welds, provided in [24] and [25]. In addition, critical welds are subject to periodical visual inspections in accordance with the requirements of GE SIL 644 SIL and BWR VIP-139 [26]. Therefore, for weld stress intensities, the allowable values are shown in Table 7. These factors (0.55 and 1.4 or 1.8) also conservatively presume that the structure is joined using fillet welds unless specified otherwise. Since fillet welds correspond to larger stress concentration factors than other types of welds, this assumption is a conservative one.

Table 7. Weld Stress Intensities.

Type	Notation	Service Limit	Allowable Value (ksi)
<i>Maximum Stress Allowables:</i>			
General Membrane	Pm	0.55 Sm	9.30
Membrane + Bending	Pm + Pb	0.825 Sm	13.94
Primary + Secondary	Pm + Pb + Q	1.65 Sm	27.89
<i>Alternating Stress Allowables:</i>			
Peak = Primary + Secondary + F	S _{alt}	Sa	13.6

Comparison of Calculated and Allowable Stress Intensities

The classification of stresses into general membrane or membrane + bending types was made according to the exact location, where the stress intensity was calculated; namely, general membrane, Pm, for middle surface of shell element, and membrane + bending, Pm + Pb, for other locations. For solid elements the most conservative, general membrane, Pm, allowable is used.

The structural assessment is carried out by computing stress ratios between the computed maximum and alternating stress intensities, and the allowable levels. Locations where any of the stresses exceed allowable levels will have stress ratios less than unity. Since computation of stress ratios and related quantities within ANSYS is time-consuming and awkward, a separate FORTRAN code was developed to compute the necessary maximum and alternating stress intensities, Pm, Pm+Pb, and S_{alt}, and then compare it to allowables. Specifically, the following quantities were computed at every node:

1. The maximum membrane stress intensity, Pm (evaluated at the mid-thickness location for shells),
2. The maximum membrane+bending stress intensity, Pm+Pb, (taken as the largest of the maximum stress intensity values at the bottom, top, and mid thickness locations, for shells),
3. The alternating stress, S_{alt}, (the maximum value over the three thickness locations is taken).
4. The stress ratio due to a maximum stress intensity assuming the node lies at a non-weld location (note that this is the minimum ratio obtained considering both membrane stresses and membrane+bending stresses):

$$SR-P(nw) = \min \{ S_m/P_m, 1.5 * S_m/(P_m+P_b) \}.$$
5. The alternating stress ratio assuming the node lies at a non-weld location,

$$SR-a(nw) = S_a / (1.1 * S_{alt}),$$
6. The same as 4, but assuming the node lies on a weld,

$$SR-P(w) = SR-P(nw) * 0.55$$
7. The same as 5, but assuming the node lies on a weld,

$$SR-a(w) = SR-a(nw) / f_{sw}.$$

Note that in steps 4 and 6, the minimum of the stress ratios based on P_m and $P_m + P_b$, is taken. The allowables listed in Table 7, $S_m = 16,900$ psi and $S_a = 13,600$ psi. The factors, 0.55 and f_{sw} , are the weld factors discussed above with $f_{sw} = 1.8$ being appropriate for a fillet weld and $f_{sw} = 1.4$ for a full penetration weld. The factor of 1.1 accounts for the differences in Young's moduli for the steel used in the steam dryer and the values assumed in alternating stress allowable. According to NG-3222.4 in subsection NG of Section III of the ASME Code [1], the effect of elastic modulus upon alternating stresses is taken into account by multiplying alternating stress S_{alt} at all locations by the ratio, $E/E_{model} = 1.1$, where:

$$E = 28.3 \cdot 10^6 \text{ psi, as shown on Fig. I-9.2.2. ASME BP\&V Code}$$

$$E_{model} = 25.55 \cdot 10^6 \text{ psi (Table 2)}$$

The appropriate maximum and alternating stress ratios, $SR-P$ and $SR-a$, are thus determined and a final listing of nodes having the smallest stress ratios is generated. The nodes with stress ratios lower than 4 are plotted in TecPlot (a 3D graphics plotting program widely used in engineering communities [27]). These nodes are tabulated and depicted in the following Results Section.

4.5 [(3)]

[[

(3)]

[[

(3)]]

Table 8. [[

(3)]]

5. Proposed Modifications to Meet EPU Stress Margins

The dryer analyzed in Section 5 [13] identified several locations with alternating stress ratios below the EPU target of 2.0 when subjected to the ACM Rev. 4.1 acoustic loads. To achieve the desired EPU stress margins several modification were proposed and analyzed in Section 6 of the same report. These evaluations were carried out using [(3)].

The present section provides definitive specifications of the required modifications and carries out stress assessments of these modifications.

The locations whose alternating stress ratios at EPU fall below 2.0 are organized into four distinct groups as follows:

- Group 1: The lifting rod bracket/side plate welds. The upper and middle brackets already have weld reinforcement, but this does not reduce stresses sufficiently under the new loads.
- Group 2: The middle hood reinforcement strip incurs a high stress due to vibration of the outboard section of the middle hood.
- Group 3: The inner hood/hood support welds that experience high stresses due to the inner hood vibrations.
- Group 4: The remaining points which are readily modified to achieve $SR-a > 2.76$.

Below, these groups are discussed in further detail.

5.1 Lifting Rod Support Brackets (Group 1)

Without any modification other than an increase in the existing weld size from $\frac{1}{4}$ " to $\frac{1}{2}$ " which, [(3)] the limiting alternating stress locations occur on the lifting rod support brackets (see Figure 15) with an alternating stress ratio below 2.76 at CLTP. The stresses are highly localized (only one node on each such bracket is affected) which is indicative of development of stress singularities at this re-entrant corner. If the lower-most brackets are modified using the same weld reinforcement planned for the middle and upper brackets then their limiting alternating stress ratio increases to 3.56. However, the middle and upper brackets are still below target stress ratios and further weld reinforcement appears unlikely by itself to achieve the necessary stress reductions. Instead a more substantial structural reinforcement is required.

The localized nature of the stress concentration calls for a corresponding localized reinforcement. Several such concepts were proposed in [13]. There it was shown that increasing the local thickness – specifically that of all elements with at least one node on the vertical plate/brace weld line – from 0.375" to 0.75" satisfactorily reduced the stress and did not significantly impact the modal properties or stresses elsewhere on the steam dryer. Of the various concepts considered, Concept 2 was recommended as it provided substantial stress reduction while requiring less severing, grinding and re-welding than some of the other concepts.

This configuration shown in Figure 16 consists of a 2" radius, 0.375" thick circular disk welded to the vertical plate and a small reinforcement plate, shaped to match the re-entrant corner contour as shown, is welded onto the support bracket to increase the effective thickness and thereby reduce the membrane stress. By examining the maximum stress in the unit solution stresses over the 128–145 Hz frequency range (which brackets the dominant frequencies for this location in the global solution) it was shown that this reinforcement reduces the maximum stress by a factor of 0.18 (Table 11 of [13]).

The design finalized here builds upon the semi-circular disc concept 2 but is modified to eliminate any cutting of existing welds. It consists of a 2.5" wide by 3" high 3/8" thick rectangular plate with a 1.5" long and 1" wide slot cut out as indicated in Figure 17. The dimensions are selected so that the plate can slide over the existing 0.25" brace attachment weld (W1). Note that the total width of the existing 0.25" double sided fillet weld is 2×0.25 " (two fillets) plus 0.375" (brace plate thickness) or 0.875". The larger 1" slot accommodates possible irregularities in the actual weld. The length of the slot is sized so that the plate can slide up to the existing weld (again accounting for possible irregularities in the wrap around portion of the existing weld) and leave sufficient room for a 0.375 fillet weld (W2) around its perimeter. The plate and slot has 1/4" rounded fillets. The installation process begins by sliding this plate over the brace and attaching it to the vertical plate by a 3/8" fillet weld as indicated in Figure 17. Next a 1/2" weld (W4) is created as shown in Figure 18 to attach the 3/8" brace reinforcement plates. These welds are continued to the right along the entire length of the vertical plate/brace joint wrapping around the end. This allows continued use of the $SRF=0.64$ for this reinforced weld line. The attachment is completed by adding a 1/4" weld W5 to attach the brace reinforcement plates to the brace. A top view of the brace reinforcement plate is shown in Figure 19. The plate is 5" long by 1.25" wide and trimmed at a 47.5 deg. angle as indicated so that the edge is parallel to the existing weld joining the two plates comprising the lifting rod brace.

This reinforcement is used for the middle and top lifting rod braces. For the lowest braces adequate stress margin is achieved by increasing the existing weld size to 1/2" allowing application of [[

(3)] to this weld as shown in [28].

Prior to final design and installation it is required that available photographs of the as-built lifting rod brace installations be reviewed to ensure that there is adequate clearance relative to existing welds and to ensure proper fitting of the new components. For example, reference to the photograph in Figure 20 suggests that proper fitting of the vertical plate will entail milling out a step on the face adjacent to the vertical plate to accommodate the closure plate and its attachment weld.

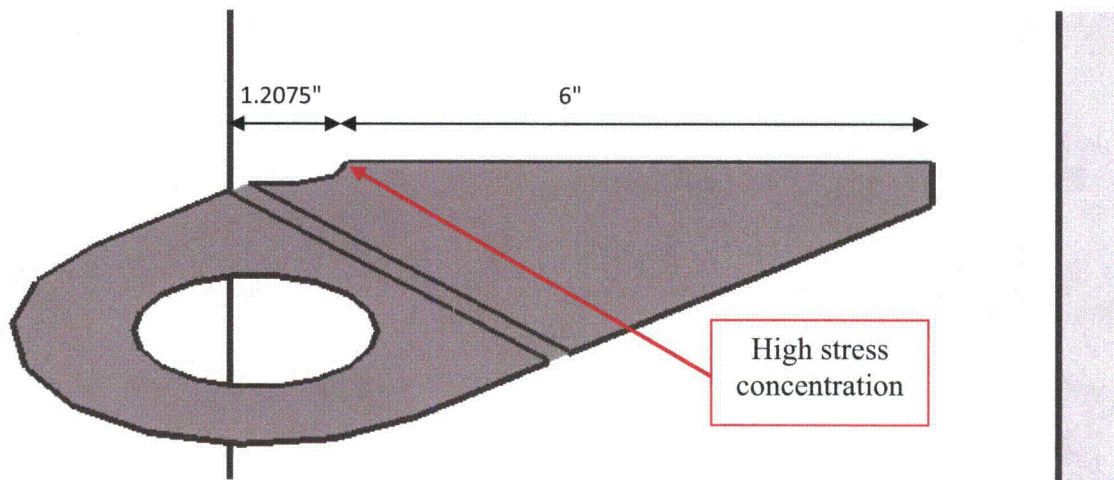


Figure 15. Basic geometry of lifting rod brace. The lifting rod slides through the circular hole and the brace is attached to the vane bank vertical plate.

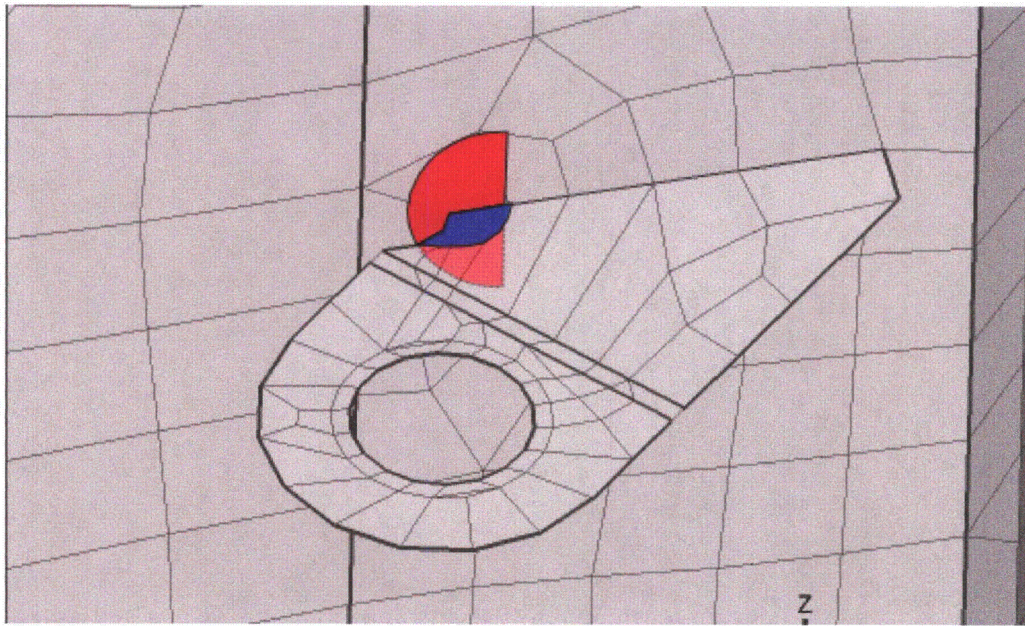


Figure 16. Reinforcement concept 2: Partial reinforcement – semi-circular plate one side plate (red) and reinforcement of re-entrant corner on support bracket (blue)

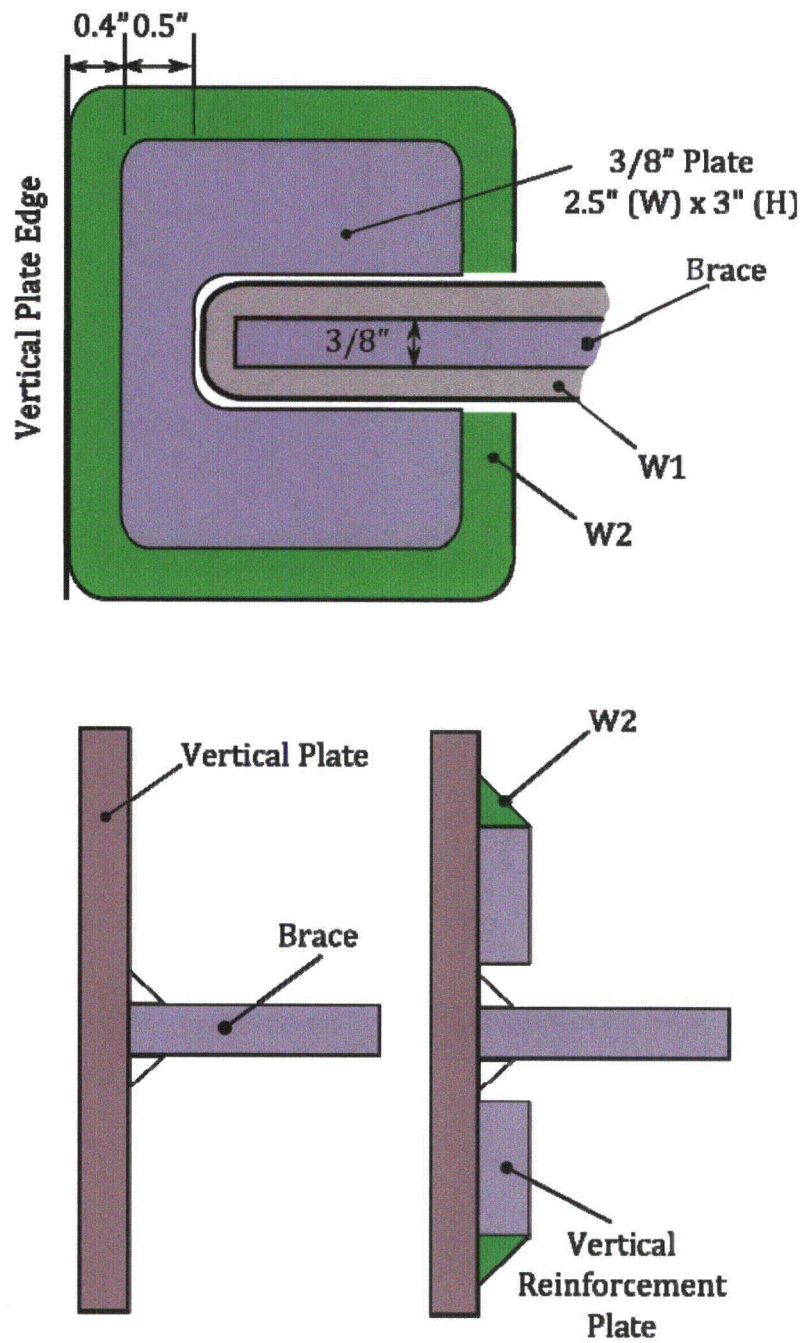


Figure 17. Schematic of reinforcement. W1 is the existing 0.25" weld; W2 is the new 0.375" weld for attaching the vertical reinforcement plate.

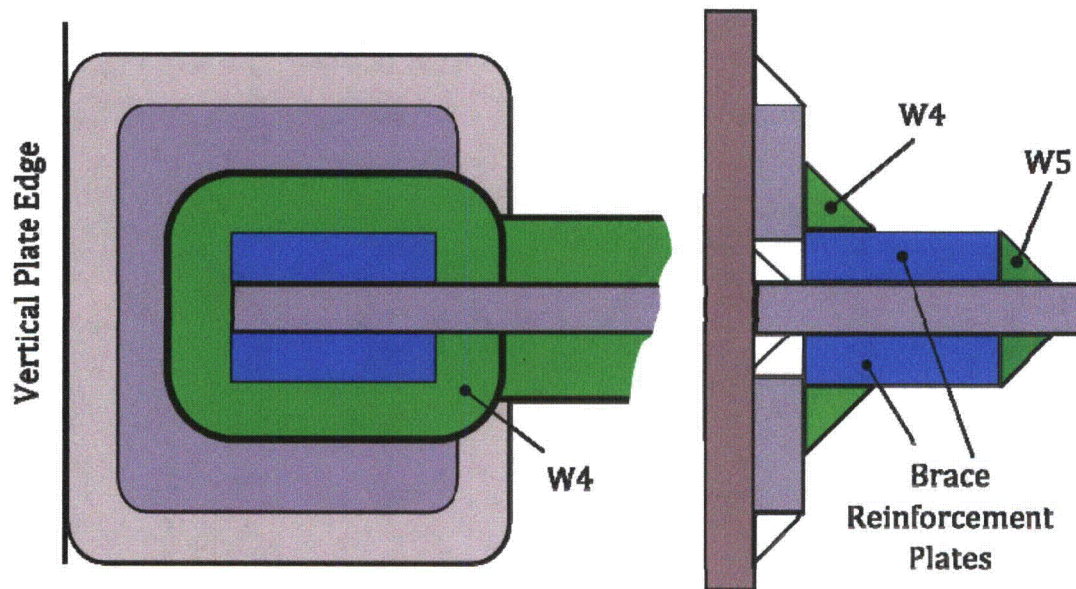


Figure 18. Additional welds. The 0.5" fillet weld, W4, attaches the 3/8" brace reinforcement plates to the vertical reinforcement plate. The weld continues on over the existing brace attachment weld. W5 attaches the brace reinforcement plates to the existing brace.

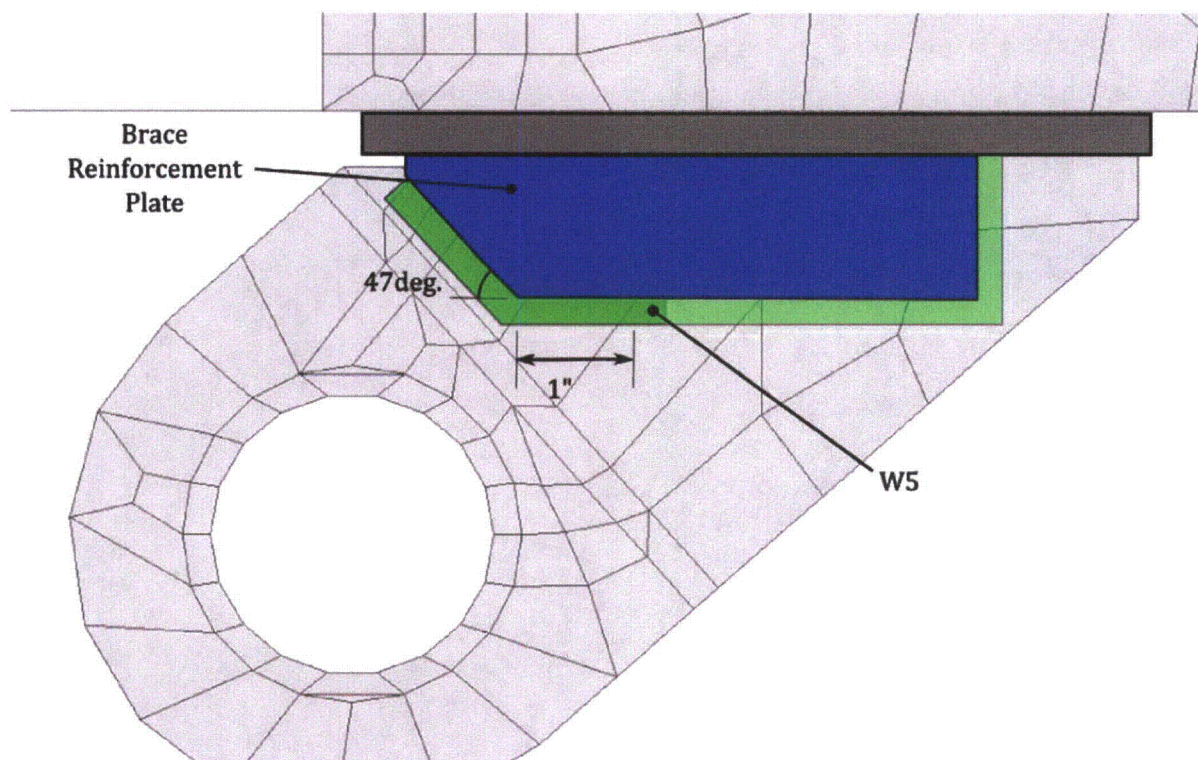


Figure 19. Depiction of brace reinforcement plate.

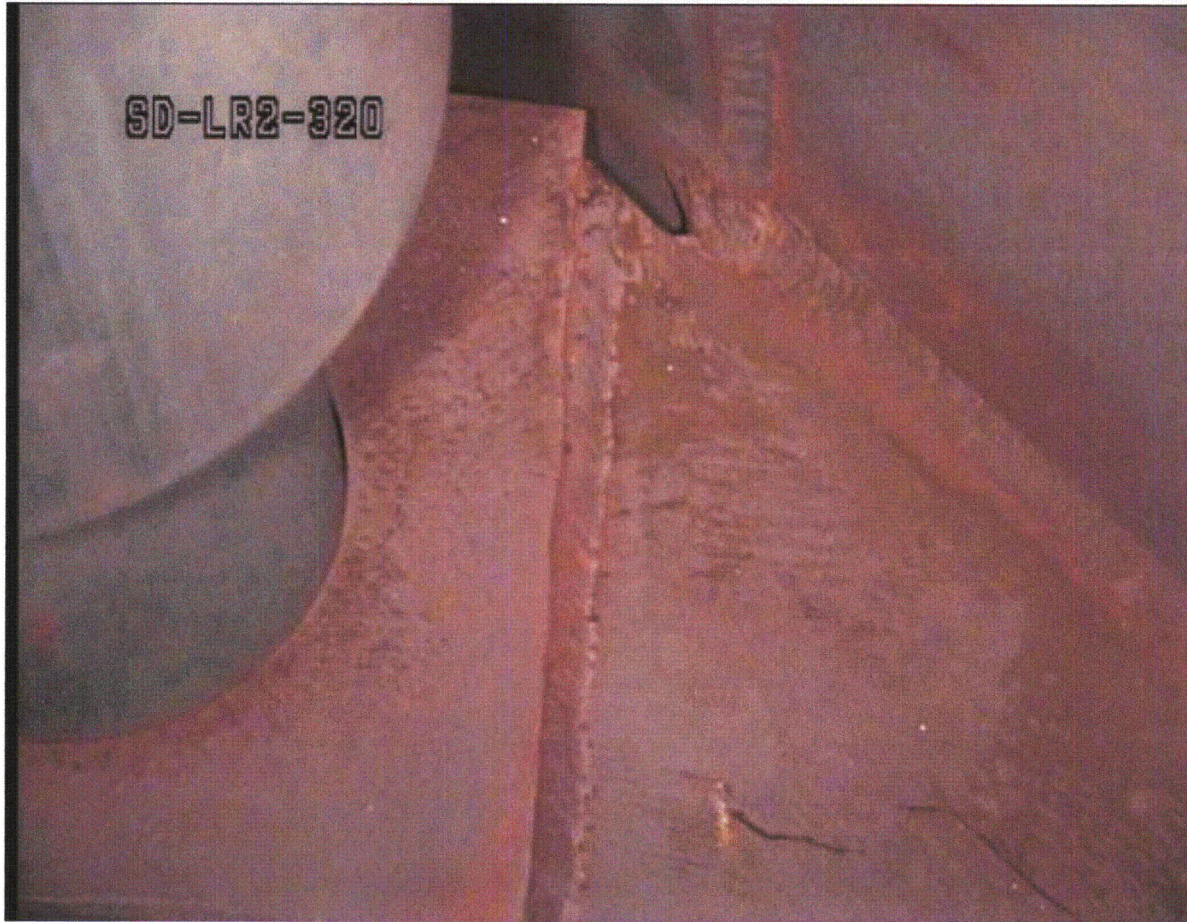


Figure 20. As built lifting rod brace.

5.2 Middle Hood/Reinforcement Strip (Group 2)

Application of the Rev. 4.1 acoustic loads induces a strong response on the section of the middle hood lying between the closure plate and the vertical reinforcement strip (see Figure 21), and generates stresses along this strip that exceed target levels. This strip was previously added to address indications on the outboard section of the middle hood. The high stresses occur on the 1/8" middle hood rather than within the much thicker strip (additional 3/8") and are dominated by a 109.0 Hz signal which, at the +10% shift, excites a structural response at 119.9 Hz.

In Section 6 of [13] it was reasoned that a local modification was unlikely to rectify the high stress, but merely shift its location slightly. Therefore, to reduce the stress it was proposed to suppress the active oscillation by covering this section of the middle hood with a 3/8" curved plate welded about its perimeter to the hood and closure plate. Manufacture of the plate is straightforward and creating the attachment weld does not pose accessibility challenges. However, since each such plate would weigh approximately 90 lbs and stress evaluations showed that all previously limiting locations on the hood acquired very high alternating stress ratios ($SR_a > 20$) after the modification it was surmised that adequate stress reduction could easily be achieved using thinner reinforcement plates.

Therefore the steam dryer stress evaluation is repeated by replacing the previous 3/8" curved reinforcement plate by one that is 1/8" thick thus increasing the effective thickness of the hood section to 1/4". Unit solution stresses of the complete steam dryer with this modified middle hood section (and also the other planned reinforcements – reinforced closure plate and added masses on the inner and middle hoods as discussed below) are developed in the 30-250 Hz frequency range. This range: (i) encompasses the frequency where stresses are highest and (ii) ensures that any higher order modes occurring at higher frequencies are fully accounted for. Recalculation of the stresses at the Group 2 locations results in stresses that are below 1300 psi which maintains ample margin for EPU operation.

It is recommended that the panels be trimmed to size such that the plate edges reach to within 1/8" of the existing welds on the closure plate and the reinforcement strip. A 3/16" inch fillet weld is then applied around the perimeter of the reinforcement plate.

Table 9. Group 2 CLTP stresses after adding 1/8th reinforcement plate over the middle hood section lying between the existing reinforcement strip and closure plate.

Location	node	Pm	Pm+Pb	Sa	SR-P	SR-a	% Freq. Shift	Dom. Freq. [Hz]
2. Hood Reinforcement/Middle Hood	98275	200	497	362	28.07	18.96	0	135.4
8. Hood Reinforcement/Middle Hood	90126	981	1462	381	9.47	18.05	5	51.2
9. Hood Reinforcement/Middle Hood	98268	352	597	377	23.34	18.24	2.5	135.4
10. Hood Reinforcement/Middle Hood	90949	993	1112	321	9.36	21.36	-5	140.9

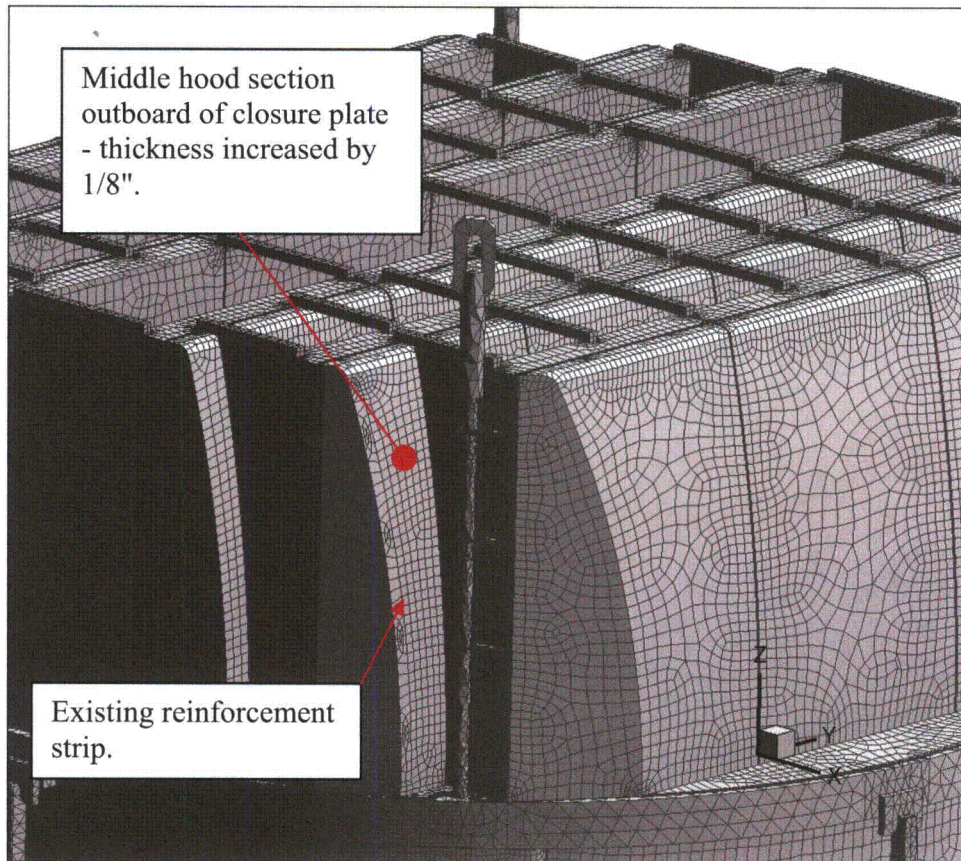


Figure 21. Middle hood section subject to modification and existing reinforcement strip.

5.3 Inner Hoods/Hood Support (Group 3)

In its present configuration the inner hoods and to a lesser extent also the middle hoods, show a strong stress response on the hood/hood support welds in the 45-60 Hz range. The stresses result from strong vibrations of the central sections of the inner and middle hoods and do not meet the required margin for EPU operation. Since the acoustic loads on these hoods are relatively low, these vibrations are caused by transmission of loads from other steam dryer components such as the directly forced outer hoods. Since the welds, particularly at higher elevations, are difficult to access and reinforce it is necessary to pursue alternate modifications. One option is to stiffen the hood panels and suppress vibrations by adding reinforcement strips at the modal displacement response peaks. This would generally result in similar response modes occurring at upward-shifted natural frequencies. However, examination of the MSL signals indicates that these signals increase with frequency so that an upward shift in the hood frequencies would place these frequencies into a range with stronger MSL signals.

Therefore the option proposed here is to add small 15 lb masses on the inner hoods. Specifically one such mass is added to each of four central inner hood sections as indicated in Figure 22. Each mass is located 18" below the top of the vane bank surface since this is approximately the reach length of a submerged diver welding the masses to the inner hoods. The addition of the masses lowers the natural response frequencies and reduces the modal amplitudes (since the generalized masses of the participating modes are reduced). These masses were added into the global model and unit solutions regenerated over the 30-250 Hz frequency range (in conjunction with the other modifications to the dryer including the thickened closure plates, middle hood masses and middle hood reinforcement described for Group 2). As shown in Section 6.2, with these masses in place all locations meet the required margins.

Using a density of 0.284 lb/in³ for stainless steel it follows that the volume of the 15 lb mass is 52.8 in³. It is here proposed to use a rounded 8"x8" 1" thick rectangular mass with two interior slits – a lower 6" slit and an upper 3" slit - added for additional weld support (see Figure 23). The mass is attached with a ¼" weld around the top and side edges (the bottom edge is considered inaccessible to diver reach) and the same sized weld around the interior perimeters of the two slits. The bottom face of the mass facing the hood is milled to accommodate the hood curvature (radius of curvature is 353") at 18" below the top of the vane bank. The upper 3" and lower 6" slots are added to allow for additional attachment welds which are placed along the interior slot perimeters. The slots are angled as shown to facilitate access with welding rods. Note that the outer perimeter welds should be sufficient to secure the masses under vibration, the interior slot welds being added for additional conservatism.

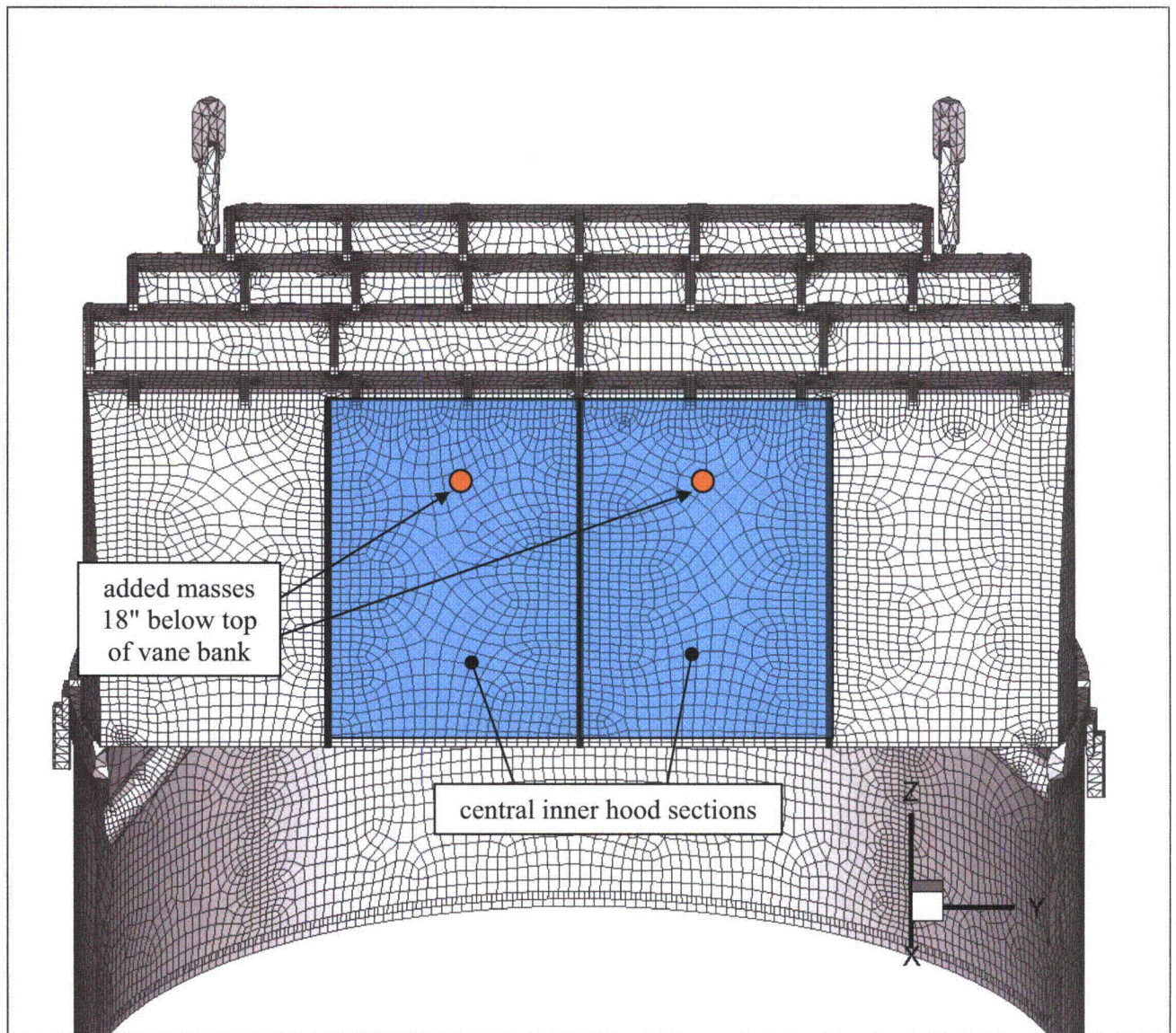


Figure 22. The inner hood sections (blue) whose response contributes to the high stresses on the central hood support/inner hood weld. Middle and outer hoods excluded from view to expose inner hood surfaces. Proposed masses are added 18" below the top of the vane bank.

[[

(3)]]

5.4 Group 4 Locations

Under a previous load definition three families of locations were identified as having alternating stress ratios between 2.65 and 2.76 before modifications [13]. Because these locations were close to, but did not meet the required margin it was natural to collect these locations into a single fourth group. To meet EPU margin, modifications were developed for the group 4 members and assessed on the basis of the older loads. The modifications identified for these locations are described below. Assessment of the modifications for the hood/hood support/base plate junction and of the bottom of the drain channel/skirt weld is [[

(3)]] In Section 6, the NMP2 steam is evaluated with these modifications in place and using the up-to-date acoustic load definition. This evaluation confirms that the modifications remain adequate for meeting the EPU stress margin.

The following locations are addressed under group 4.

(a) *Outer hood/hood support/cover plate junctions.* These points lie on the common intersection between the hood, hood support and base plate. To alleviate the stress a stress relief cut-out hole in the hood support is proposed. A detailed evaluation of this modification is developed in Section 3.4 and Appendix A.11 of [5] showing that the stress reduction factor achieved with [[

(3)]] The semi-circular stress relief cut-out hole can be generated using electrical discharge machining (EDM) that can be implemented remotely thus reducing diver dose to at most the period required to attach the device to the hood support. When the circular cut-out is considered the limiting stress ratio (at CLTP) at these locations is 2.83 which is above the target value (2.76 at CLTP).

(b) *Bottoms of the drain channel/skirt welds.* These locations are easily accessible and can be reinforced by adding a wrap-around reinforcement weld to alleviate the stress. Specifically, the existing bottom 4" of weld are increased to a thickness of 0.25" and the weld wraps around the bottom of the drain channel and 1" up on the interior side of the junction. In Section 3.1 of [5] a stress reduction factor of [[

(3)]] Without application of the SRF, the limiting alternating stress ratio at CLTP is $SR-a=3.06$. Therefore, this location now (i.e., with the up-to-date load definition) meets the required stress margin without any modification needed. When the stress reduction factor is invoked the limiting stress ratio for this weld increases to $SR-a=4.84$ and occurs on a point that is 1" above the bottom of the drain channel/skirt junction where the SRF is in fact not applied.

(c) *Middle hood/hood support welds.* High stresses occur on the middle hood/hood support welds due to vibrations of the middle hoods. The stresses at these locations are addressed by adding a total of four 10 lb masses on the central sections of the middle hoods. These function in a manner similar to the masses employed for the inner hoods. However, because a lesser reduction is needed the masses are smaller than those proposed for the inner hoods. The detailed design is the same as for the inner hoods except that the thickness of the rectangular plate is reduced from 1" to 11/16". The middle hood masses are placed at the same 18" depth measured from the top of the vane bank as the inner hood masses. The impact on stress of adding these masses in and also the other reinforcements including the reinforced closure plates, inner hood

masses and reinforced middle hood section outboard of the closure plate is quantified by generating unit solutions with all modifications implemented over the 30-250 Hz frequency range and applying the ACM Rev. 4.1 loads. With these modifications the limiting alternating stress ratio at this location $SR-a=3.71$.

The resulting changes in the stress ratios for the Group 4 locations when implementing all steam dryer modifications are summarized in Table 10.

Table 10. Alternating stress ratios for group 4 locations before and after modifications.

Location	Modification	SR-a	
		Pre-modification	Post-Modification
(a) Hood Support/Outer Base Plate/Middle Backing Bar	Cut-out in hood support (SRF=0.80, Section 3.4 and Appendix A.11 in [5])	2.29	2.83
(b) Submerged Drain Channel/Submerged Skirt	Wrap around weld (SRF=0.56, Section 3.1 in [5])	3.06	4.84
(c) Hood Support/Middle Hood	Added 10 lb mass	2.94 (1)	3.71

Note: (1). Pre-modification value is estimated as follows. In [29] it was shown that the limiting alternating stress ratios on the middle hood/hood support weld were 2.68 before modification (Table 6 in [29]) and 3.38 after modification (Entry 16 in Table 10 of [29]). This implies a stress increase of 26% when removing the middle hood masses. The pre-modification value is thus estimated as $SR-a=3.71/1.26$.

5.5 Modification of Closure Plates

The presently installed closure plates are 1/8 in thick and contain a structural mode near 128 Hz. This mode is a second order mode in the vertical direction and first order in the horizontal direction. In preliminary analyses of the dryer these plates were found to respond strongly to a 135.7 Hz component in the acoustic signal which when shifted by -10% during frequency shifting, couples closely to the closure plate frequency. The response mode induces high stresses along the lateral welds connecting the closure plate to the vane bank (a straight vertical weld) and to the adjacent hood (a mostly vertical weld, but curved to accommodate the hood geometry). The highest stresses generally occur at the top of this weld. However, significant stresses also develop on these weld lines between 10-20 inches below the top of the weld. This corresponds to the weld locations nearest the maximum displacement of this mode. In preliminary stress assessments made for the dryer where noise was filtered from the signal on the basis of low power measurements, several locations on the closure plate welds emerged as having stress ratios that do not meet target levels at EPU. These locations were addressed by performing a [[

(3)]. In some cases, addition of an interior weld or thickening of the existing weld (see Section 2.2) was required to achieve acceptable stress ratios.

With the more recent acoustic loads processed with the ACM Rev. 4.1 (and where low power subtraction is not performed) the closure plate weld reinforcements are insufficient to achieve the

target EPU stress margin. Rather than pursue further weld reinforcement, which is limited in regard to both access (finite arm reach limits the length of weld that can be produced on the interior side of the closure plate) and prospect for improvement (making weld legs significantly larger than the plate thickness does not necessarily improve the stresses), it was decided to reinforce the closure plate itself to simultaneously reduce stresses and separate structural mode and peak acoustic frequencies.

[[

(3)]]

With the closure plate reinforcement and other steam dryer modifications it is determined that the previous closure plate attachment weld reinforcements are no longer needed and the existing welds are sufficient to meet the EPU stress margins. [[

(3)]]

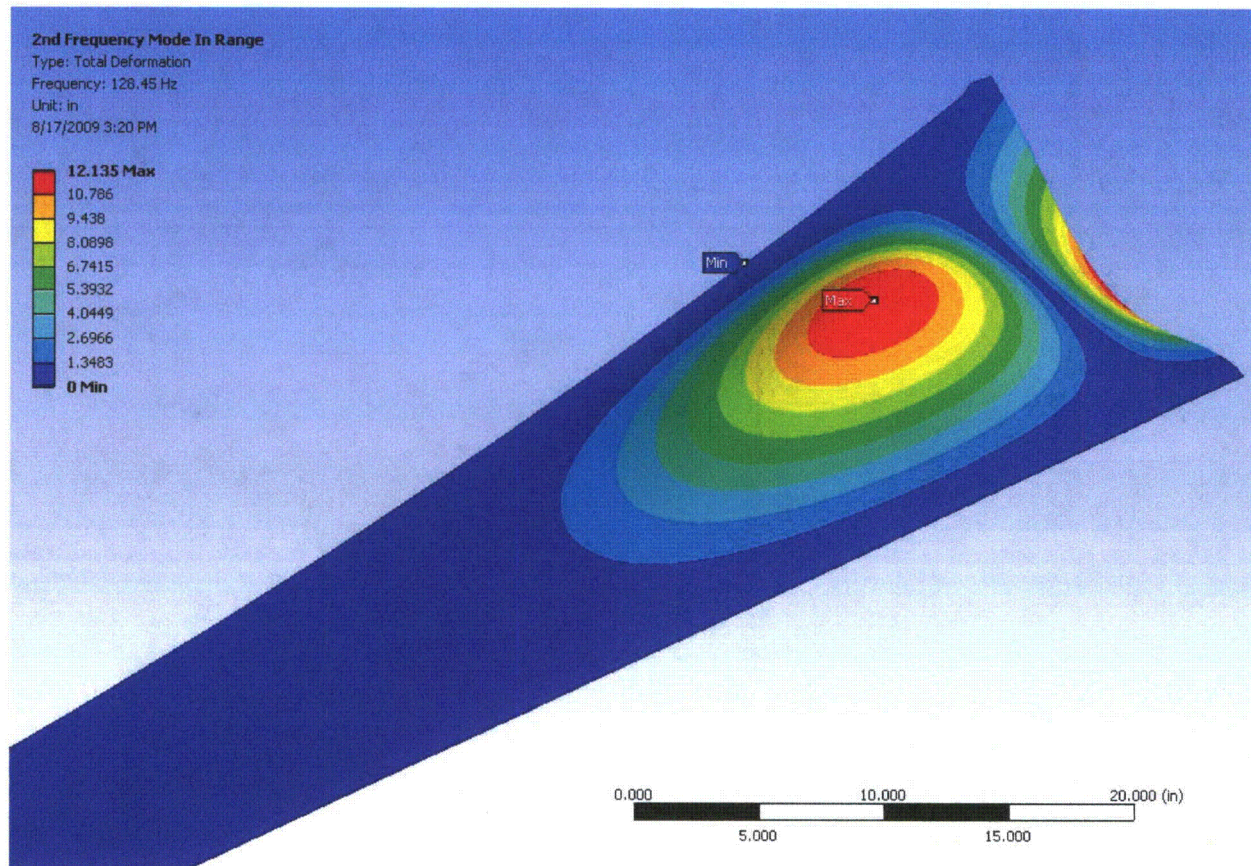


Figure 24: Second mode shape ($f=128.45$ Hz) of unmodified closure plates

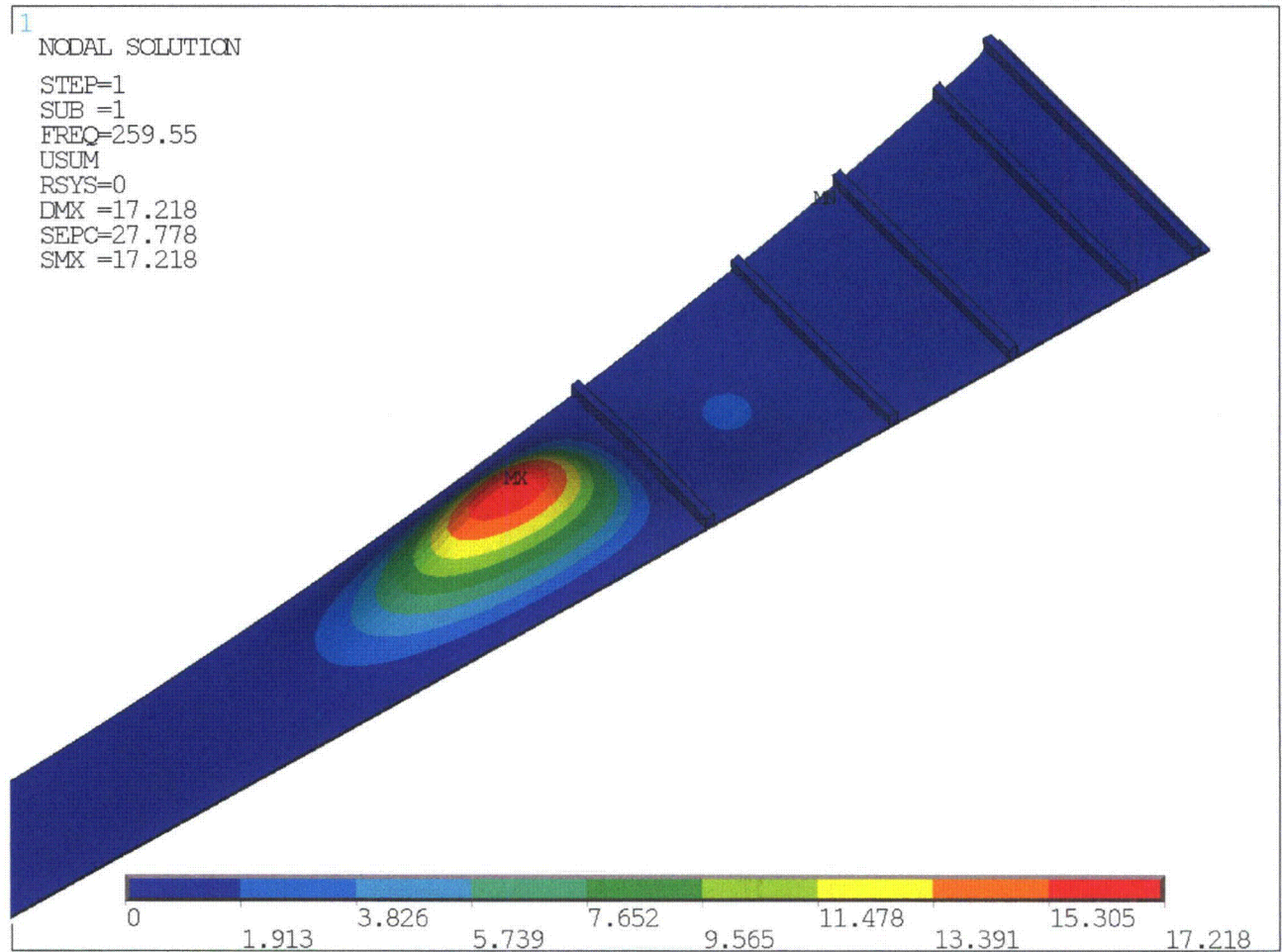


Figure 25: Fundamental mode shape ($f=259.6$ Hz) of modified closure plate.

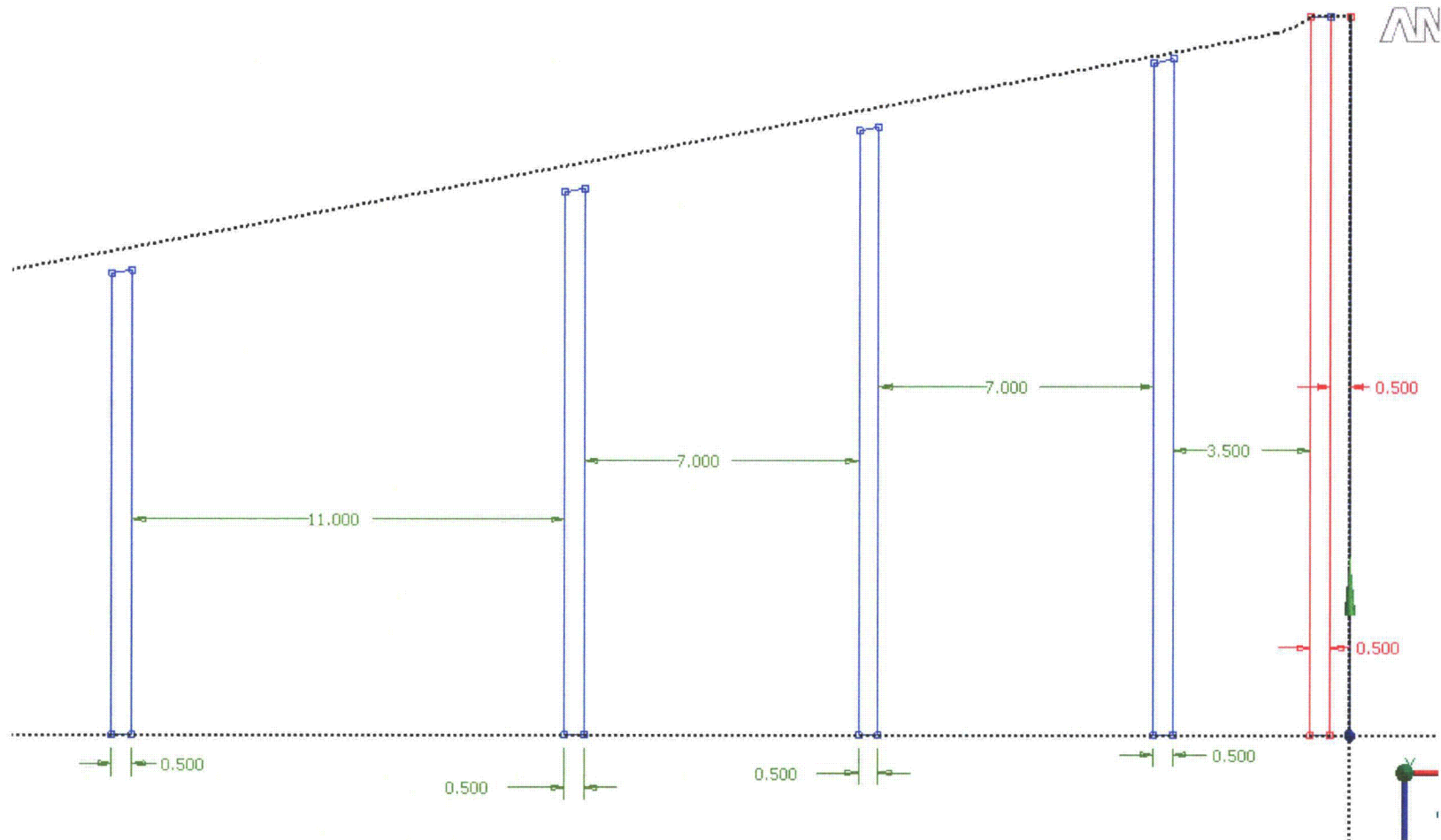


Figure 26. Closure Plate Modification – Geometry (0.5" w x 0.75" h Beam (from [30]))

5.6 Summary of Modifications

The dryer modifications are summarized in Table 11. To implement the modifications 1, 4, 5 and 8 unit solutions are regenerated over the 30-250 Hz frequency range with these modifications in place. Below 30 Hz the unit solutions for the original unmodified dryer are used. Since the original dryer had no significant stress response below 30 Hz, the splitting of the unit solutions in this manner is acceptable. For the remaining locations [[

(3)]]]. The unit solutions are combined with the MSL signals in the manner described in Section 2.

Table 11. Summary of modifications made to the NMP2 steam dryer.

Reinforcement / Modification	Details	FEA Implementation
1. Add reinforcement ribs to all (8) closure plates.	Section 5.5	Closure plates are thickened to obtain dynamically equivalent structure a described in Section 3.5
2. Increase weld of the lowest lifting rod brace/vertical plate welds to 0.5"	Section 5.4; Section 3.5 in [5]	[[(3)]]
3. Reinforce middle and upper lifting rod braces to eliminate stress concentration on weld to vertical plate.	Section 5.1	Reduce stresses by 0.18 at this location based on FEA reductions shown for Concept 2 in Table 11 of [13])
4. Add 1/8" thick plate over the middle hood section lying between the closure plate and existing reinforcement strip.	Section 5.2	Thicken the existing plate by 1/8".
5. Add total of four 15 lb masses to the central sections of the inner hoods.	Section 5.3	Place 15 lb point masses on the inner hoods at the mass centers.
6. Add stress relief cut-out at the bottom edge of the outer hood supports.	Section 5.4; Section 3.4 in [5]	[[(3)]]
7. Reinforce the bottom of the drain channel/skirt weld with thickened wrap-around weld.	Section 5.4; Section 3.1 in [5]	[[(3)]]
8. Add total of four 10 lb masses to the central sections of the middle hoods.	Section 5.4	Place 10 lb point masses on the middle hoods at the mass centers.

6. Results

The stress intensities and associated stress ratios resulting from the Rev. 4.1 acoustic/hydrodynamic loads [4, 8] with associated biases and uncertainties factored in, are presented below. The bias due to finite frequency discretization and uncertainty associated with the finite element model itself, are also factored in. In the following sections the highest maximum and alternating stress intensities are presented to indicate which points on the dryer experience significant stress concentration and/or modal response (Section 5.1). The lowest stress ratios obtained by comparing the stresses against allowable values, accounting for stress type (maximum and alternating) and location (on or away from a weld), are also reported (Section 5.2). Finally the frequency dependence of the stresses at nodes experiencing the lowest stress ratios is depicted in the form of accumulative PSDs (Section 5.3).

In each section results are presented both at nominal conditions (no frequency shift) and with frequency shift included. Unless specified otherwise, frequency shifts are generally performed at 2.5% increments. The tabulated stresses and stress ratios are obtained using a 'blanking' procedure that is designed to prevent reporting a large number of high stress nodes from essentially the same location on the structure. In the case of stress intensities this procedure is as follows. The relevant stress intensities are first computed at every node and then nodes sorted according to stress level. The highest stress node is noted and all neighboring nodes within 10 inches of the highest stress node and its symmetric images (i.e., reflections across the $x=0$ and $y=0$ planes) are "blanked" (i.e., excluded from the search for subsequent high stress locations). Of the remaining nodes, the next highest stress node is identified and its neighbors (closer than 10 inches) blanked. The third highest stress node is similarly located and the search continued in this fashion until all nodes are either blanked or have stresses less than half the highest value on the structure. For stress ratios, an analogous blanking procedure is applied. Thus the lowest stress ratio of a particular type in a 10" neighborhood and its symmetric images is identified and all other nodes in these regions excluded from listing in the table. Of the remaining nodes, the one with the lowest stress ratio is reported and its neighboring points similarly excluded, and so on until all nodes are either blanked or have a stress ratio higher than 4.

The acoustic loads applied to the steam dryer are obtained using the most recent and complete strain gage signals [4] and processed using the ACM Rev. 4.1 analysis with associated biases and uncertainties updated to reflect the new revision as described in [3]. For the FEM structural model there are three main contributors to the bias and uncertainty. The first is an uncertainty (21.5%) that accounts for modeling idealizations (e.g., vane bank mass model), geometrical approximations and other discrepancies between the modeled and actual dryer such as neglecting of weld mass and stiffness in the FEA. The second contributor is a bias of 9.53% accounting for discretization errors associated with using a finite size mesh, upon computed stresses. The third contributor is also a bias and compensates for the use of a finite discretization schedule in the construction of the unit solutions. The frequencies are spaced such that at 1% damping the maximum (worst case) error in a resonance peak is 5%. The average error for this frequency schedule is 1.72%.

6.1 General Stress Distribution and High Stress Locations

The maximum stress intensities obtained by post-processing the ANSYS stress histories for CLTP at nominal frequency and with frequency shift operating conditions are listed in Table 12. Contour plots of the stress intensities over the steam dryer structure are shown on Figure 27 (nominal frequency) and Figure 28 (maximum stress over all nine frequency shifts including nominal). The figures are oriented to emphasize the high stress regions. Note that these stress intensities *do not* account for weld factors but include end-to-end bias and uncertainty. Further, it should be noted that since the allowable stresses vary with location, stress intensities do not necessarily correspond to regions of primary structural concern. Instead, structural evaluation is more accurately made in terms of the stress ratios which compare the computed stresses to allowable levels with due account made for stress type and weld. Comparisons on the basis of stress ratios are made in Section 6.2.

The maximum stress intensities in most areas are low (less than 1000 psi). For the membrane stresses (P_m) the high stress regions tend to occur at: (i) the bottom of the central vertical side plate that joins the innermost vane banks (stress concentrations occur where this plate is welded to the inner base plates resting on the upper support ring); (ii) the welds joining the tie bars to the top cover plates on the vane banks; (iii) the seismic blocks that rest on the steam dryer supports; (iv) the bottoms of the inner vane bank side plates where they connect to the USR; and (v) the closure plate welds. For these locations the stresses are dominated by the static contribution as can be inferred from the small alternating stress intensities (S_{alt}) tabulated in Table 12 for the high P_m locations. The exception to this general pattern is the common junction of the outer hood, hood support and cover plate (the 5th entry in Table 12b). From Figure 27a and Figure 28a higher P_m regions are seen to be in the vicinity of the supports where all of the dryer deadweight is transmitted, the closure plates connecting the inner hoods to the middle vane banks, and various localized concentrations such those along the bottom of the outer hood.

The membrane + bending stress ($P_m + P_b$) distributions evidence a more pronounced modal response especially on the inner and middle hood structures. High stress concentrations are recorded on the bottom edge of the central vertical plate where it joins to the USR (immediately above the support blocks) and the inner vane bank. Other areas with high $P_m + P_b$ stress concentrations include: (i) the tops of the closure plates where they are welded to a hood or vane bank end plates; (ii) the skirt/drain channel welds; (iii) the outer cover plates connecting to the upper support ring and bottom of the outer hoods; (iv) the common junction between each hood, its hood support (or stiffener), and (v) the central panels of the inner and (to a lesser extent) middle hoods (see Figure 28b-c).

The alternating stress, S_{alt} , distributions are most pronounced on the inner and middle hoods. The highest stress intensity at any frequency shift at a non-weld location occurs on the inner hood. Though not exposed directly to the MSL acoustic sources, these hoods are thinner than the outer ones and their response is driven mainly by structural coupling rather than direct forcing. Significant response is also observed on the outer hoods nearest the MSL inlet acoustics. Numerous weld locations also show significant stress including the bottoms of drain channels and the junctions between the hoods, hood supports and base plates. These locations are characterized by localized stress concentrations as indicated in Figure 28e and have emerged as

high stress locations in other steam-dryers also. Other locations with high alternating stress intensities include the tie bar/top cover plate weld, the weld joining the lifting rod braces to the vertical vane bank end plate and welds involving the closure plate.

Comparing the nominal results (12a) and results with frequency shifting it can be seen that maximum stress intensities, P_m and P_m+P_b , do not differ significantly. The highest alternating stress is approximately 9.0% higher when frequency shifts are considered.

Table 12a. Locations with highest predicted stress intensities for CLTP conditions with no frequency shift.

Stress Category	Location	Weld	SRF(a)	Location (in)			node	Stress Intensities (psi)			Dom. Freq. (Hz)
				x	y	z		Pm	Pm+Pb	Salt	
Pm	Inner Side Plate	No		3.1	119	0.5	37229	7472	8918	575	45.0
"	Upper Support Ring (USR)/Support/Seismic Block	Yes		-6.9	-122.3	-9.5	113554	7380	7380	967	15.4
"	Side Plate Ext/Inner Base Plate	Yes		16.3	119	0	94143	6930	9812	491	45.0
"	Tie Bar	Yes		-49.3	-108.1	88	143795	6168	6168	1086	71.4
	Closure Plate/Backing Bar/Inner Hood	Yes		-39.9	-108.6	0.5	84198	4926	4947	623	71.1
Pm+Pb	Side Plate Ext/Inner Base Plate	Yes		16.3	119	0	94143	6930	9812	491	45.0
"	Inner Side Plate	No		3.1	119	0.5	37229	7472	8918	575	45.0
"	Side Plate/Top Plate	No		49.6	108.6	88	93256	2547	8676	1447	69.2
"	USR/Support/Seismic Block	Yes		-6.9	-122.3	-9.5	113554	7380	7380	967	15.4
"	Side Plate/Top Plate	No		17.6	119	88	91215	922	7326	1451	72.1
Salt	Inner Hood	No		-32.4	27	72.4	81316	1469	4404	3884	45.5
"	Brace	No		-79.6	-85.5	75.8	37724	2909	3049	3015	19.8
"	Middle Hood	No		63.6	-30	73.3	34302	975	3152	2917	60.8
"	Inner Hood	No		31.4	-36.1	77.1	70582	1022	2889	2840	55.2
"	Inner Hood	No		31.8	-16.2	75.4	70627	761	2437	2434	55.2

Notes: (a) [(3)] Entry is empty if no SRF is applied.

(b) Full penetration weld so that weld factor, WF=1.4.

(1-5) Number referring to the [(3)]

Table 12b. Locations with highest predicted stress intensities taken over all frequency shifts at CLTP conditions.

Stress Category	Location	Weld	SRF(a)	Location (in)			node	Stress Intensities (psi)			% Freq. Shift	Dom. Freq. (Hz)
				x	y	z		Pm	Pm+Pb	S _{alt}		
Pm	Inner Side Plate	No		3.1	119	0.5	37229	7500	9030	662	5	69.6
"	USR/Support/Seismic Block	Yes		-6.9	-122.3	-9.5	113554	7380	7380	1062	0	14.0
"	Side Plate Ext/Inner Base Plate	Yes		16.3	119	0	94143	7018	9923	535	2.5	14.9
"	Tie Bar	Yes		-49.3	-108.1	88	143795	6169	6169	1086	2.5	71.4
"	Hood Support/Outer Cover Plate/Outer Hood ⁽⁴⁾	Yes	0.80	-102.8	28.4	0	95267	5167	5194	2424	5	60.5
Pm+Pb	Side Plate Ext/Inner Base Plate	Yes		16.3	119	0	94143	7018	9923	535	2.5	14.9
"	Inner Side Plate	No		3.1	119	0.5	37229	7500	9030	662	5	69.6
"	Side Plate/Top Plate	Yes		49.6	108.6	88	93256	2573	8687	1447	-7.5	69.2
"	Middle Base Plate/Inner Backing Bar/Inner Hood	Yes		-39.9	-108.6	0	84197	565	7503	1555	2.5	52.0
"	Side Plate/Top Plate	Yes		17.6	119	88	91215	941	7445	1710	5	69.2
S _{alt}	Inner Hood	No		-32.4	27	72.4	81316	1469	4502	4233	-7.5	60.8
"	Inner Hood	No		31.4	-36.1	77.1	70582	1022	3049	3033	2.5	53.8
"	Brace	No		-79.6	-85.5	75.8	37724	2954	3049	3015	0	19.8
"	Middle Hood	No		-64.8	24.8	67.6	30488	840	3051	2943	2.5	60.6
"	Middle Hood	No		63	-32.6	76.3	34771	815	2697	2673	0	60.8

Notes: (a) [[(3)]] Entry is empty if no SRF is applied.

(b) Full penetration weld so that weld factor, WF=1.4.

(1-5) Number referring to the [[(3)]]

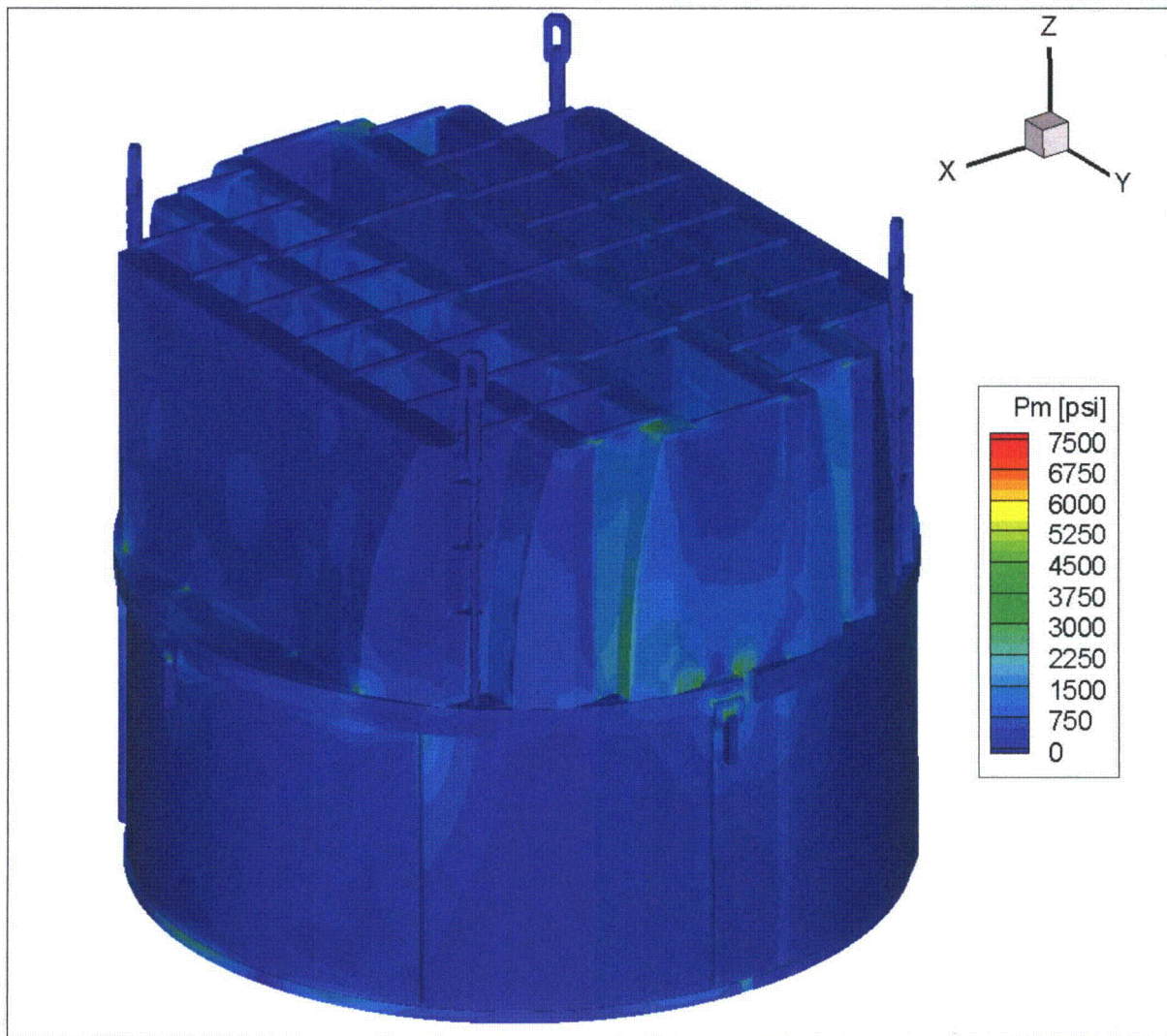


Figure 27a. Contour plot of maximum membrane stress intensity, P_m , for CLTP load. The maximum stress intensity is 7472 psi.

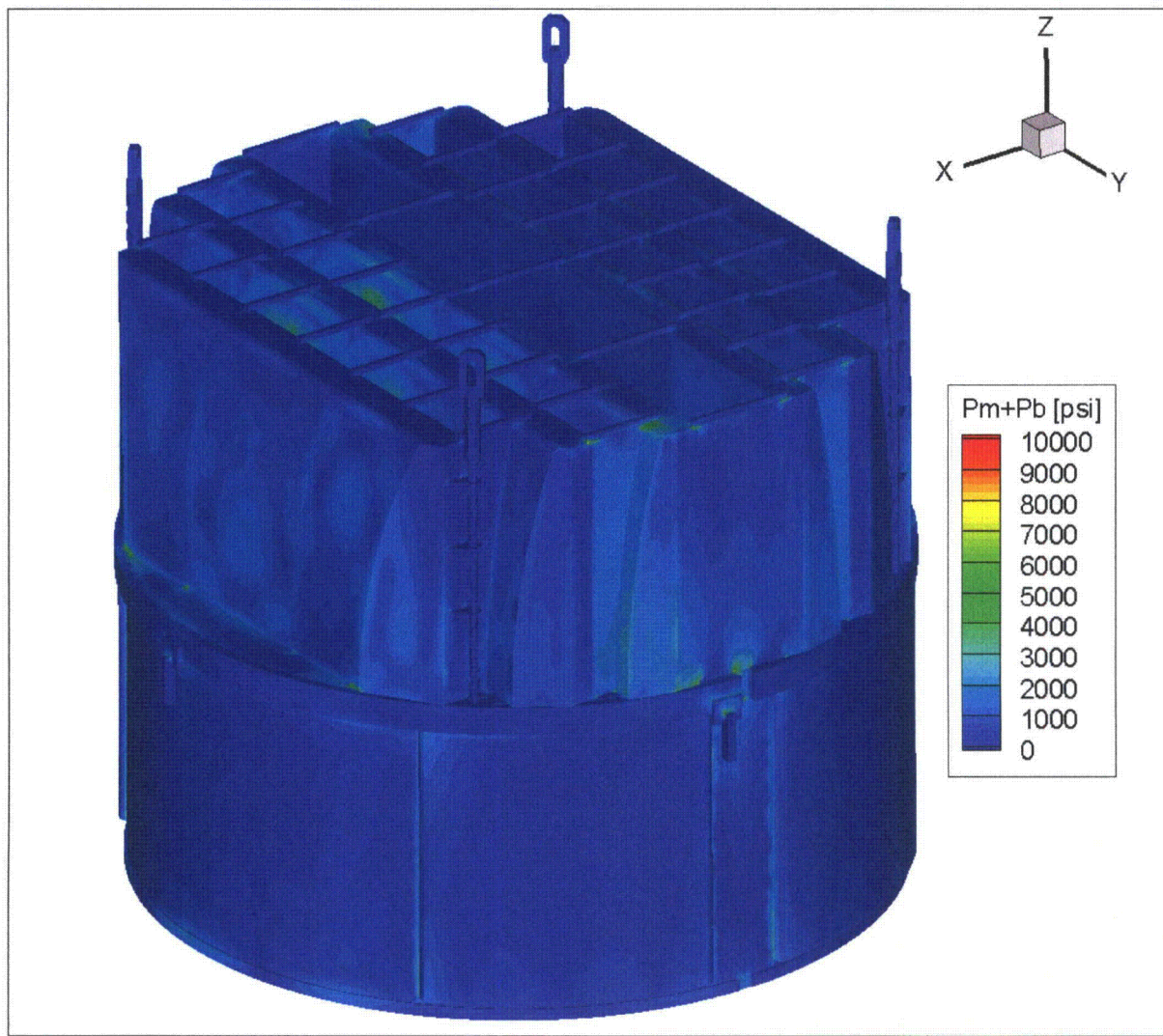


Figure 27b. Contour plot of maximum membrane+bending stress intensity, P_m+P_b , for CLTP load. The maximum stress intensity is 9812 psi. First view.

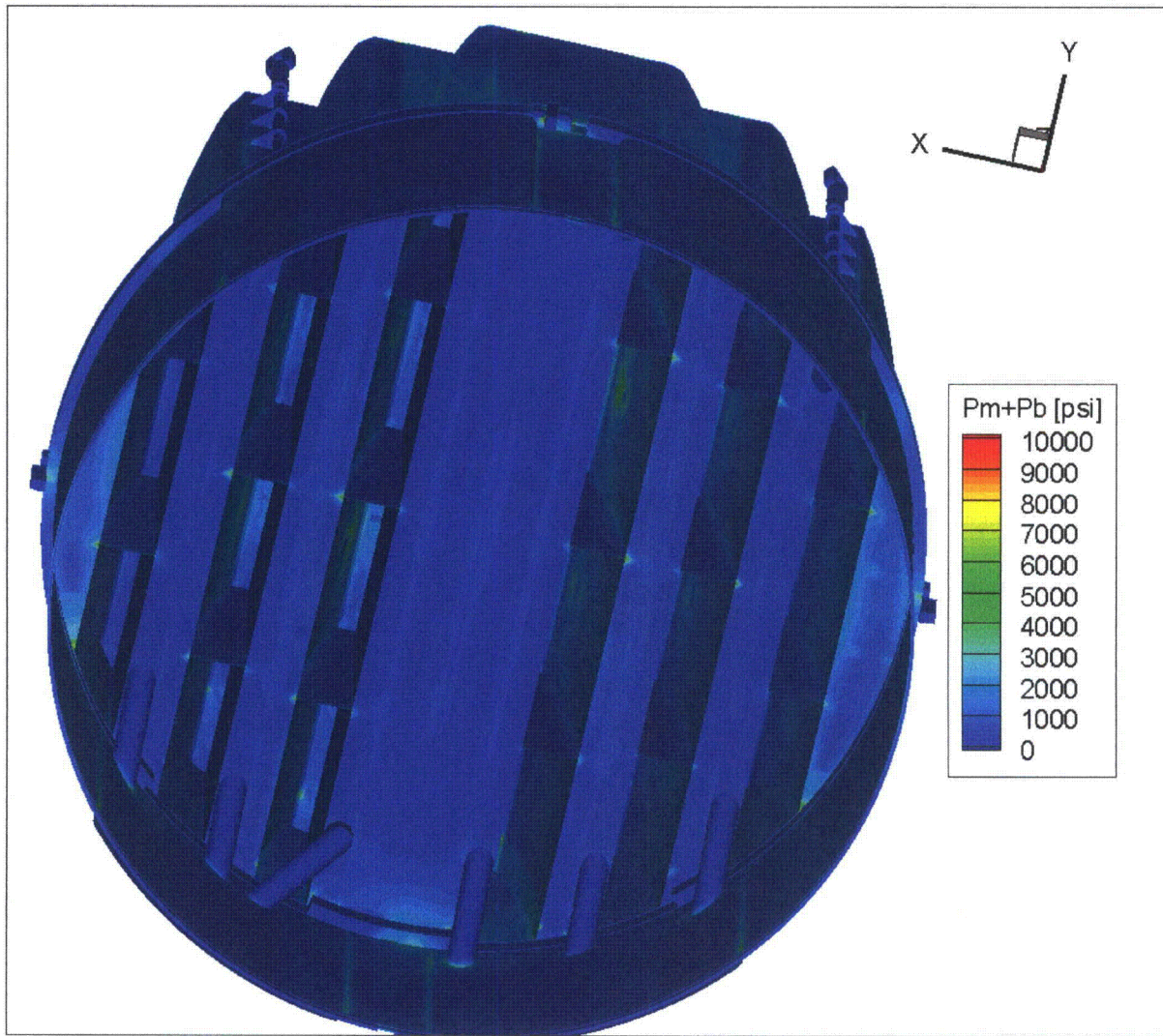


Figure 27c. Contour plot of maximum membrane+bending stress intensity, $P_m + P_b$, for CLTP load. This second view from below shows the high stress intensities at the hood/stiffener/base plate junctions and drain channel/skirt welds.

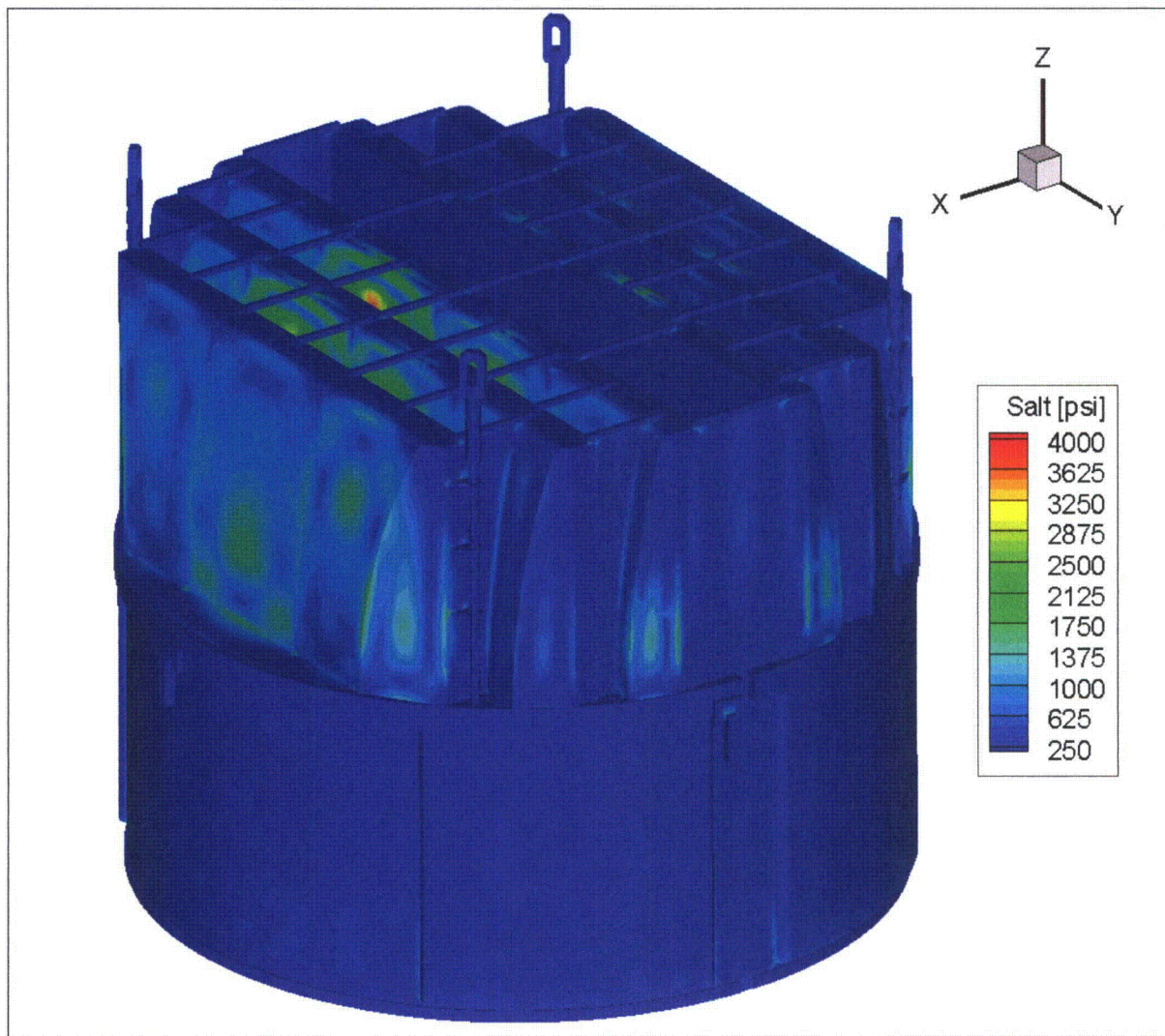


Figure 27d. Contour plot of alternating stress intensity, S_{alt} , for CLTP load. The maximum alternating stress intensity is 3884 psi. First view.

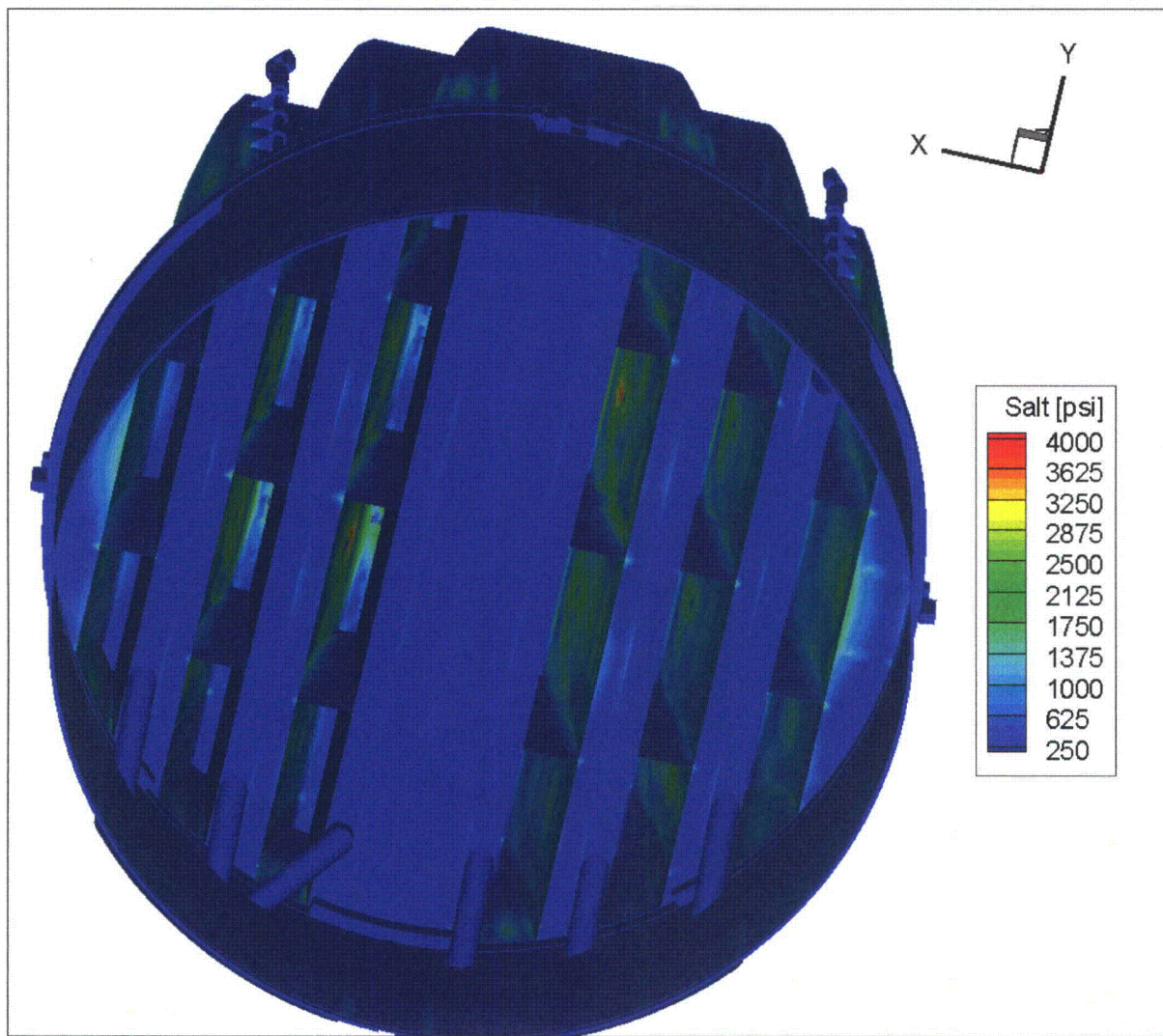


Figure 27e. Contour plot of alternating stress intensity, S_{alt} , for CLTP load. Second view from below.

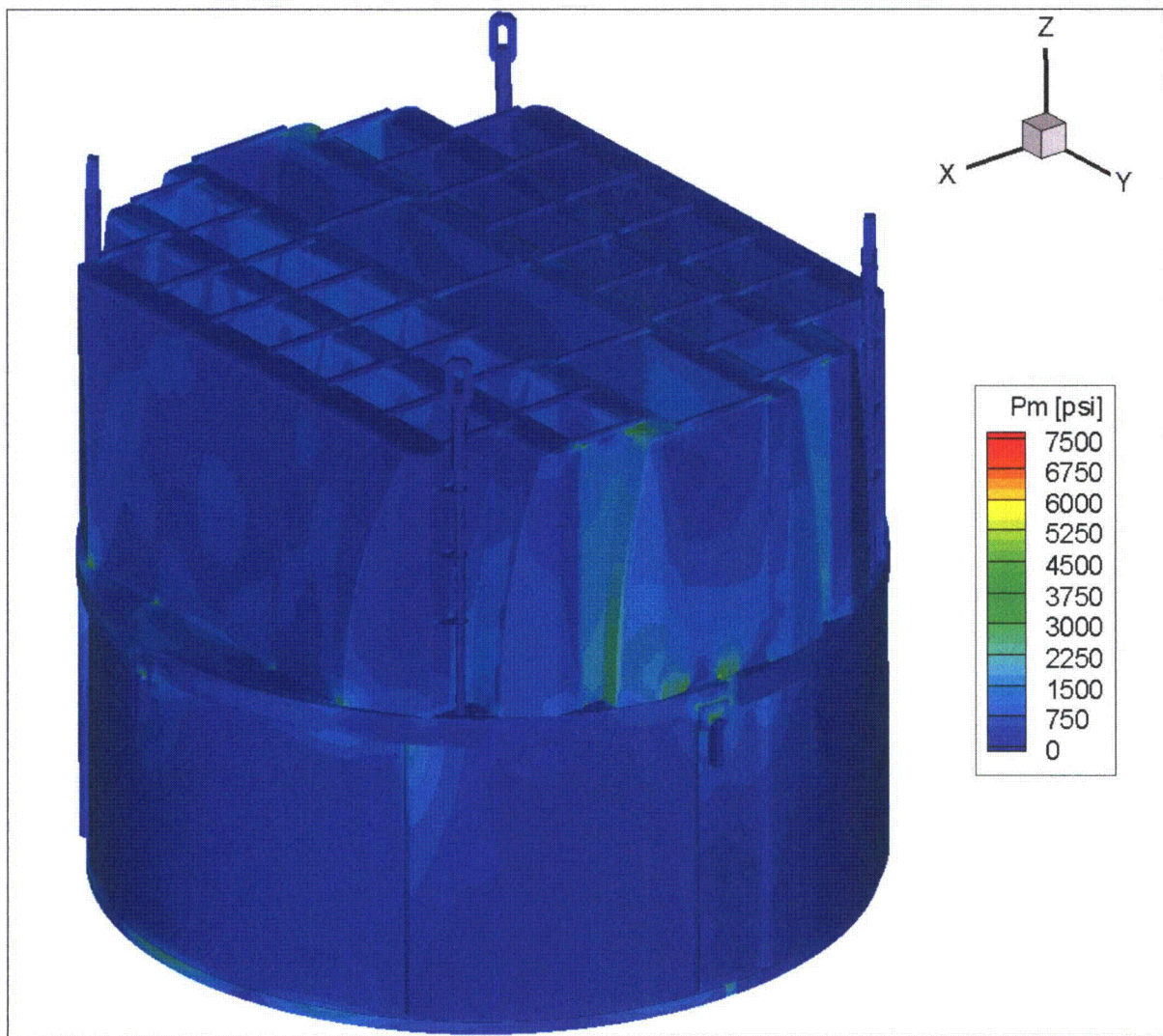


Figure 28a. Contour plot of maximum membrane stress intensity, P_m , for CLTP operation with frequency shifts. The recorded stress at a node is the maximum value taken over all frequency shifts. The maximum stress intensity is 7500 psi.

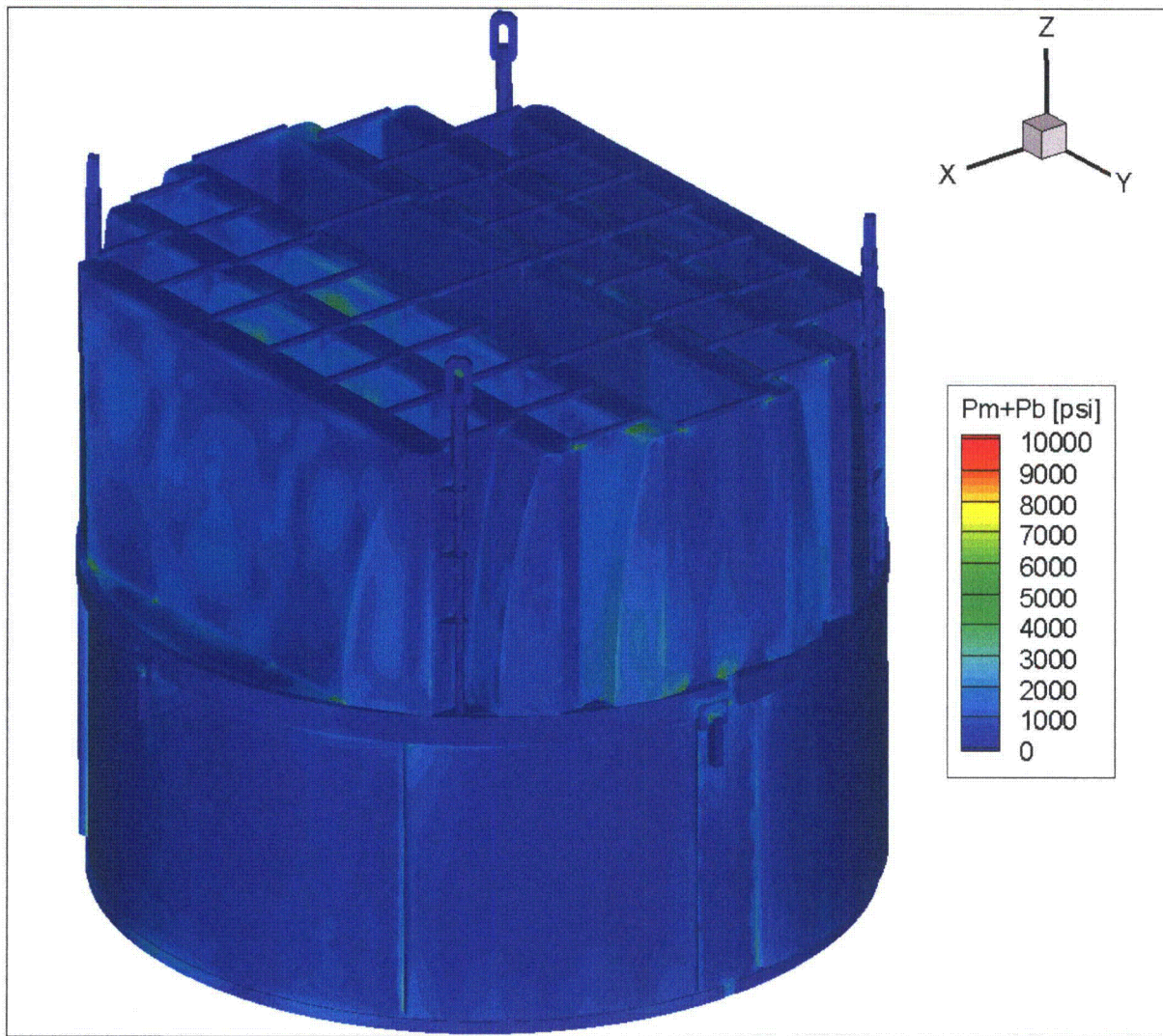


Figure 28b. Contour plot of maximum membrane+bending stress intensity, $P_m + P_b$, for CLTP operation with frequency shifts. The recorded stress at a node is the maximum value taken over all frequency shifts. The maximum stress intensity is 9923 psi. First view.

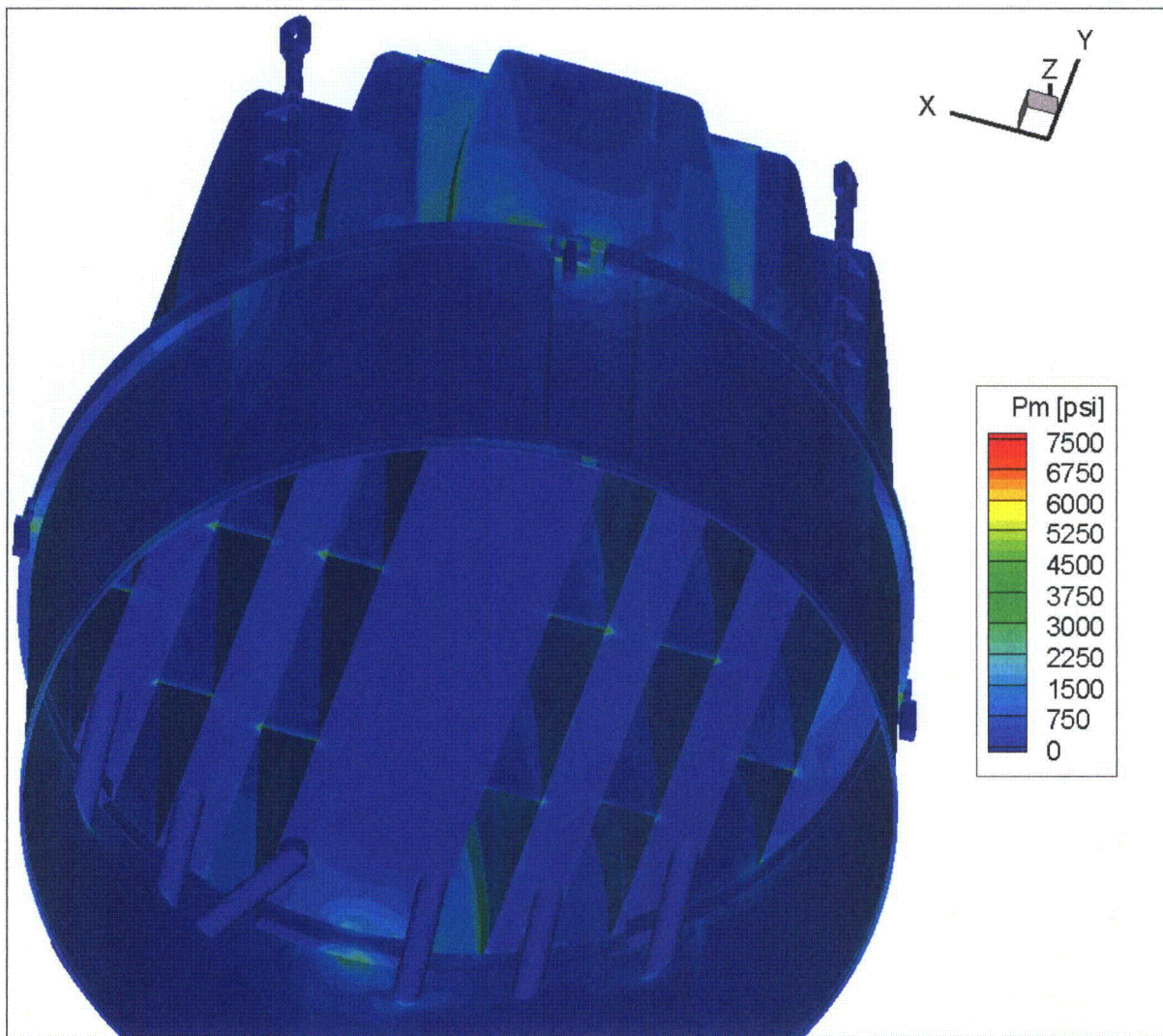


Figure 28c. Contour plot of maximum membrane+bending stress intensity, $P_m + P_b$, for CLTP operation with frequency shifts. Second view from beneath.

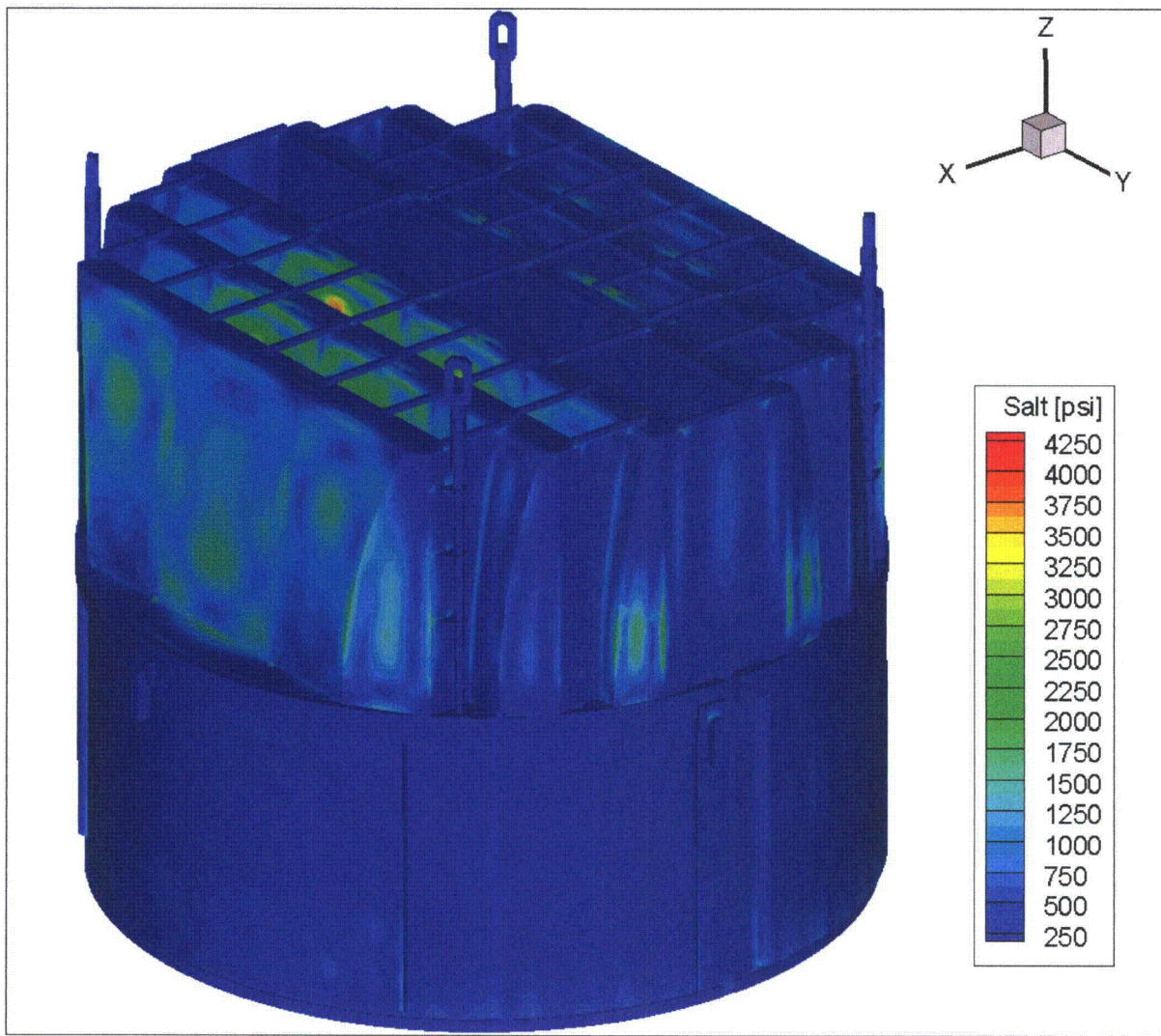


Figure 28d. Contour plot of alternating stress intensity, S_{alt} , for CLTP operation with frequency shifts. The recorded stress at a node is the maximum value taken over all frequency shifts. The maximum alternating stress intensity is 4233 psi. First view.

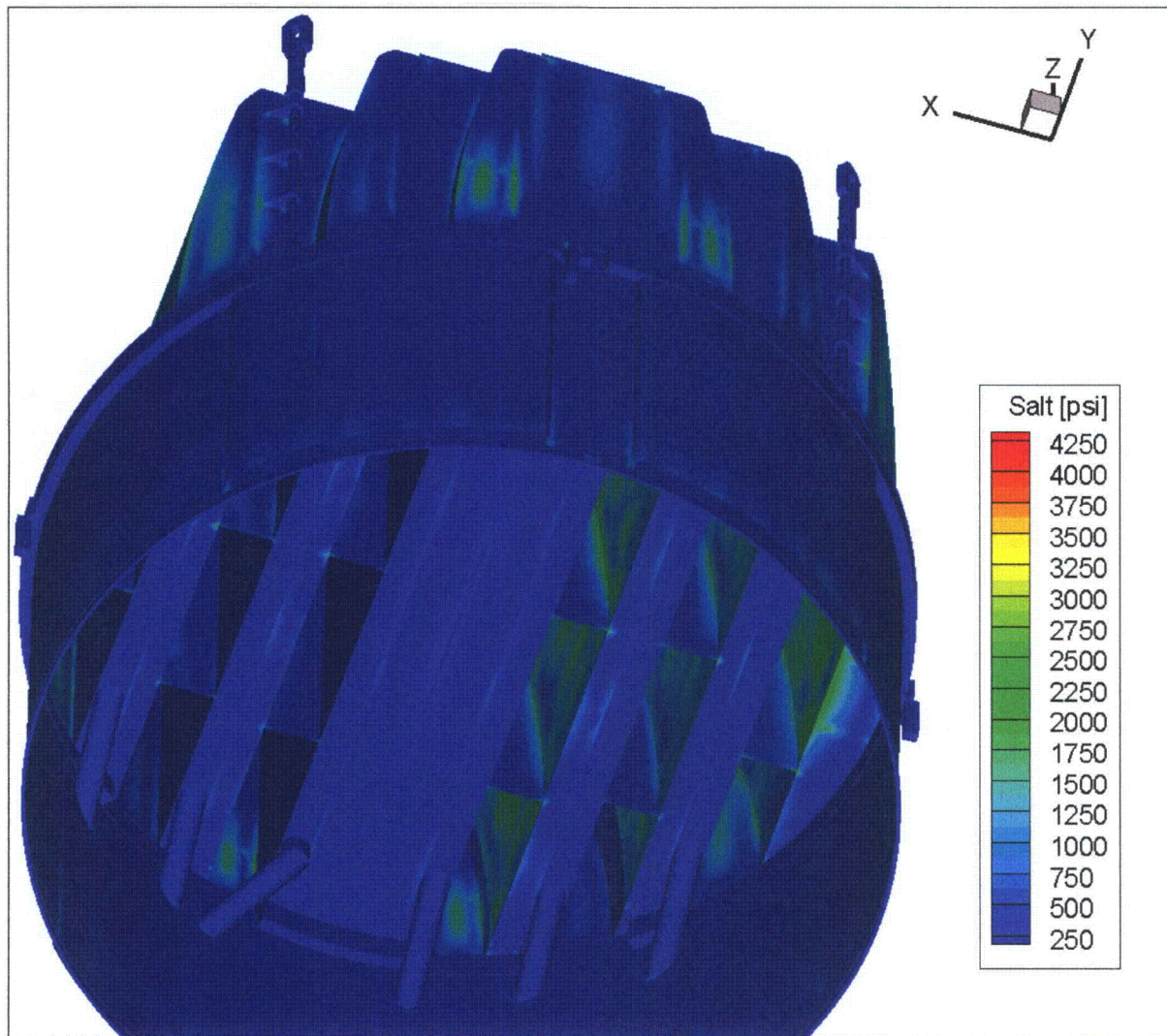


Figure 28e. Contour plot of alternating stress intensity, S_{alt} , for CLTP operation with frequency shifts. The recorded stress at a node is the maximum value taken over all frequency shifts. Second view from below.

6.2 Load Combinations and Allowable Stress Intensities

The stress ratios computed for CLTP at nominal frequency and with frequency shifting are listed in Table 13 (without frequency shifting) and Table 14 (with frequency shifting). The stress ratios are grouped according to type (SR-P for maximum membrane and membrane+bending stress, SR-a for alternating stress) and location (away from welds or on a weld). The tabulated nodes are also depicted in Figure 29 (no frequency shift) and Figure 30 (all frequency shifts included). The plots corresponding to maximum stress intensities depict all nodes with stress ratios less than 5 as indicated, and the plots of alternating stress ratios display all nodes with $SR-a \leq 5$.

For CLTP operation at nominal frequency the minimum stress ratio is identified as a maximum stress, $SR-P=1.26$, and is recorded on upper support ring where it rests on the support block. This stress at this location is dominated by the static stress due to deadweight and is only weakly responsive to acoustic loads as can be seen from the high alternating stress ratio at this location ($SR-a > 6.47$ at all frequency shifts). This is true for all four nodes having the lowest values of $SR-P$, all having $SR-a > 6.32$ at all frequency shifts. The minimum alternating stress ratio at zero frequency shift, $SR-a=3.29$, occurs on the weld connecting the outer hood, hood support and cover plate. At zero shift the lower lifting rod brace has the lowest alternating stress ratio ($SR-a=3.87$). This is because, unlike the middle and upper braces which experience higher alternating lateral loads, the lower brace is only reinforced by an increase in the weld size.

The effects of frequency shifts can be conservatively accounted for by identifying the minimum stress ratio at every node, where the minimum is taken over all the frequency shifts considered (including the nominal or 0% shift case). The resulting stress ratios are then processed as before to identify the smallest stress ratios anywhere on the structure, categorized by stress type (maximum or alternating) and location (on or away from a weld). The results are summarized in Table 14 and show that the lowest stress ratio, $SR-P=1.26$, occurs at the same location as in the nominal case and retains the same value. Moreover, the next three lowest $SR-P$ locations in Table 14b are the same as in Table 13b. The lowest alternating stress ratio also occurs at the same location as without shifting on the common junction of the outer hood, hood support and cover plate. However the alternating stress ratio reduces from $SR-a=3.29$ to $SR-a=2.83$. The next collection of high stress locations involves the inner hood and adjoining structures and is associated with hood vibration. A similar, but weaker response is observed in the middle hood/hood support weld. Other points with low alternating stress ratios include the tie bar/top vane bank plate welds, some locations on the closure plate attachment welds and welds joining the lifting rod brace (lower-most) to the vane bank end plate.

The estimated alternating stress ratio at EPU operation is obtained by scaling the corresponding value at CLTP by the square of the ratio of the steam flow velocities at EPU and CLTP conditions. Since this ratio, $(U_{EPU}/U_{CLTP})^2 = 1.1756^2 = 1.382$, the limiting alternating stress ratio at any frequency shift for EPU is estimated as $SR-a = 2.83/1.382 = 2.05$ which meets the EPU target of 2.0. The lowest stress ratio associated with a maximum stress is $SR-P=1.25$ at CLTP. This value is dominated by the static component and is only weakly altered by acoustic loads and reduces to 1.22 at EPU.

Table 13a. Limiting non-weld locations with at CLTP conditions with no frequency shift. Stress ratios are grouped according to stress type (maximum – SR-P; or alternating – SR-a). Locations are depicted in Figure 29.

Stress Ratio	Location	Location (in.)			node	Stress Intensity (psi)			Stress Ratio		Dom. Freq. (Hz)
		x	y	z		Pm	Pm+Pb	S _{alt}	SR-P	SR-a	
SR-P	1. Inner Side Plate	3.1	119	0.5	37229	7472	8918	575	2.26	21.49	45.0
"	2. Thin Vane Bank Plate	-15.6	-118.4	0.6	2558	4829	5238	<250	3.5	>40	0
"	3. Support/Seismic Block	10.2	123.8	-9.5	113286	4482	4482	1429	3.77	8.65	15.4
SR-a	1. Brace	-32.4	27	72.4	81316	1469	4404	3884	5.76	3.18	45.5
"	2. Inner Hood	-79.6	-85.5	75.8	37724	2909	3049	3015	5.81	4.1	19.8
"	3. Middle Hood	63.6	-30	73.3	34302	975	3152	2917	8.04	4.24	60.8

Table 13b. Limiting peak stress ratios, SR-P, on welds at CLTP conditions with no frequency shift. Bold text indicates minimum stress ratio on the structure. Locations are depicted in Figure 29.

Location	SRF(a)	Location (in.)			node	Stress Intensity (psi)			Stress Ratio		Dom. Freq. (Hz)
		x	y	z		Pm	Pm+Pb	S _{alt}	SR-P	SR-a	
1. USR/Support/Seismic Block		-6.9	-122.3	-9.5	113554	7380	7380	967	1.26	7.11	15.4
2. Side Plate Ext/Inner Base Plate		16.3	119	0	94143	6930	9812	491	1.34	13.99	45.0
3. Tie Bar		-49.3	-108.1	88	143795	6168	6168	1086	1.51	6.32	71.4
4. Inner Side Plate/Inner Base Plate		-2.3	-119	0	99200	4479	7931	564	1.76	12.18	73.0
5. Closure Plate/Backing Bar/Inner Hood		-39.9	-108.6	0.5	84198	4926	4947	623	1.89	11.03	71.1
6. Side Plate/Top Plate		17.6	119	88	91215	922	7326	1451	1.9	4.73	72.1
7. Hood Support/Middle Base Plate/Backing Bar/Inner Hood ^(b)		-39.9	0	0	85723	4790	4976	1551	1.94	4.43	45.5
8. Cover Plate/Outer Hood		102.8	-58.1	0	94498	1040	7178	908	1.94	7.57	11.6
9. Thin Vane Bank Plate/Hood Support/Inner Base Plate		24.1	-59.5	0	85191	4755	4761	1137	1.95	6.04	55.2
10. Hood Support/ Cover Plate/Outer Hood ⁽⁴⁾	0.8	-102.8	28.4	0	95267	4642	4855	2087	2	3.29	54.3
11. Hood Support/Outer Base Plate/Middle Backing Bar		-71.3	0	0	95428	4641	4861	1914	2	3.59	52.1
12. Hood Support/Middle Base Plate/Backing Bar/Inner Hood ^(b)		-39.9	59.5	0	90468	4433	4525	1347	2.1	5.1	45.5

Notes: (a) [[(3)]] Entry is empty if no SRF is applied.

(b) Full penetration weld so that weld factor, WF=1.4.

(1-5) Number referring to the [[(3)]]

Table 13c. Limiting alternating stress ratios, SR-a, on welds at CLTP conditions with no frequency shift. Locations are depicted in Figure 29.

Location	SRF(a)	Location (in.)			node	Stress Intensity (psi)			Stress Ratio		Dom. Freq. (Hz)
		x	y	z		Pm	Pm+Pb	S _{alt}	SR-P	SR-a	
1. Hood Support/Cover Plate/Outer Hood(4)	0.80	-102.8	28.4	0	95267	4642	4855	2087	2	3.29	54.3
2. Top Thick Plate/Inner Hood/Top Plate		24.1	-30.6	88	85512	744	2179	2030	6.4	3.38	55.2
3. Hood Support/Inner Hood(b)		-36.8	0	46.9	95644	760	2092	2013	6.66	3.41	44.9
4. Hood Support/Outer Base Plate/Backing Bar		71.3	0	0	98067	4292	4583	1996	2.17	3.44	44.4
5. Top Thick Plate/Middle Hood/Top Plate		55.6	-27.9	88	90947	701	2250	1915	6.2	3.59	60.8
6. Side Plate/Top Plate		-80.2	85.2	88	99455	556	4590	1895	3.04	3.62	71.4
7. Hood Support/Inner Hood(b)		32.4	0	72.5	99540	537	2155	1870	6.47	3.67	55.2
8. Top Thick Plate/Inner Hood/Top Plate(2)	0.83	24.1	-27.8	88	90897	831	2208	1854	6.31	3.71	55.2
9. Closure Plate/Middle Hood		60.2	-85.2	87	89317	1190	4673	1822	2.98	3.77	71.1
10. Hood Support/Inner Hood(b)		-36.8	59.5	46.9	90431	703	1992	1792	7	3.83	45.5
11. Side Plate/Brace(5)	0.64	-79.7	-85.2	31.2	84708	1606	1950	1774	5.79	3.87	108.0
12. Double Side Plate/Top Plate		-49.3	0	88	97693	907	2541	1769	5.49	3.88	71.1
13. Hood Support/Middle Hood(b)		63.8	0	72.5	98462	537	1997	1757	6.98	3.91	60.8
14. Double Side Plate/Top Plate/Tie Bar		-17.6	0	88	100166	980	2332	1737	5.98	3.95	72.3
15. Hood Support/Inner Hood(b)		-38.9	0	27	95634	660	1774	1736	7.86	3.96	45.5

Notes: (a) [[(3)]] Entry is empty if no SRF is applied.
 (b) Full penetration weld so that weld factor, WF=1.4.
 (1-5) Number referring to the [[(3)]]

Table 14a. Limiting non-weld locations with at CLTP conditions with frequency shifts. Stress ratios are grouped according to stress type (maximum – SR-P; or alternating – SR-a). Locations are depicted in Figure 30.

Stress Ratio	Location	Location (in.)			node	Stress Intensity (psi)			Stress Ratio		% Freq. Shift	Dom. Freq. (Hz)
		x	y	z		Pm	Pm+Pb	S _{alt}	SR-P	SR-a		
SR-P	1. Inner Side Plate	3.1	119	0.5	37229	7500	9030	662	2.25	18.67	5	69.6
"	2. Thin Vane Bank Plate	-15.6	-118.4	0.6	2558	4855	5272	255	3.48	48.57	-2.5	45.9
"	3. Support/Seismic Block	10.2	123.8	-9.5	113286	4570	4570	1521	3.7	8.13	10	14.0
SR-a	1. Inner Hood	-32.4	27	72.4	81316	1469	4502	4233	5.63	2.92	-7.5	60.8
"	2. Inner Hood	31.4	-36.1	77.1	70582	1022	3049	3033	8.31	4.08	2.5	53.8
"	3. Brace	-79.6	-85.5	75.8	37724	2954	3049	3015	5.72	4.1	0	19.8
"	4. Middle Hood	-64.8	24.8	67.6	30488	840	3051	2943	8.31	4.2	2.5	60.6

Table 14b. Limiting peak stress ratios, SR-P, on welds at CLTP conditions with frequency shifts. Bold text indicates minimum stress ratio on the structure. Locations are depicted in Figure 30.

Location	SRF(a)	Location (in.)			node	Stress Intensity (psi)			Stress Ratio		% Freq. Shift	Dom. Freq. (Hz)
		x	y	z		Pm	Pm+Pb	S _{alt}	SR-P	SR-a		
1. USR/Support/Seismic Block		-6.9	-122.3	-9.5	113554	7380	7380	1062	1.26	6.47	0	14.0
2. Side Plate Ext/Inner Base Plate		16.3	119	0	94143	7018	9923	535	1.32	12.83	2.5	14.9
3. Tie Bar		-49.3	-108.1	88	143795	6169	6169	1086	1.51	6.32	2.5	71.4
4. Inner Side Plate/Inner Base Plate		-2.3	-119	0	99200	4488	8084	769	1.72	8.93	7.5	70.6
5. Hood Support/ Cover Plate/Outer Hood ⁽⁴⁾	0.8	-102.8	28.4	0	95267	5167	5194	2424	1.8	2.83	5	60.5
6. Thin Vane Bank Plate/Hood Support/Inner Base Plate		24.1	-59.5	0	85191	5056	5181	1415	1.84	4.85	5	52.1
7. Closure Plate/Backing Bar/Inner Hood		39.9	108.6	0.5	93062	5021	5078	695	1.85	9.89	7.5	51.2
8. Side Plate/Top Plate		17.6	119	88	91215	941	7445	1710	1.87	4.02	5	69.2
9. Hood Support/Middle Base Plate/Inner Backing Bar/Inner Hood ^(b)		-39.9	0	0	85723	4844	5095	1837	1.92	3.74	2.5	70.6
11. Outer Cover Plate/Outer Hood		102.8	-58.1	0	94498	1052	7231	951	1.93	7.22	2.5	11.2
11. Hood Support/Outer Base Plate/Middle Backing Bar		-71.3	0	0	95428	4713	5234	2030	1.97	3.38	5	51.2
12. Hood Support/Middle Base Plate/Backing Bar/Inner Hood ^(b)		-39.9	59.5	0	90468	4433	4525	1347	2.1	5.1	0	45.5

Notes: (a) [[(3)]] Entry is empty if no SRF is applied.
 (b) Full penetration weld so that weld factor, WF=1.4.
 (1-5) Number referring to the [[(3)]]

Table 14 c. Limiting alternating stress ratios, SR-a, on welds at CLTP conditions with frequency shifts. Locations are depicted in Figure 30.

Location	SRF(a)	Location (in.)			node	Stress Intensity (psi)			Stress Ratio		% Freq. Shift	Dom. Freq. (Hz)
		x	y	z		Pm	Pm+Pb	S _{alt}	SR-P	SR-a		
1. Hood Support/Cover Plate/Outer Hood ⁽⁴⁾	0.8	-102.8	28.4	0	95267	5167	5194	2424	1.8	2.83	-10	60.5
2. Outer Cover Plate/Outer Hood		-102.8	1	0	95237	1200	2624	2251	5.31	3.05	-10	60.5
3. Hood Support/Inner Hood ^(b)		32.4	0	72.5	99540	592	2520	2164	5.53	3.17	5	52.1
4. Top Thick Plate/Tie Bar/Inner Hood		-24.1	23.9	88	99104	751	2190	2137	6.37	3.21	-7.5	60.8
5. Hood Support/Outer Base Plate/Backing Bar		71.3	0	0	98067	4438	4682	2088	2.09	3.29	2.5	52.0
6. Top Thick Plate/Tie Bar/Inner Hood ⁽³⁾	0.83	-24.1	26.8	88	99130	643	2229	2059	6.26	3.34	-7.5	60.8
7. Hood Support/Inner Hood ^(b)		-36.5	0	48.8	95645	784	2256	2049	6.18	3.35	-10	49.4
8. Vane Bank Plate/Side Plate/End Plate		24.1	119	11.6	91091	1602	2716	2024	5.13	3.39	5	143.9
9. Double Side Plate/Top Plate		-49.3	0	88	97693	1012	2790	1996	5	3.44	5	69.2
10. Entry Bottom Perf/Side Plate/End Plate		24.1	119	23.7	91154	1283	2728	1995	5.11	3.44	-5	160.2
11. Closure Plate/Middle Hood		60.2	-85.2	87	89317	1251	4916	1981	2.84	3.47	2.5	70.6
12. Double Side Plate/Top Plate/Tie Bar		17.6	0	88	95617	1064	2592	1965	5.38	3.5	5	69.2
13. Side Plate/Top Plate		80.2	-85.2	88	91054	596	4693	1954	2.97	3.51	2.5	70.6
14. Hood Support/Inner Hood ^(b)		-38.2	0	34.9	95638	796	1980	1952	7.04	3.52	-2.5	45.5
15. Side Plate/Brace ⁽⁵⁾	0.64	79.7	-85.2	31.2	87633	2130	2443	1930	4.36	3.56	10	194.5

Notes: (a) [[(3)]] Entry is empty if no SRF is applied.
 (b) Full penetration weld so that weld factor, WF=1.4.
 (1-5) Number referring to the [[(3)]]

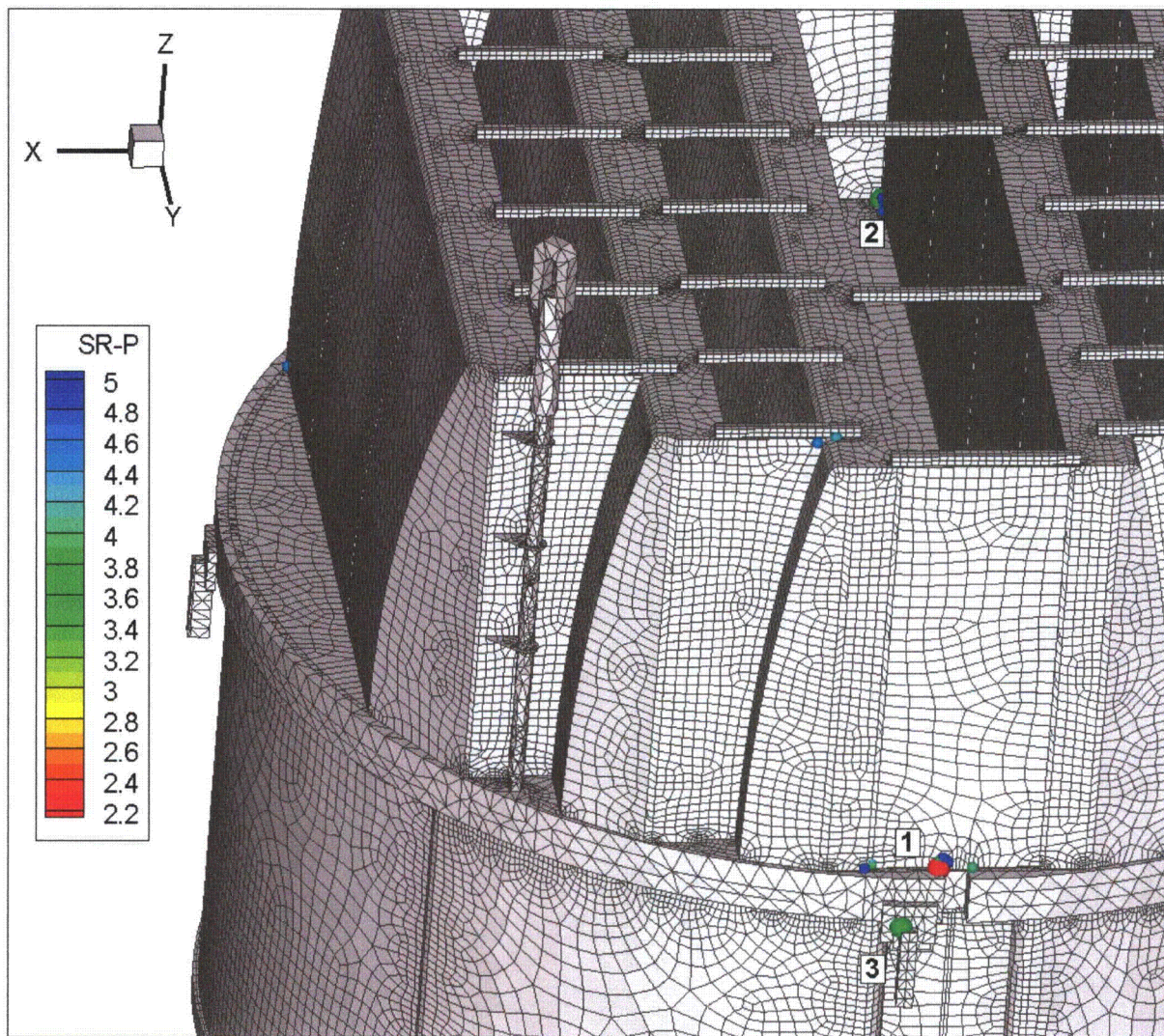


Figure 29a. Locations of nodes with stress ratios, $SR-P \leq 5$, associated with a maximum stress at non-welds for nominal CLTP operation. Numbers refers to the enumerated locations for SR-P values at non-welds in Table 13a.

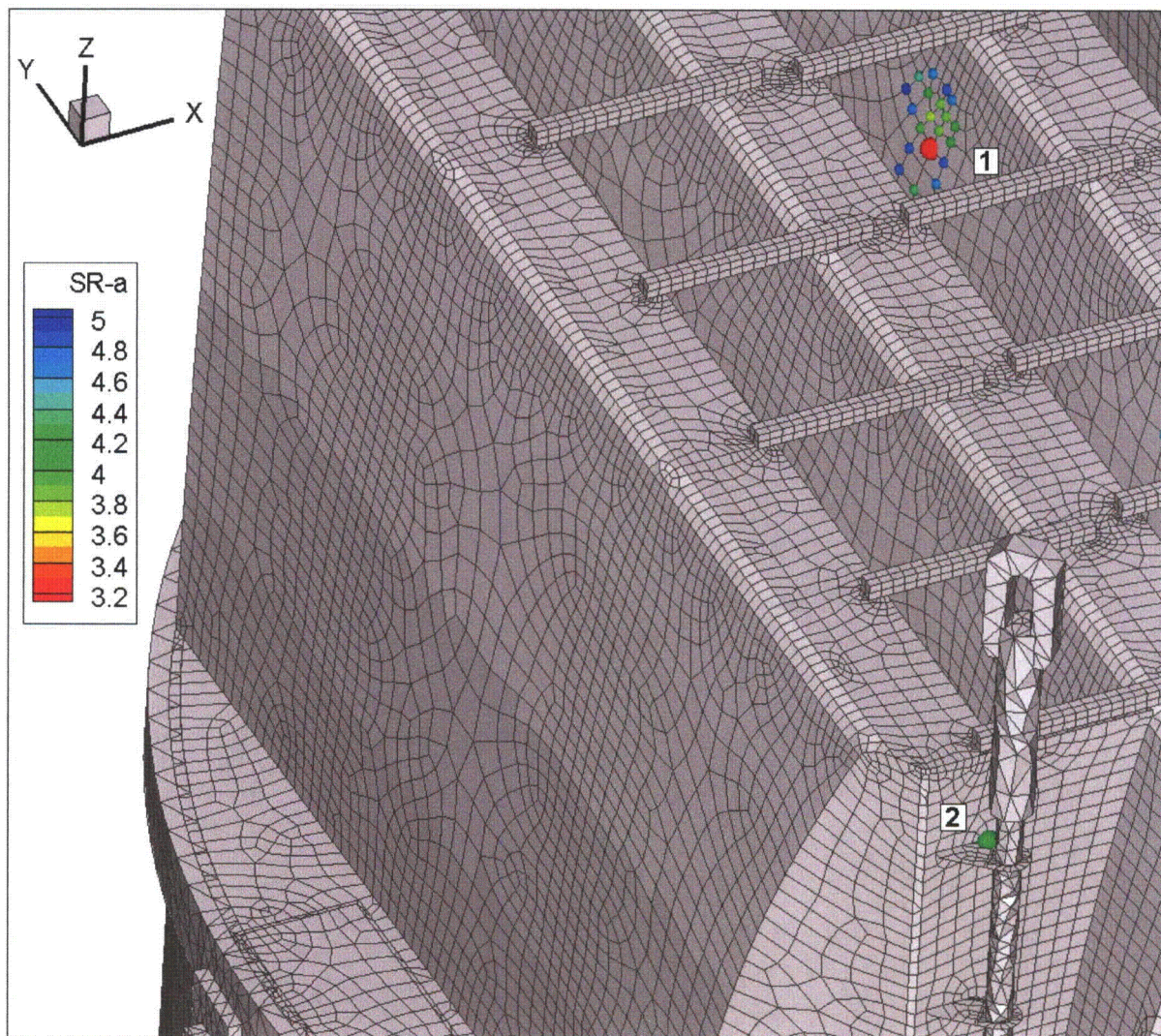


Figure 29b. Locations of smallest alternating stress ratios, $SR-a \leq 5$, at non-welds for nominal CLTP operation. Numbers refer to the enumerated locations for $SR-a$ values at non-welds in Table 13a. View showing locations 1 and 2.

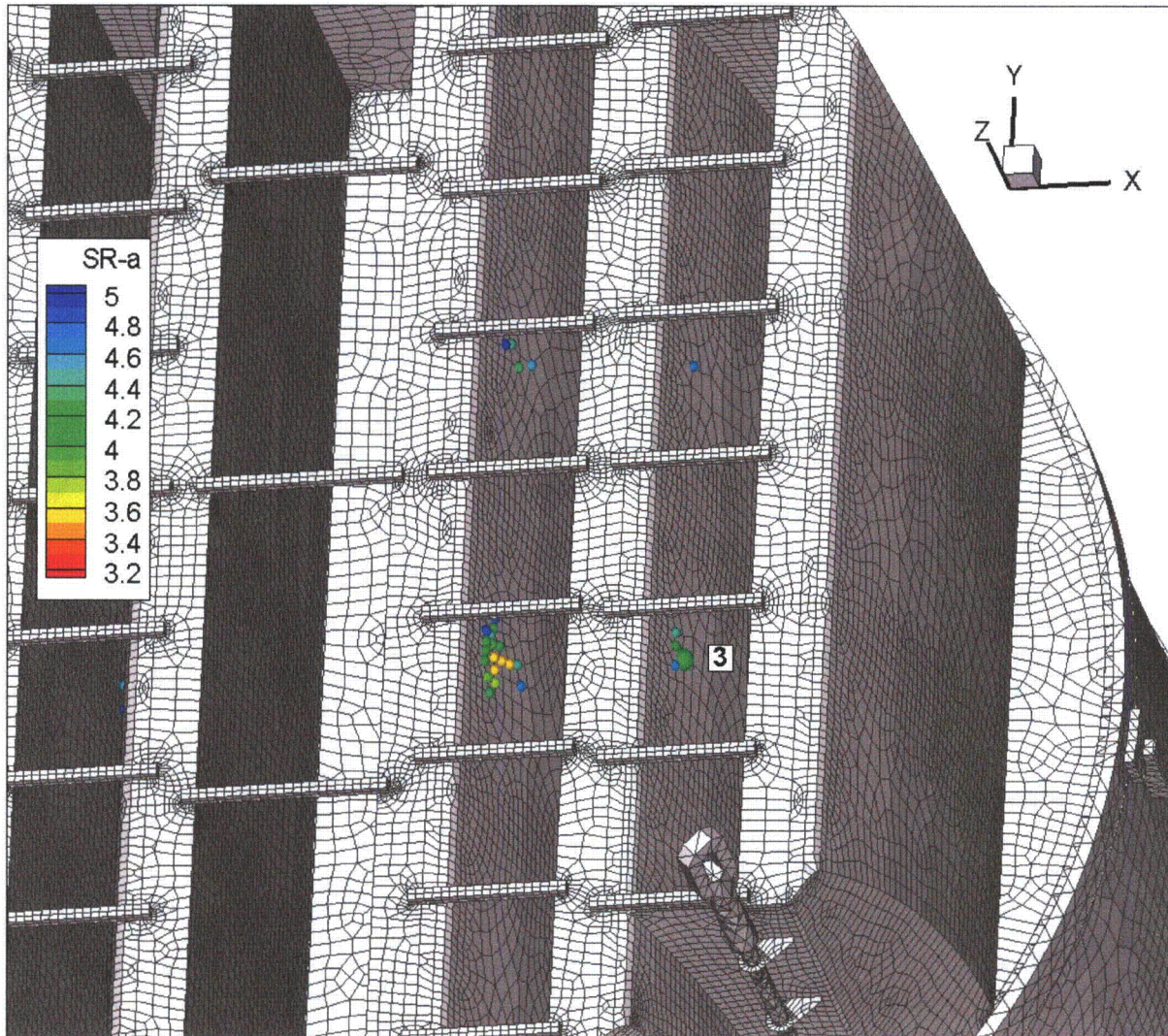


Figure 29c. Locations of smallest alternating stress ratios, $SR-a \leq 5$, at non-welds for nominal CLTP operation. Numbers refer to the enumerated locations for SR-a values at non-welds in Table 13a. View showing location 2.

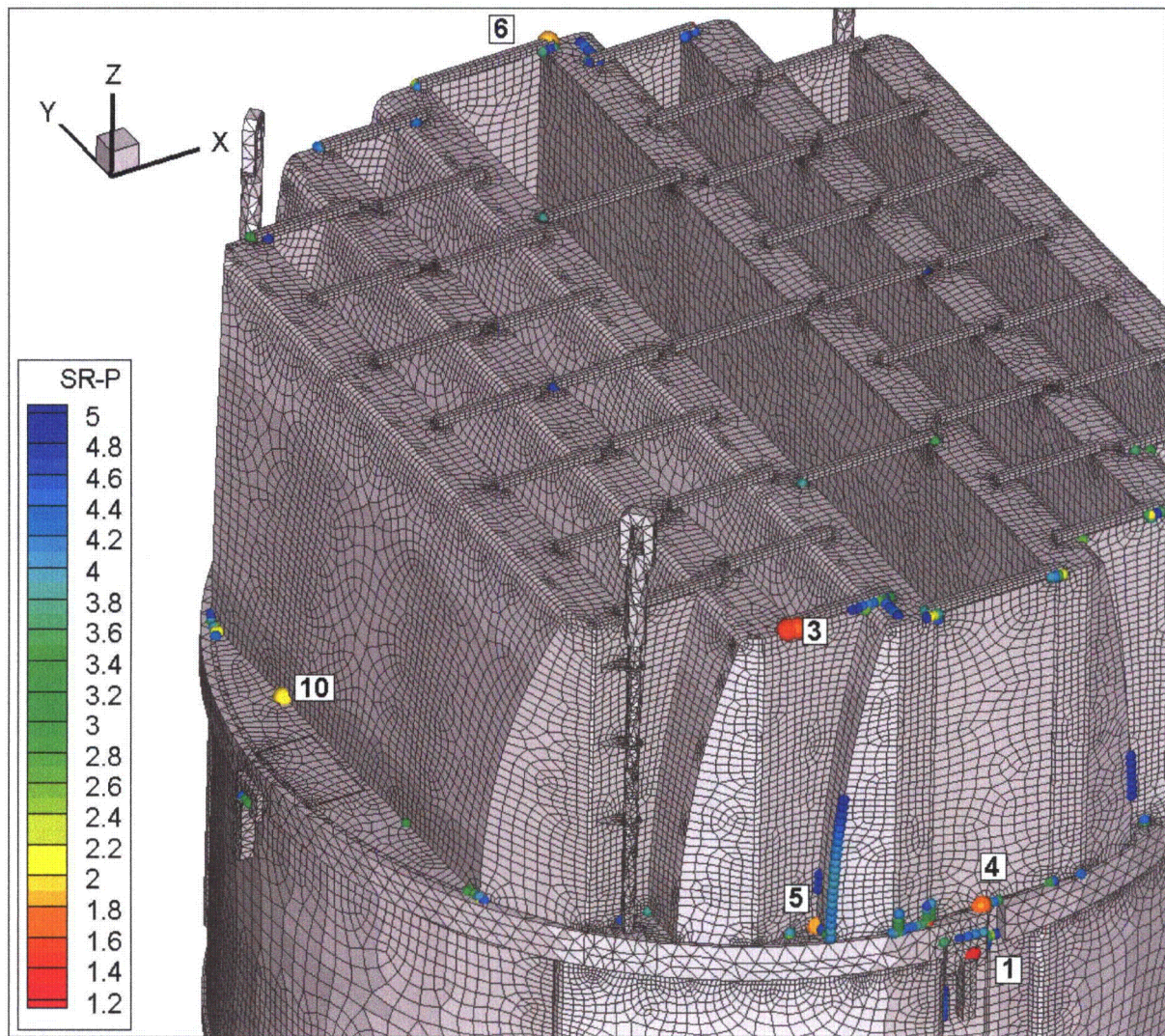


Figure 29d. Locations of smallest stress ratios, $SR-P \leq 5$, associated with maximum stresses at welds for nominal CLTP operation. Numbers refer to the enumerated locations for SR-P values at welds in Table 13b. This view shows locations 1, 3-6 and 10.

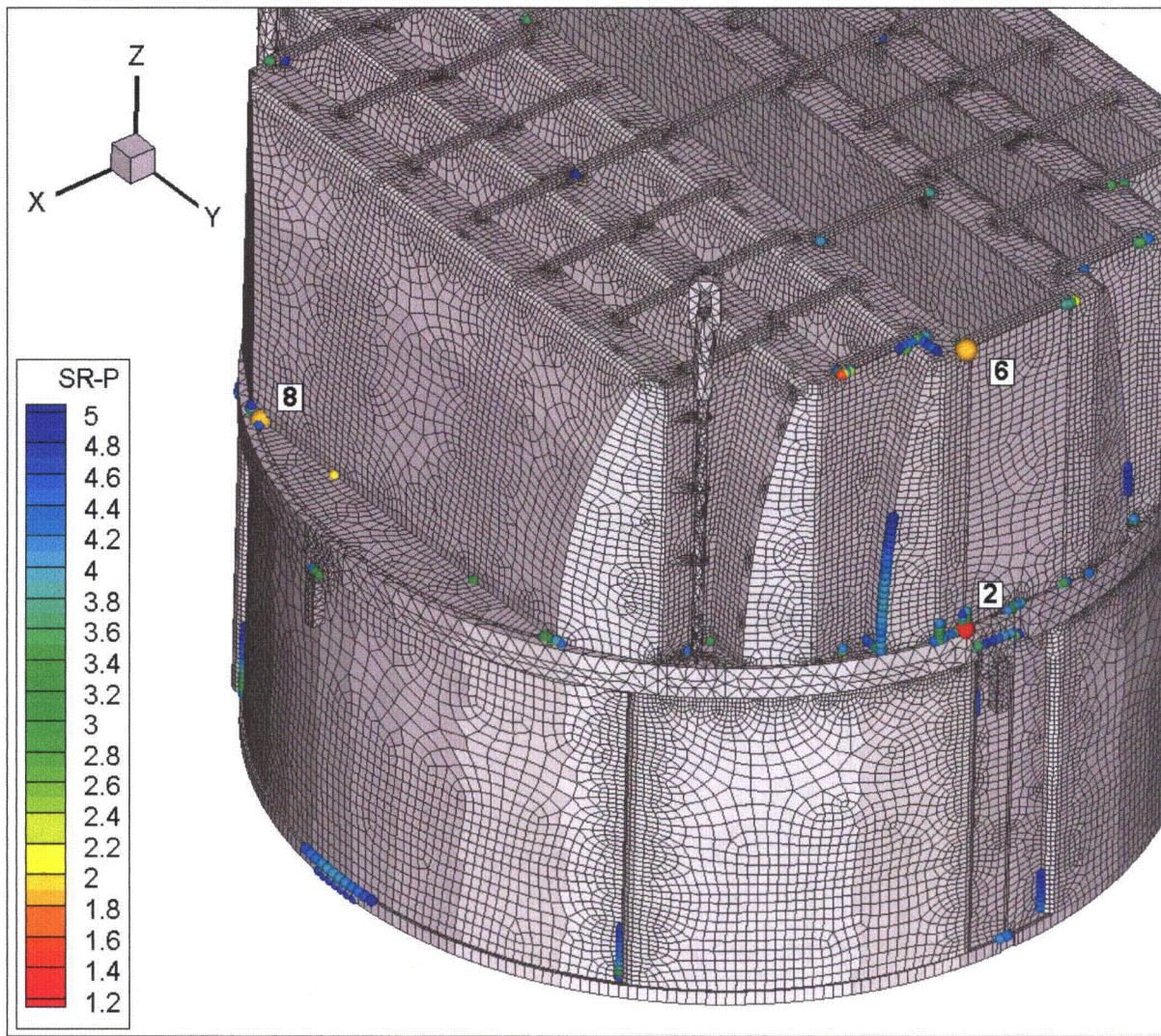


Figure 29e. Locations of minimum stress ratios, $SR-P \leq 5$, associated with maximum stresses at welds for nominal CLTP operation. Numbers refer to the enumerated locations for SR-P values at welds in Table 13b. This view shows locations 2, 6 and 8.

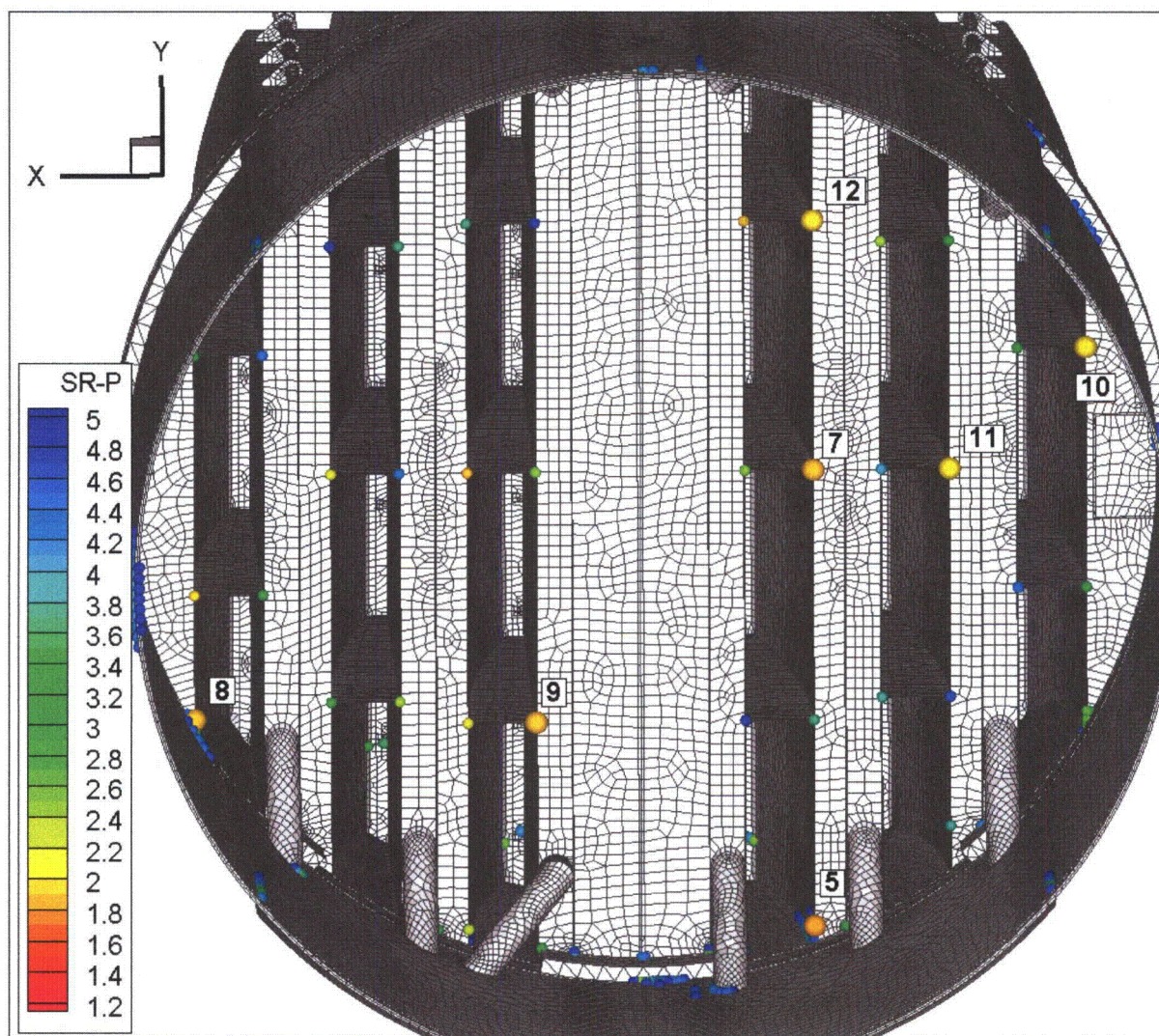


Figure 29f. Locations of minimum stress ratios, $SR-P \leq 5$, associated with maximum stresses at welds for nominal CLTP operation. Numbers refer to the enumerated locations for SR-P values at welds in Table 13b. This view shows locations 5 and 7-12

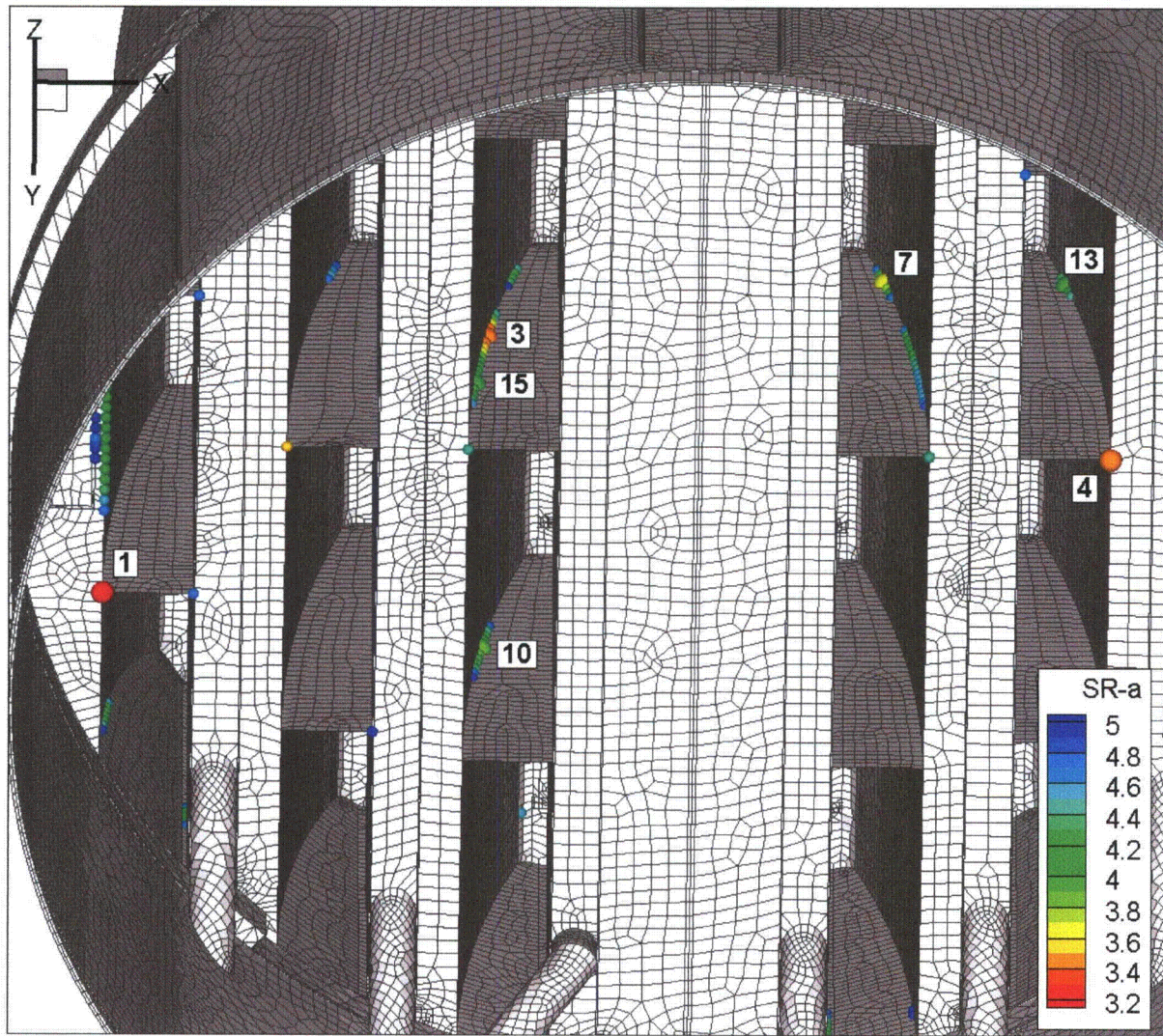


Figure 29g. Locations of minimum alternating stress ratios, $SR-a \leq 5$, at welds for nominal CLTP operation. Numbers refer to the enumerated locations for $SR-a$ values at welds in Table 13c. Locations 1, 3, 4, 7, 10, 13 and 15 are shown.

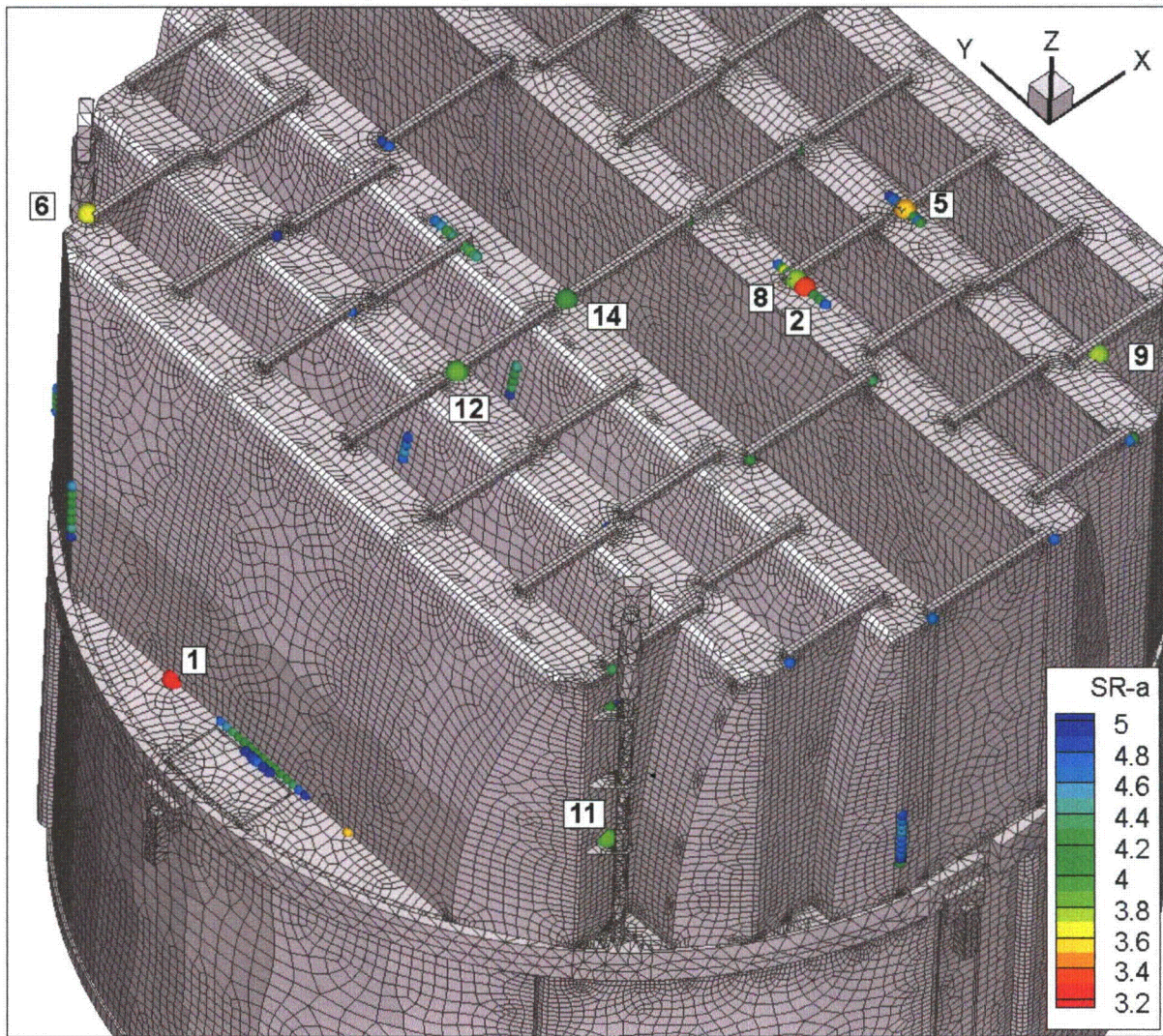


Figure 29h. Locations of minimum alternating stress ratios, $SR-a \leq 5$, at welds for nominal CLTP operation. Numbers refer to the enumerated locations for $SR-a$ values at welds in Table 13c. Locations 2, 5, 6, 8, 9, 11, 12 and 14 shown.

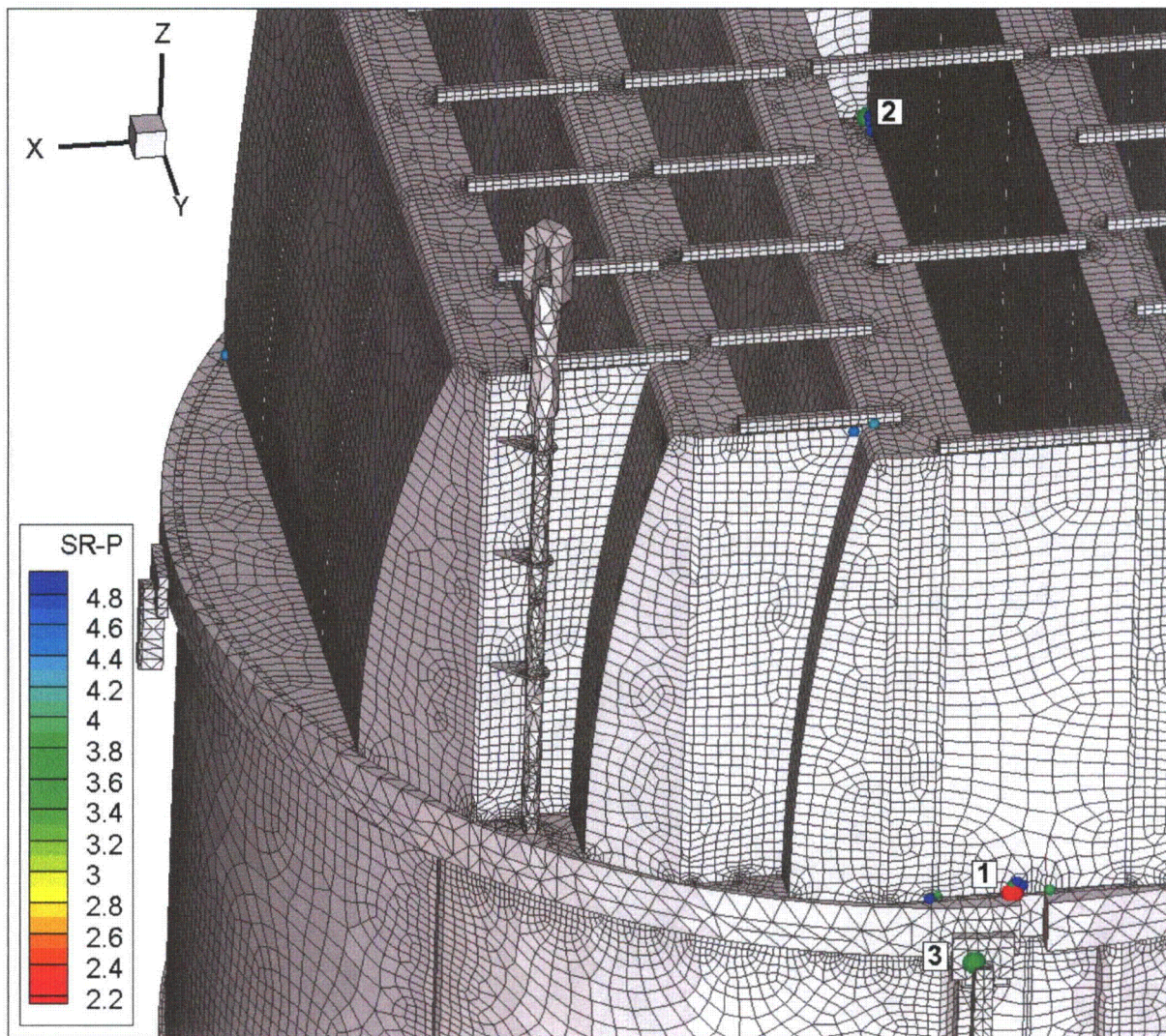


Figure 30a. Locations of minimum stress ratios, $SR-P \leq 5$, associated with maximum stresses at non-welds for CLTP operation with frequency shifts. The recorded stress ratio is the minimum value taken over all frequency shifts. The numbers refers to the enumerated location for SR-P values at non-welds in Table 14a.

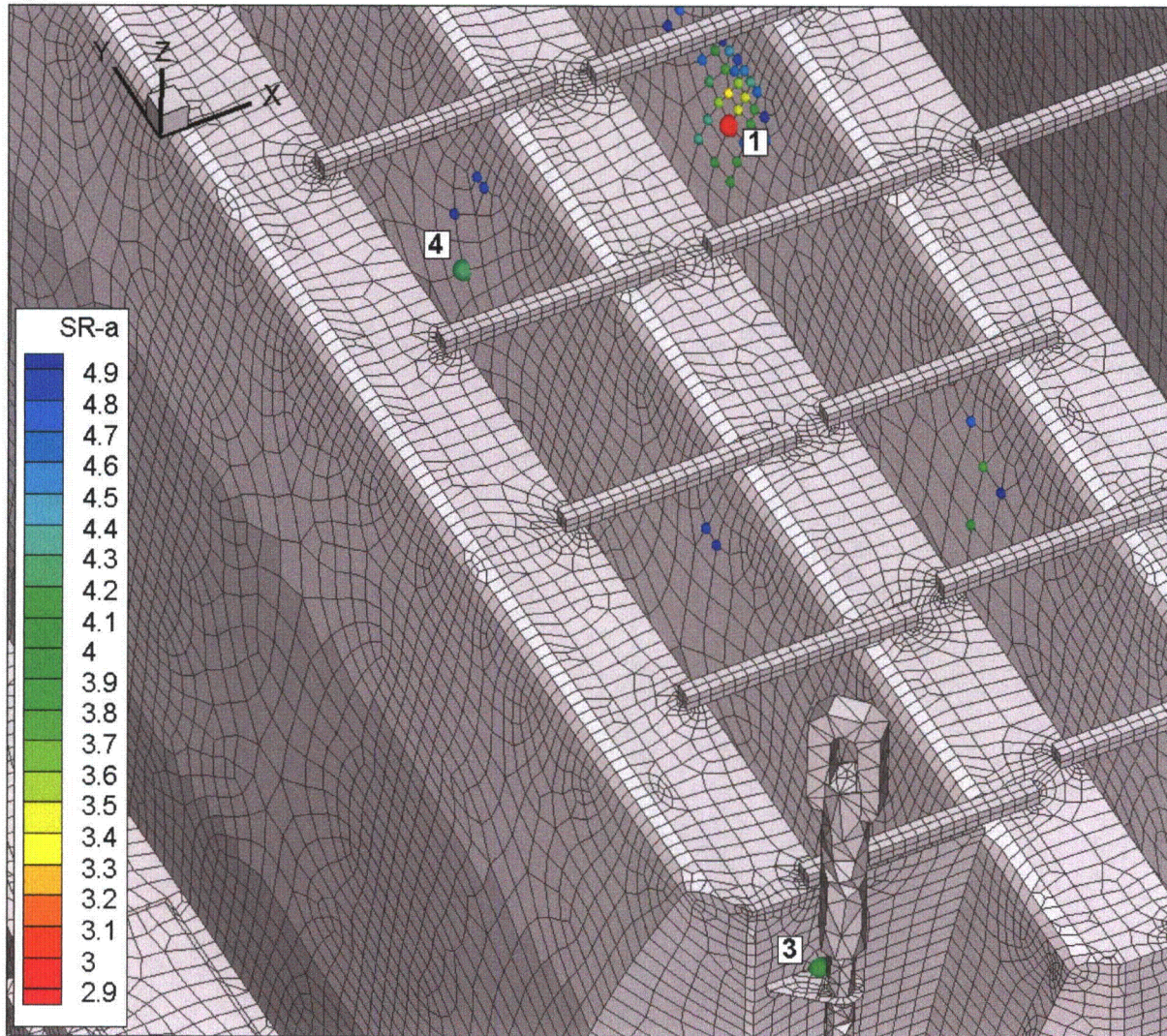


Figure 30b. Locations of minimum alternating stress ratios, $SR-a \leq 5$, at non-welds for CLTP operation with frequency shifts. The recorded stress ratio at a node is the minimum value taken over all frequency shifts. Numbers refer to the enumerated locations for $SR-a$ values at non-welds in Table 14a. View showing locations 1, 3 and 4.

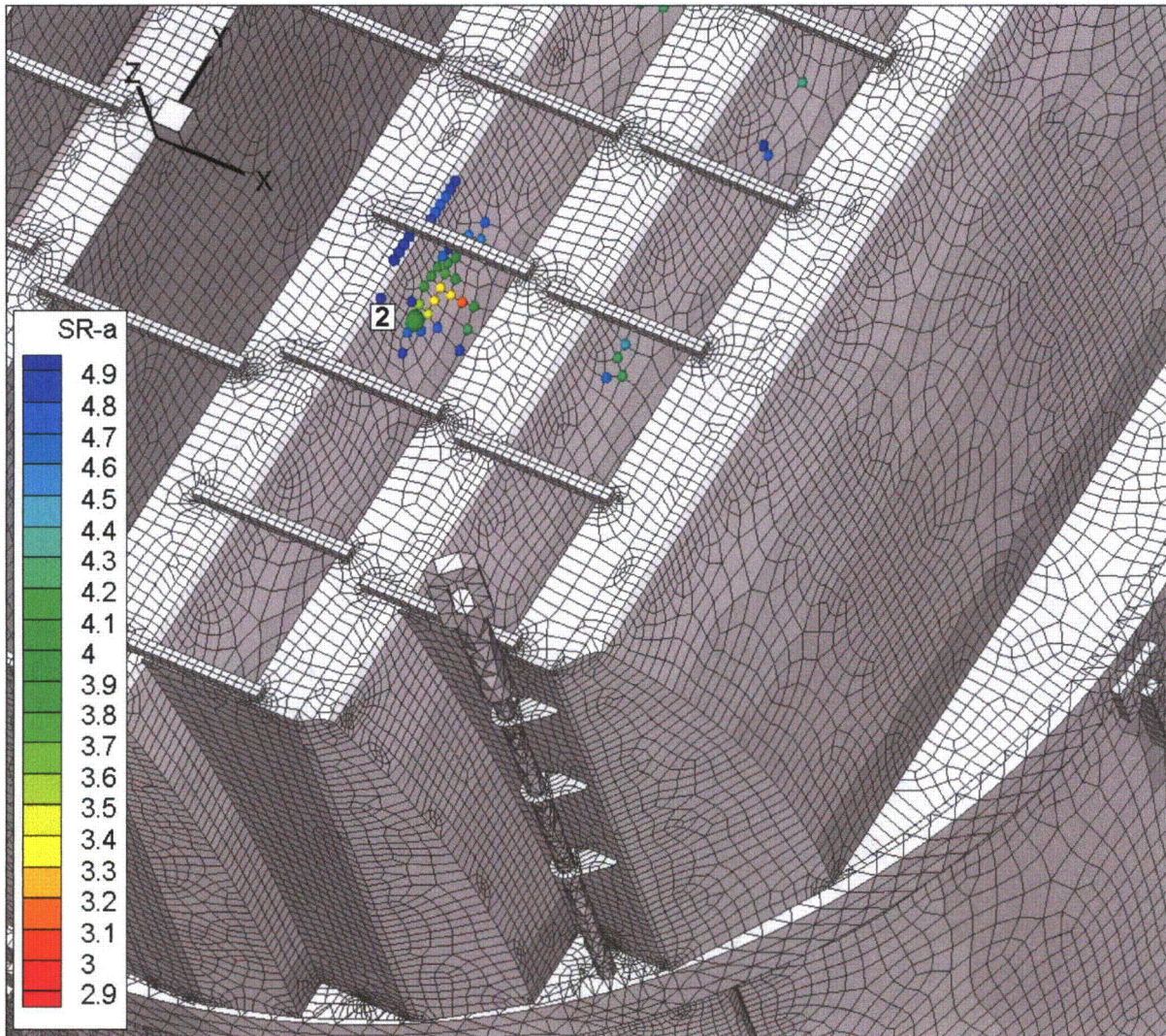


Figure 30c. Locations of minimum alternating stress ratios, $SR-a \leq 5$, at non-welds for CLTP operation with frequency shifts. The recorded stress ratio at a node is the minimum value taken over all frequency shifts. Numbers refer to the enumerated locations for $SR-a$ values at non-welds in Table 14a. View showing location 2.

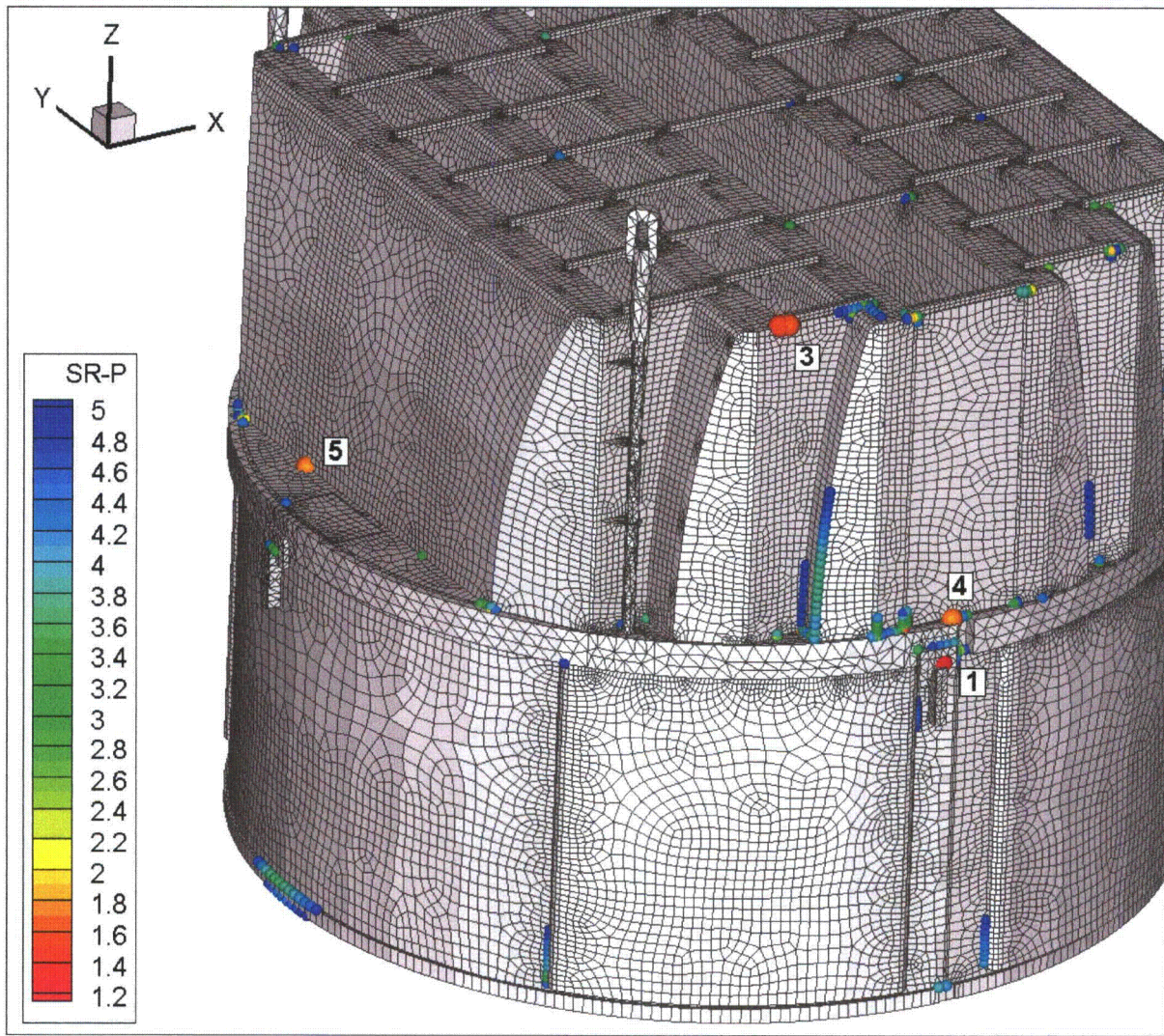


Figure 30d. Locations of minimum stress ratios, $SR-P \leq 5$, associated with maximum stresses at welds for CLTP operation with frequency shifts. The recorded stress ratio at a node is the minimum value taken over all frequency shifts. Numbers refer to the enumerated locations for SR-P values at welds in Table 14b. This view shows locations 1 and 3-5.

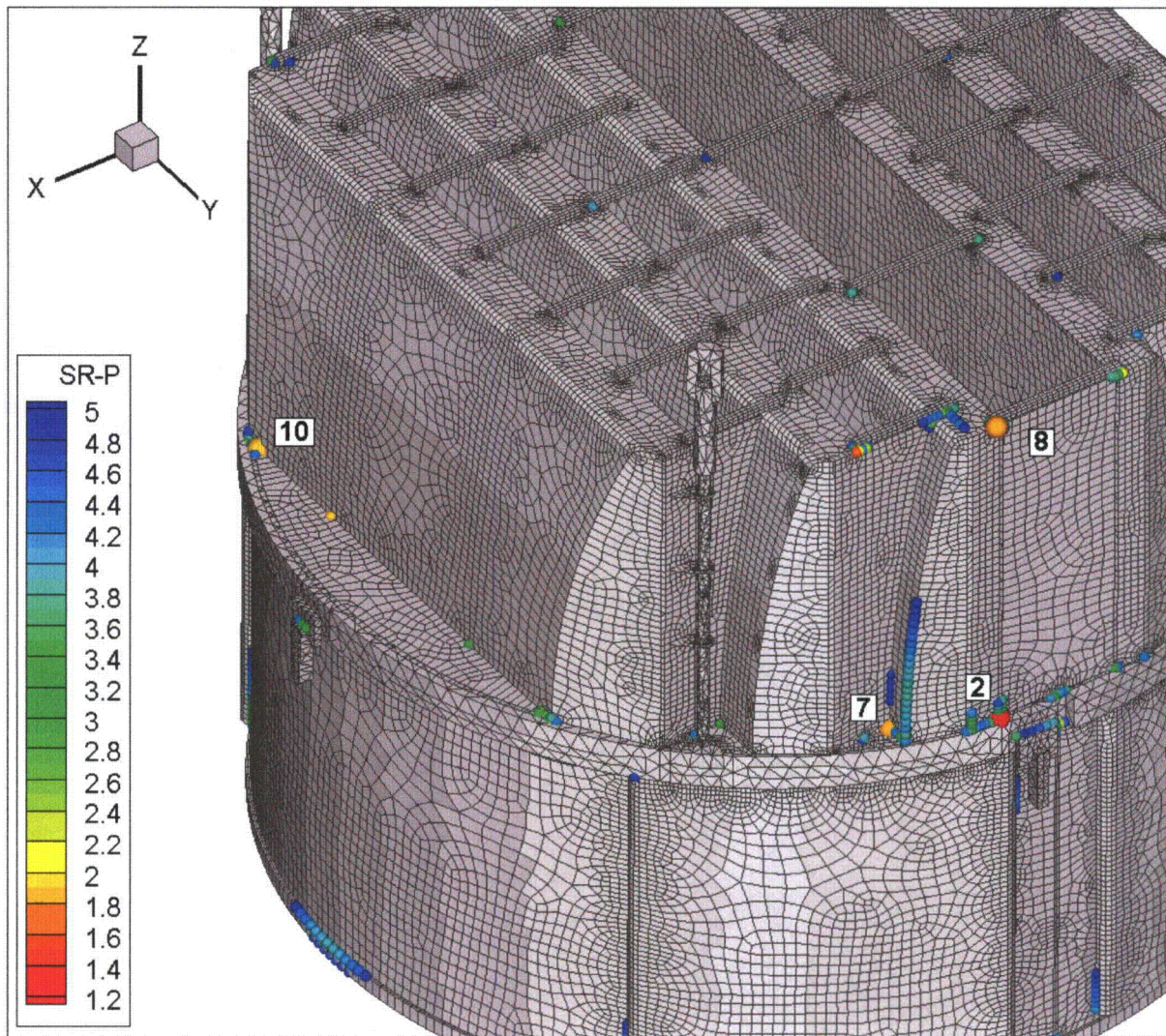


Figure 30e. Locations of minimum stress ratios, $SR-P \leq 5$, associated with maximum stresses at welds for CLTP operation with frequency shifts. The recorded stress ratio at a node is the minimum value taken over all frequency shifts. Numbers refer to the enumerated locations for SR-P values at welds in Table 14b. This view shows locations 2, 7, 8 and 10.

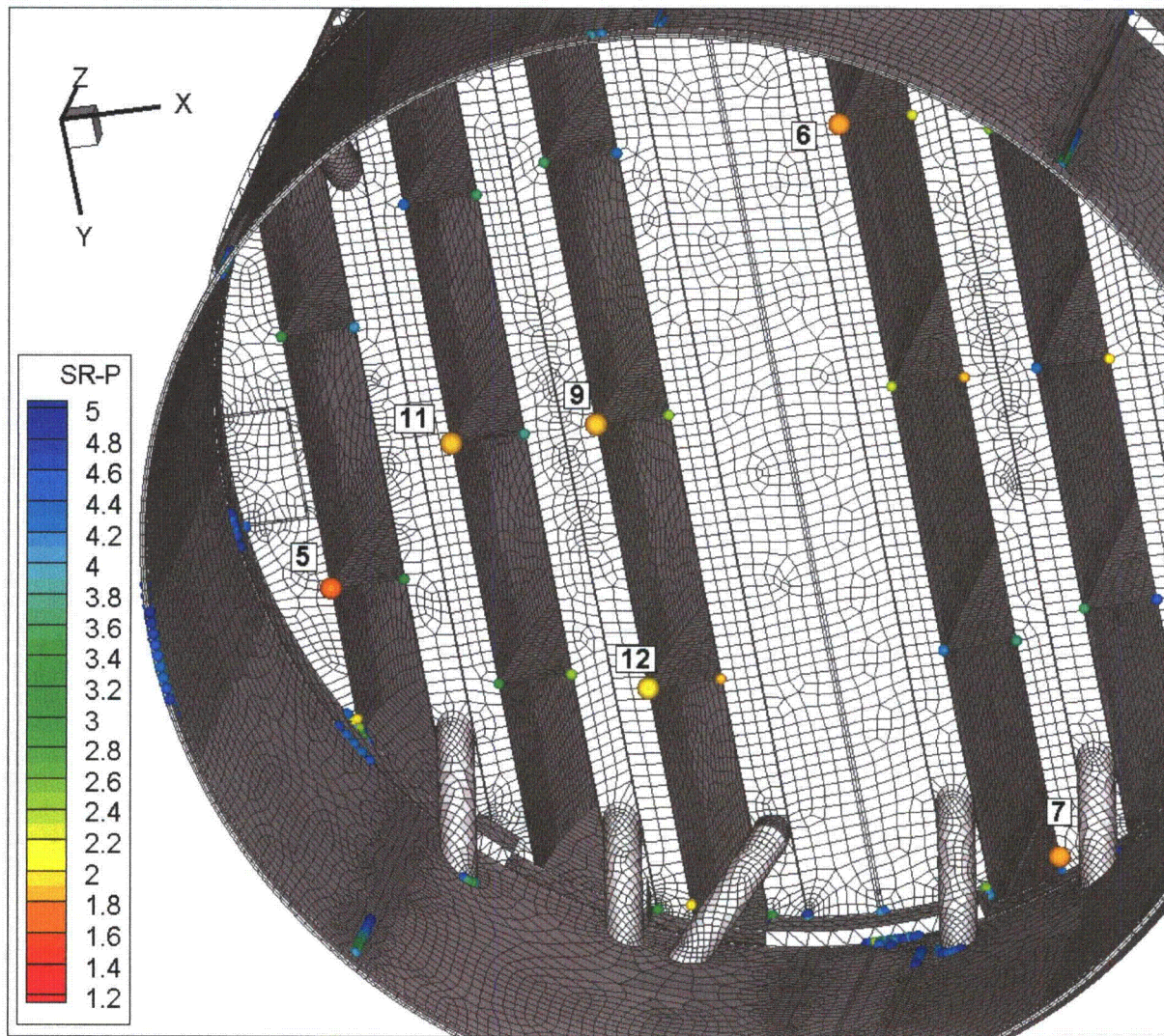


Figure 30f. Locations of minimum stress ratios, $SR-P \leq 5$, at welds for CLTP operation with frequency shifts. The recorded stress ratio at a node is the minimum value taken over all frequency shifts. Numbers refer to the enumerated locations for SR-P values at welds in Table 14b. This view from below shows locations 5-7, 9, 11 and 12.

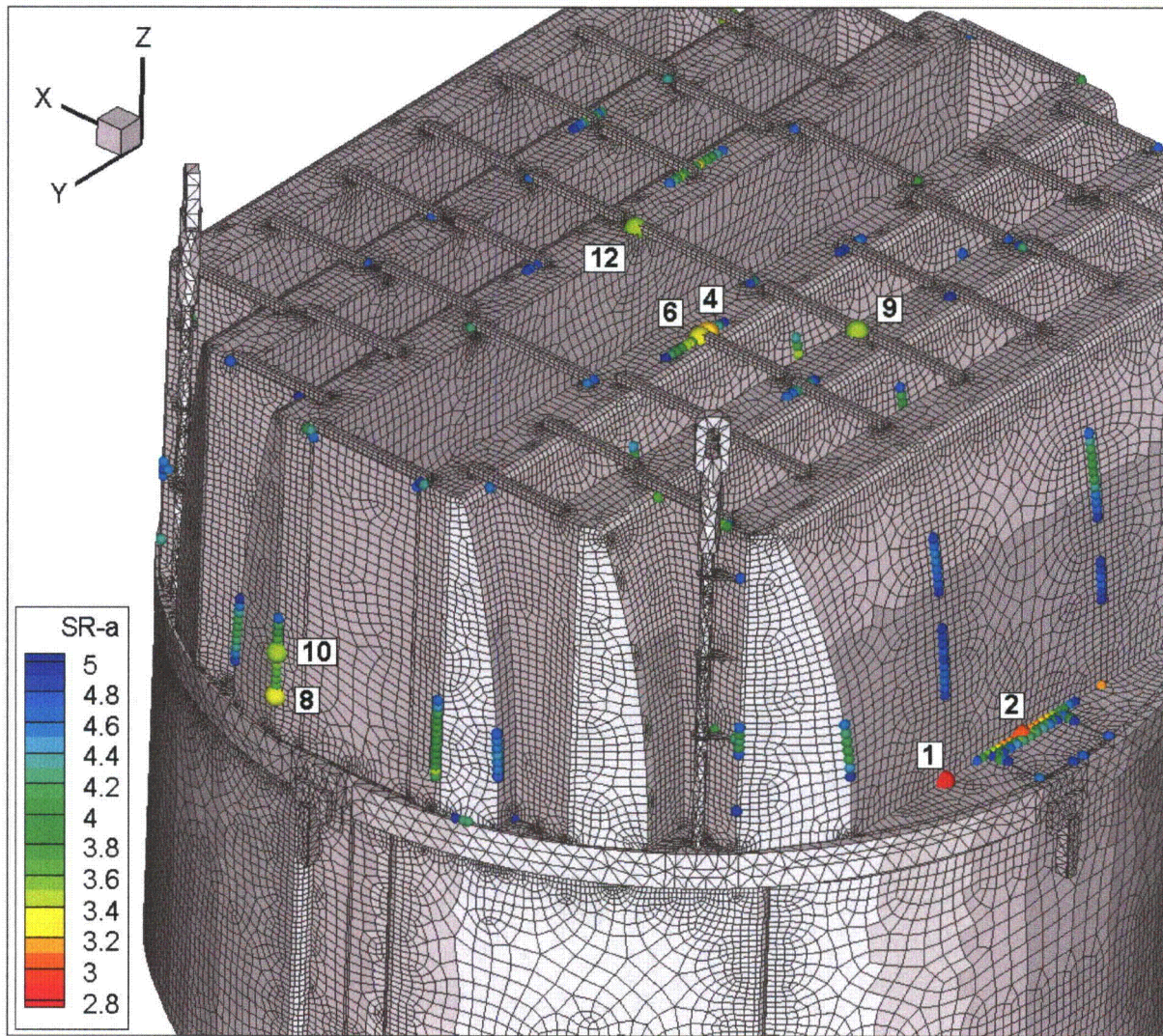


Figure 30g. Locations of minimum alternating stress ratios, $SR-a \leq 5$, at welds for CLTP operation with frequency shifts. The recorded stress ratio at a node is the minimum value taken over all frequency shifts. Numbers refer to the enumerated locations for $SR-a$ values at welds in Table 14c. This view shows locations 1, 2, 4, 6, 8-10 and 12.

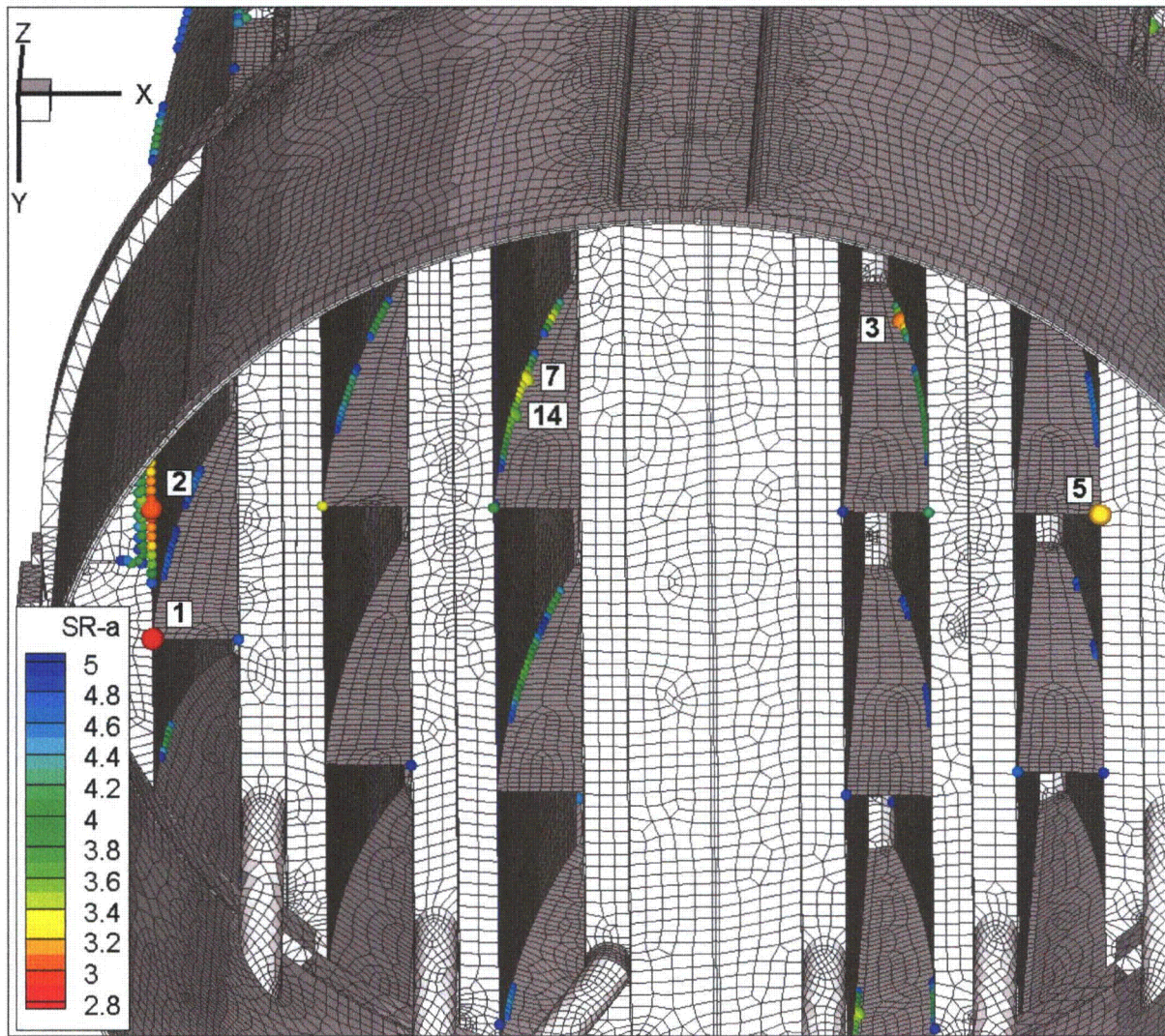


Figure 30h. Locations of minimum alternating stress ratios, $SR-a \leq 5$, at welds for CLTP operation with frequency shifts. The recorded stress ratio at a node is the minimum value taken over all frequency shifts. Numbers refer to the enumerated locations for $SR-a$ values at welds in Table 14c. View showing locations 1-3, 5, 7 and 14.

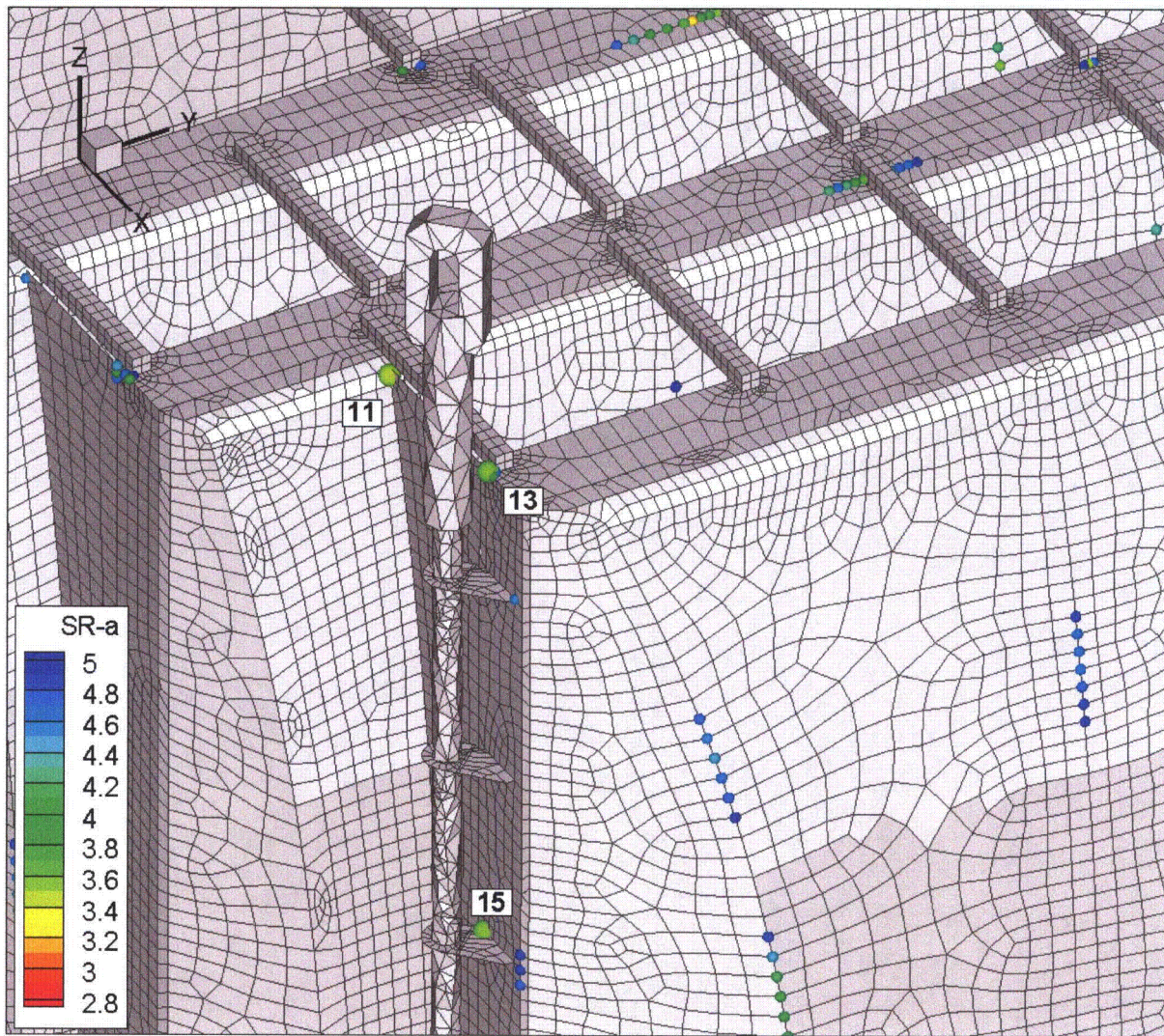


Figure 30i. Locations of minimum alternating stress ratios, $SR-a \leq 5$, at welds for CLTP operation with frequency shifts. The recorded stress ratio at a node is the minimum value taken over all frequency shifts. Numbers refer to the enumerated locations for $SR-a$ values at welds in Table 14c. View around locations 11, 13 and 15.

6.3 Frequency Content and Filtering of the Stress Signals

The frequency contribution to the stresses can be investigated by examining the power spectral density (PSD) curves and accumulative PSDs for selected nodes having low alternating stress ratios. The accumulative PSDs are computed directly from the Fourier coefficients as

$$\Sigma(\omega_n) = \sqrt{\sum_{k=1}^n |\tilde{\sigma}(\omega_k)|^2}$$

where $\tilde{\sigma}(\omega_k)$ is the complex stress harmonic at frequency, ω_k . Accumulative PSD plots are useful for determining the frequency components and frequency ranges that make the largest contributions to the fluctuating stress. Unlike PSD plots, no “binning” or smoothing of frequency components is needed to obtain smooth curves. Steep step-like rises in $\Sigma(\omega)$ indicate the presence of a strong component at a discrete frequency whereas gradual increases in the curve imply significant content over a broader frequency range. From Parseval’s theorem, equality between $\Sigma(\omega_N)$ (where N is the total number of frequency components) and the RMS of the stress signal in the time domain is established.

The selected nodes are the ones having the lowest alternating stress ratios (at a weld) in Table b. These are:

- Node 95267 – located on the welded common junction between the outer hood, hood support and outer cover plate. The associated PSDs are shown in Figure 31a.
- Node 99540 – located on the weld joining the inner hood and hood support. The associated PSDs are shown in Figure 31b.
- Node 99130 – located on the weld joining the tie bar and inner vane bank top plate. The associated PSDs are shown in Figure 31c.
- Node 91091 – located on the weld joining the tie bar and vane bank top plate and end plate. The associated PSDs are shown in Figure 31d.
- Node 87633 – located on the lifting rod brace/vane bank end plate connection. The associated PSDs are shown in Figure 31e.

These are the nodes labeled 1, 3, 6, 8 and 15 in Table c for alternating stresses on a weld and accompanying Figure 30g-i.

In each case, since there are six stress components and up to three different section locations for shells (the top, mid and bottom surfaces), there is a total of 18 stress histories per component. Moreover, at junctions there are at least two components that meet at the junction. The particular stress component that is plotted is chosen as follows. First, the component and section location (top/mid/bottom) is taken as the one that has the highest alternating stress. This narrows the selection to six components. Of these, the component having the highest Root Mean Square (RMS) is selected.

The first node (95267) is dominated by a peak centered at near 60.5 Hz for the -10% shifted case. From the accumulative PSD it is evident that frequency shifting increases this peak, but

does not shift its frequency. This is indicative of a peak in the signal moving closer to a structural resonance. A very similar behavior is observed for node 99540 which has dominant frequencies at 60.5 Hz and 52.1 Hz. At the limiting +5% frequency shift the former peak grows with the frequency shift whereas the second one attenuates. The third node (99130) also follows the same behavior with two dominant peaks being present at the same frequencies and behaving in a similar manner when moving to the limiting frequency shift. The fourth location (node 910091) is characterized by a dominant peak at 143.9 Hz which at the +5% shift produces a strong resonance at 151.1 Hz. Finally for node 87633, several peaks are present whose relative dominance changes with frequency shifting from 108 Hz (no shift) to 213.9 Hz at the +10% shift.

Another way to characterize the dominant frequencies is to plot the dominant frequency over the dryer surface. For each finite element node the frequency associated with the largest stress harmonic (at any frequency shift) is recorded. A contour map of this dominant frequency is shown in Figure 32. This map is useful in a qualitative sense for identifying what dryer components appear most responsive to particular frequencies. For most of the dryer, including the central section of the outer hoods, the inner hoods and most of the skirt the dominant frequencies are in the 50-55 Hz range as indicated in Figure 32a. From Figure 32b the outer sections of the outer hoods show peak frequencies near 65-75 Hz. The middle and inner hoods respond in the ranges 58-62 Hz.

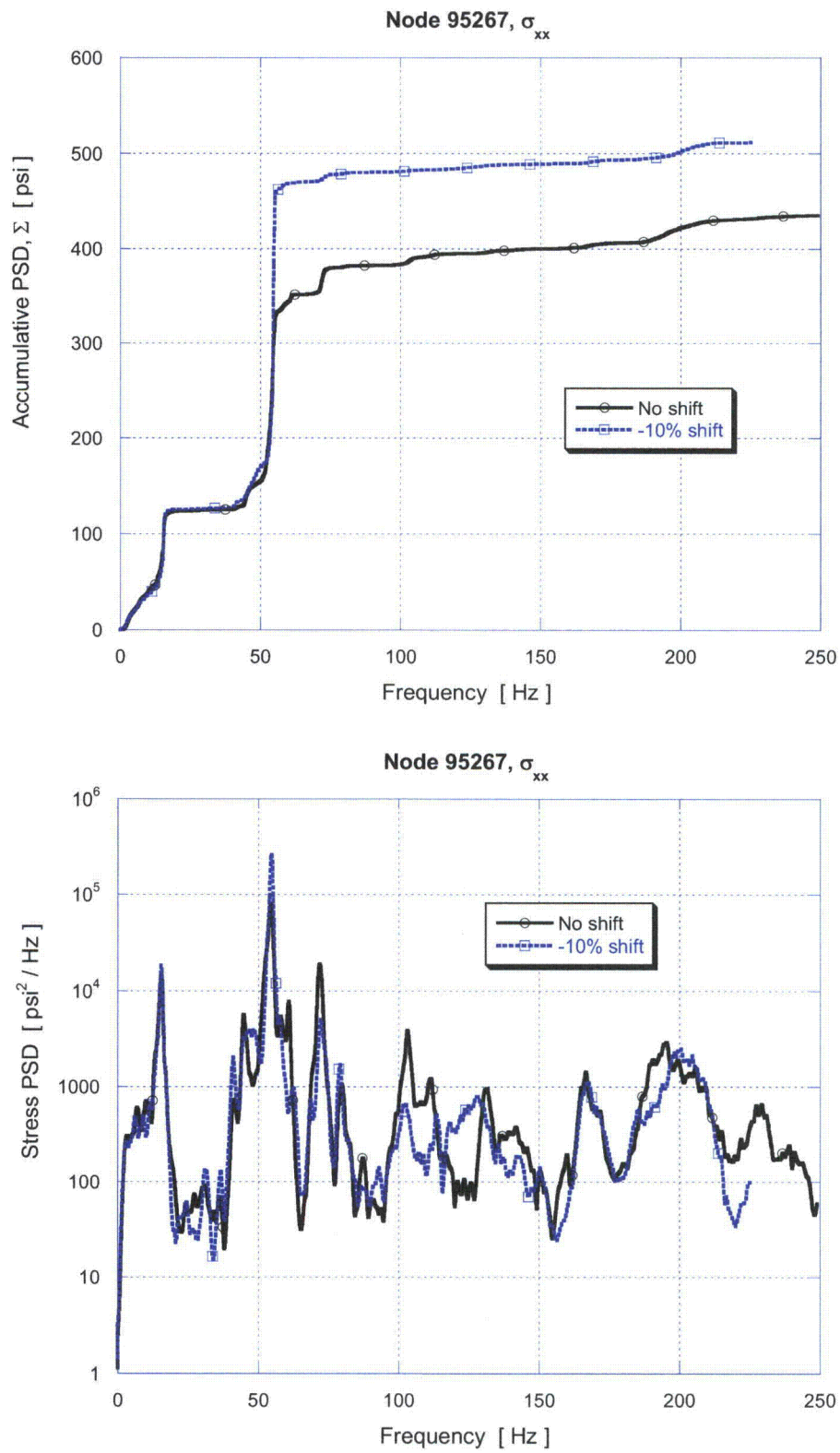


Figure 31a. Accumulative PSD and PSD curves of the σ_{xx} stress response at node 95267.

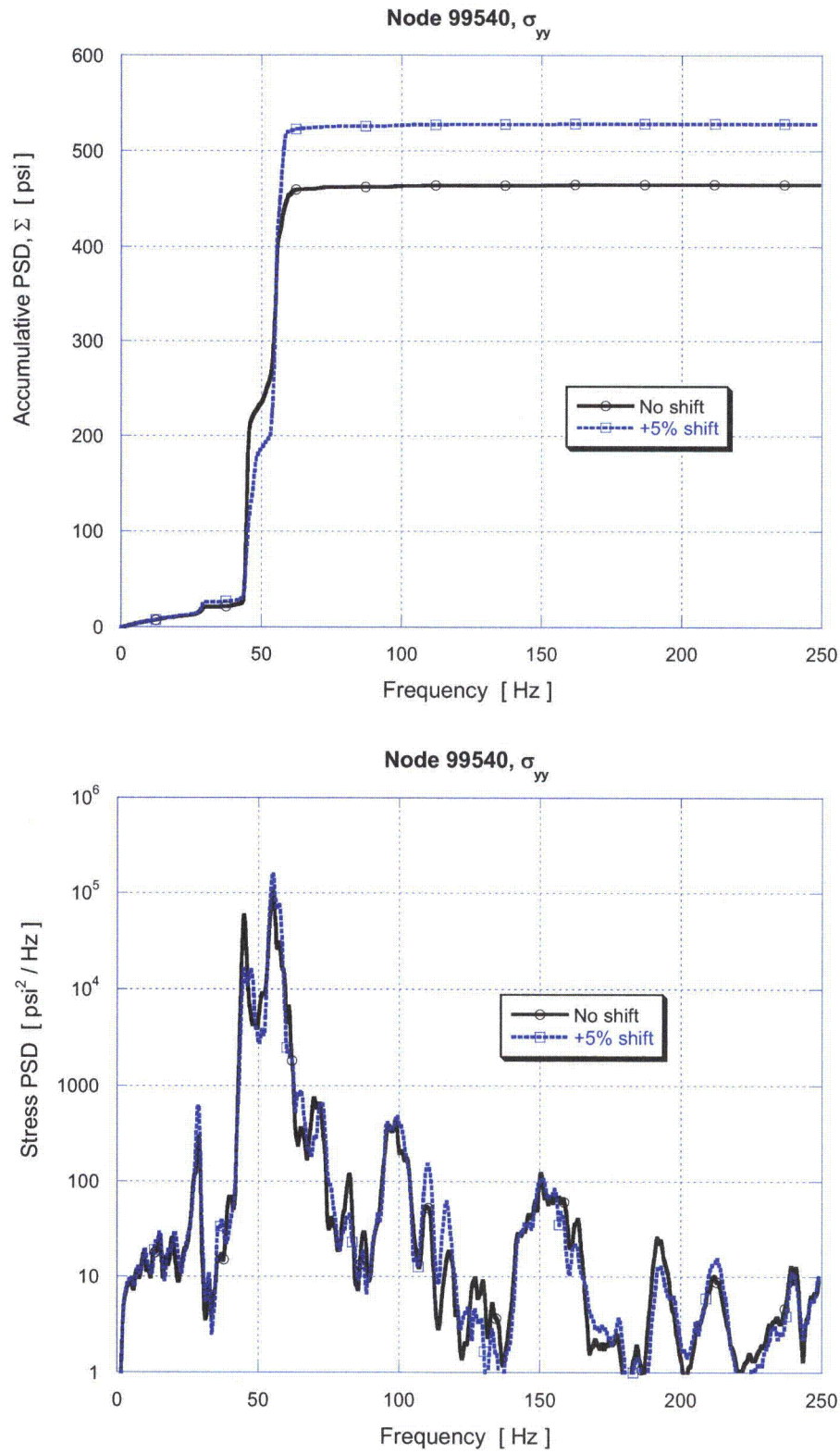


Figure 31b. Accumulative PSD and PSD of the σ_{yy} stress response at node 99540.

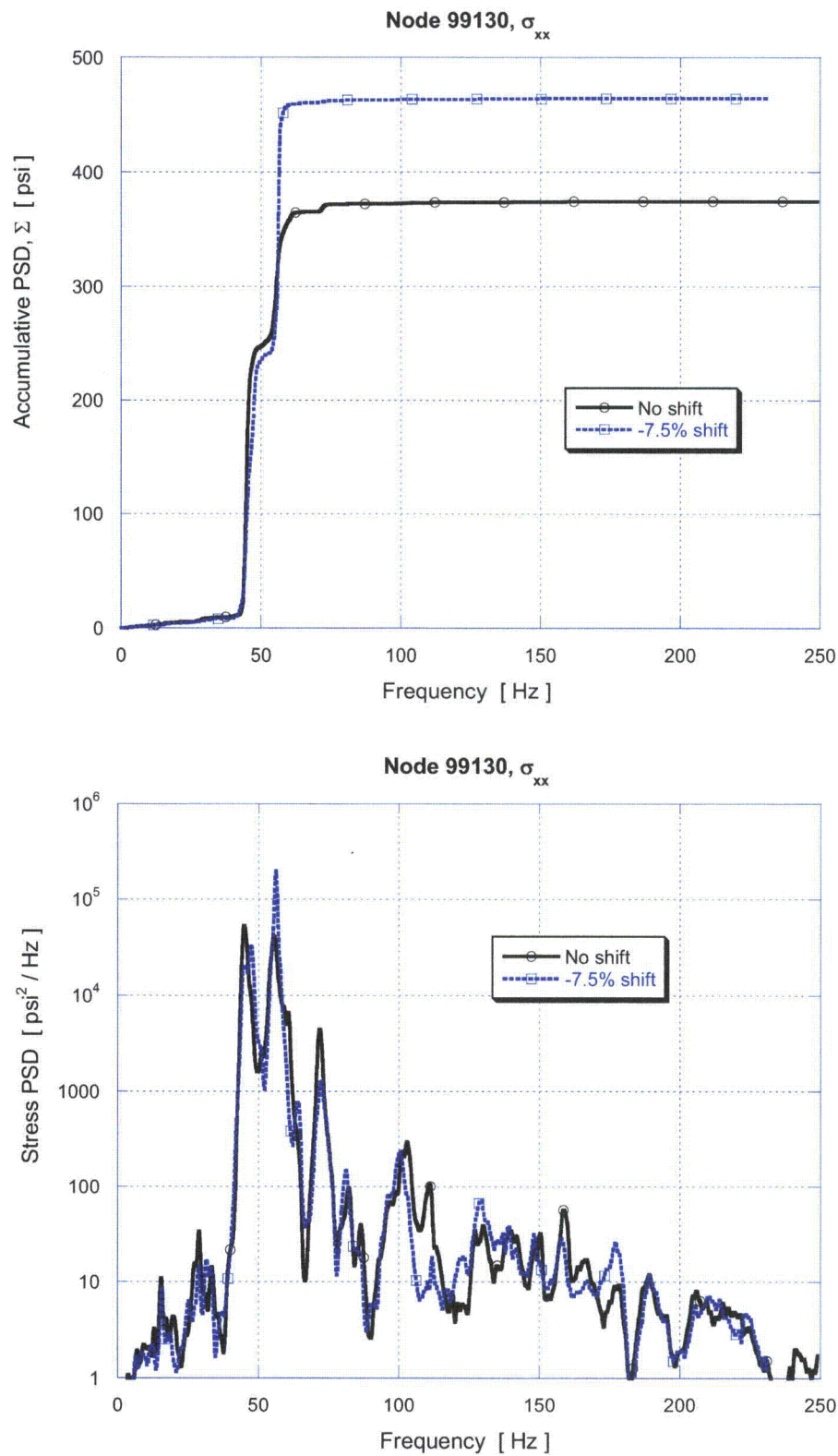


Figure 31c. Accumulative PSD and PSD of the σ_{xx} stress response at node 99130.

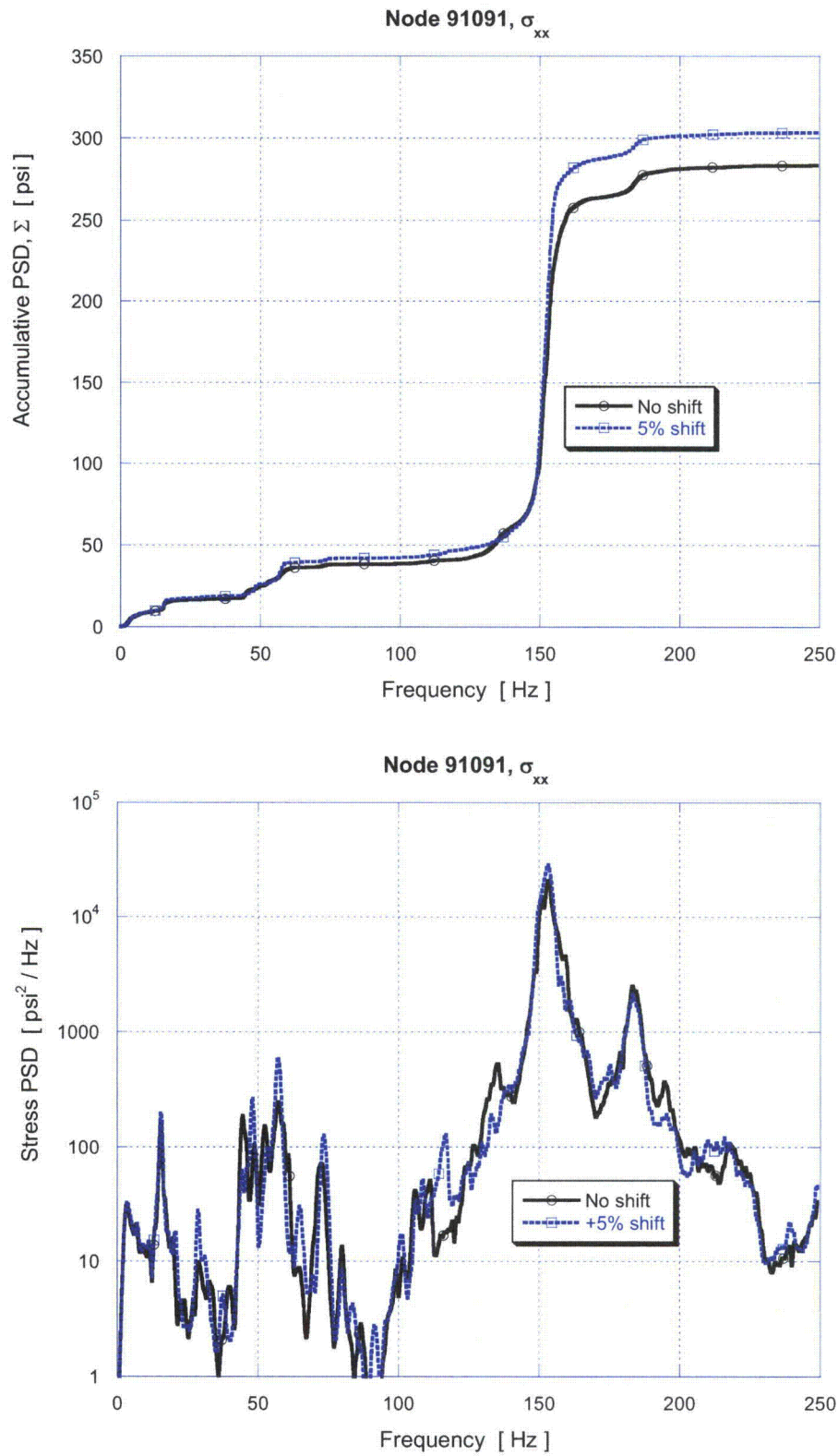


Figure 31d. Accumulative PSD and PSD of the σ_{xx} stress response at node 91091.

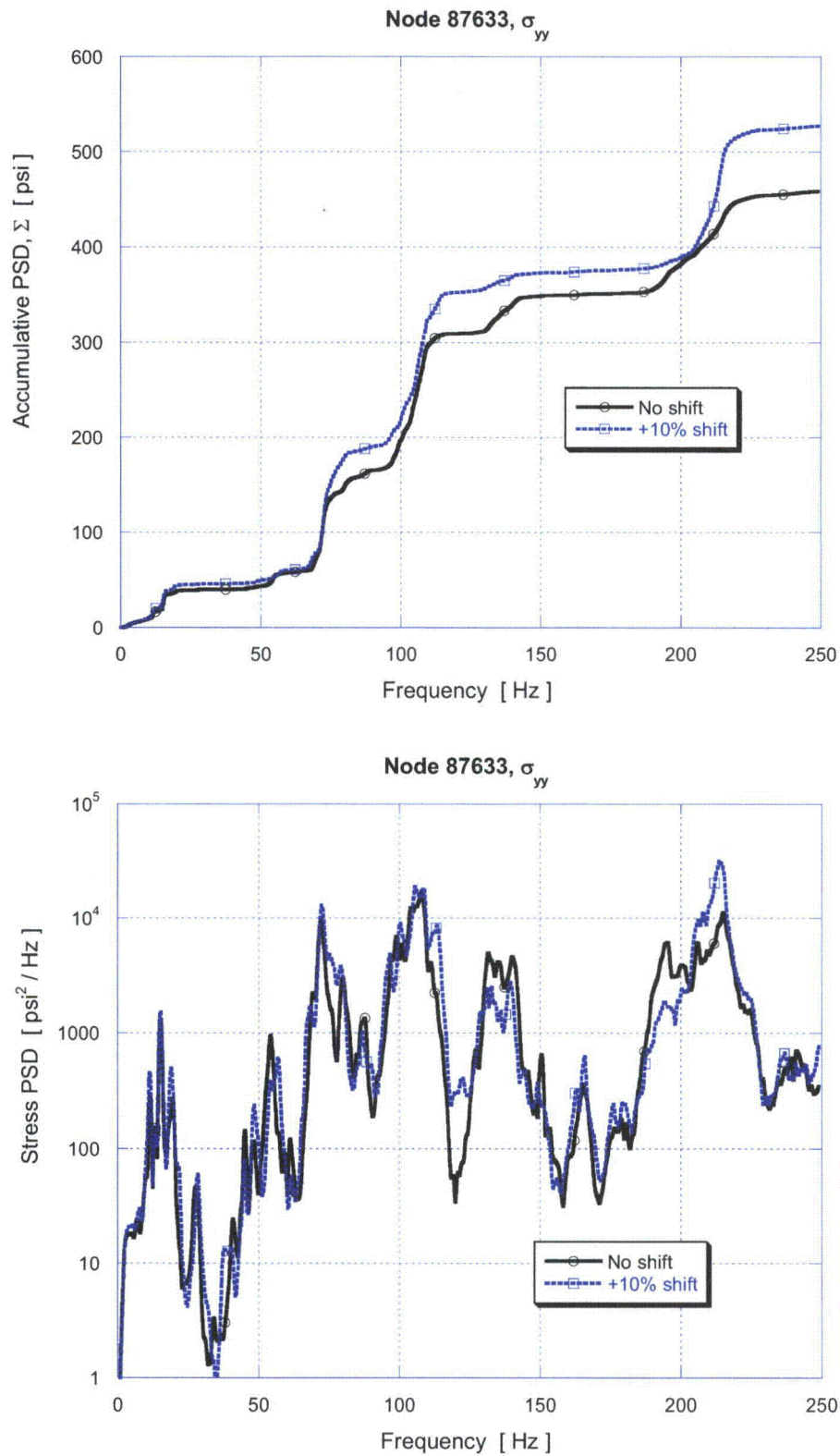


Figure 31e. Accumulative PSD and PSD of the σ_{yy} stress response at node 87633.

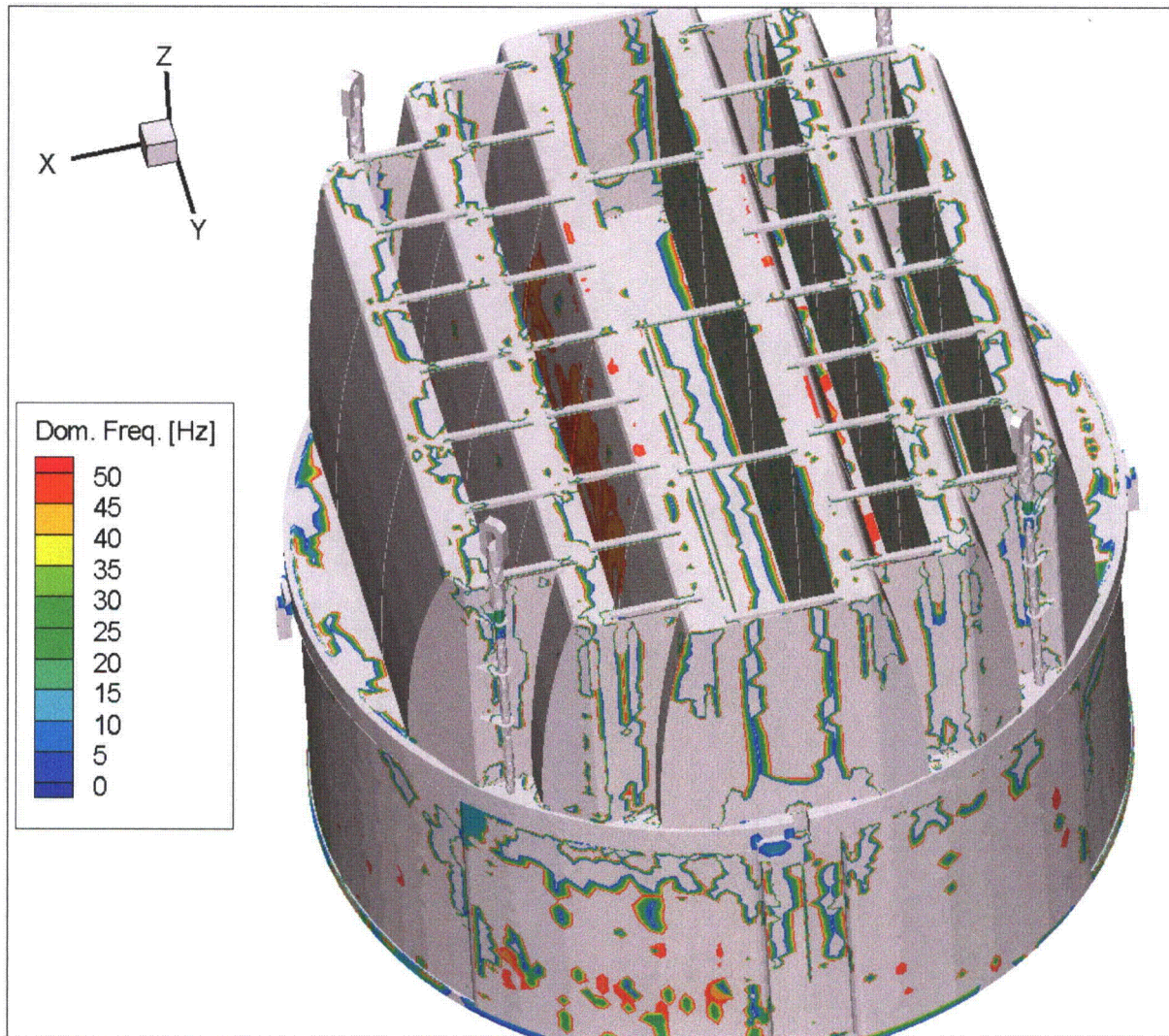


Figure 32a. Contour map showing the dominant frequencies (i.e., the frequency with the largest stress harmonic). This shows locations with dominant frequencies in the range 0-50 Hz.

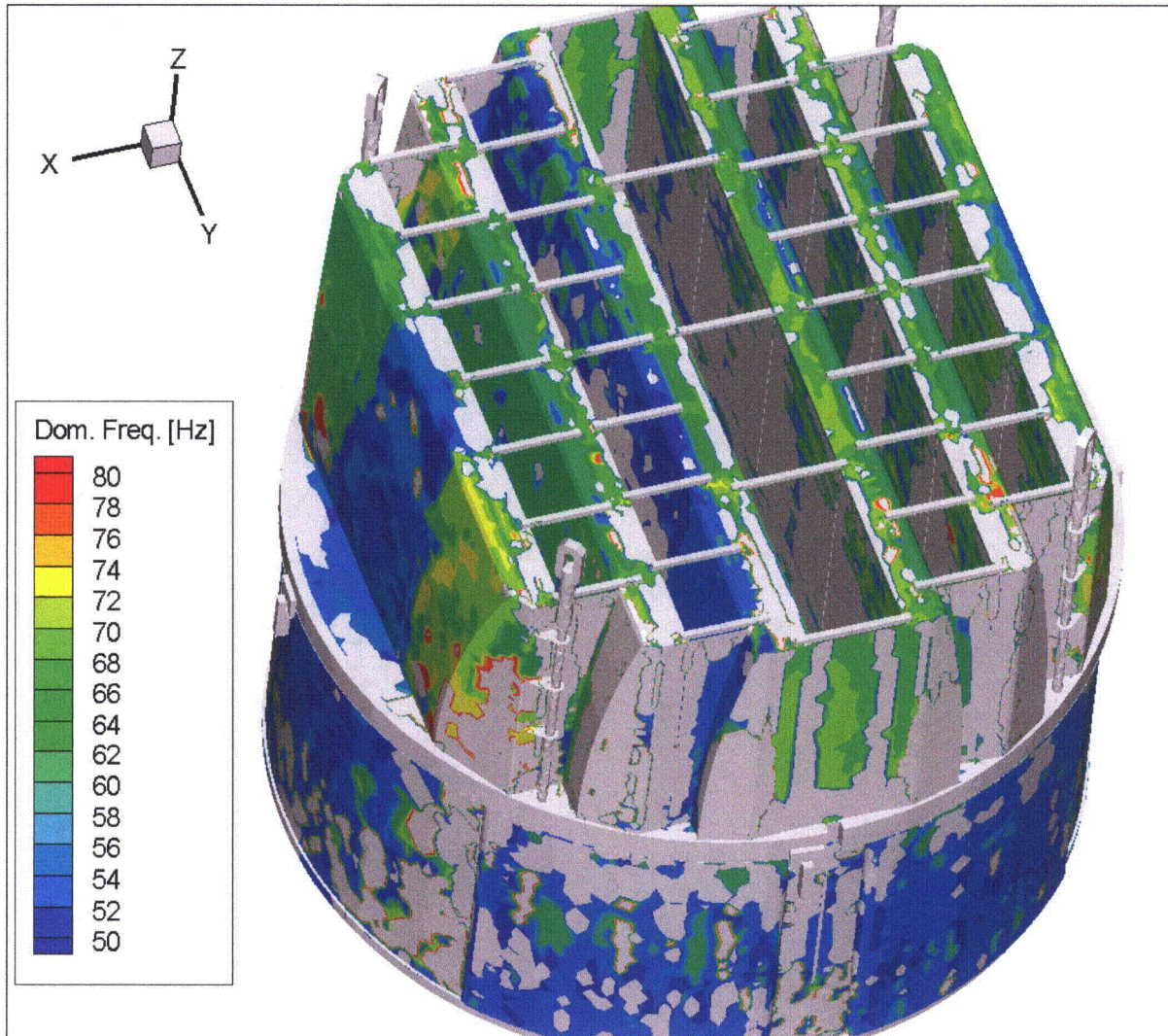


Figure 32b. Contour map showing the dominant frequencies (i.e., the frequency with the largest stress harmonic). This shows locations with dominant frequencies in the range 50-80 Hz.

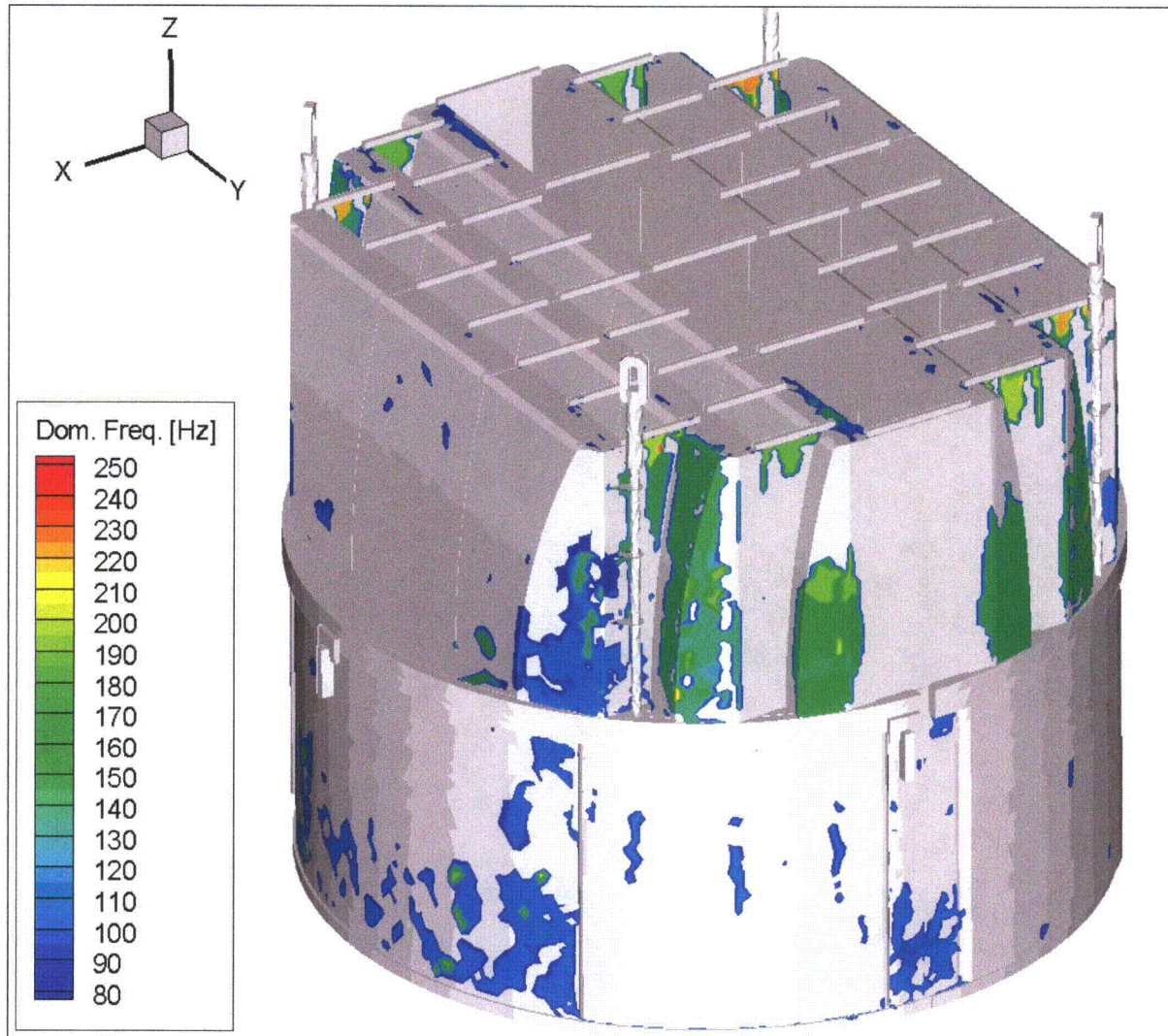


Figure 32c. Contour map showing the dominant frequencies (i.e., the frequency with the largest stress harmonic). This shows locations with dominant frequencies in the range 80-250 Hz.

7. Conclusions

The NMP2 steam dryer with the modifications described in Section 5 and summarized in Table 11 to allow operation of the NMP2 steam dryer at EPU conditions has been evaluated using a harmonic stress analysis. The analysis calculates the stresses arising when the steam dryer is subjected to acoustic loads inferred from strain gage measurements on the main steam lines and a calibrated acoustic circuit model (ACM, Rev. 4.1) that uses these measurements to obtain the acoustic loads on the dryer. The ANSYS FEA package is then used to acquire the dryer stress response resulting from these acoustic loads and post-processed to obtain the limiting alternating stress ratios. The results account for all biases and uncertainties identified for both the ACM Rev. 4.1 and the FEA harmonic analysis.

The stress evaluation shows that the limiting alternating stress ratio on the dryer with all modifications implemented is $SR-a=2.83$ and occurs on the outer hood/hood support/cover plate junction and is addressed using a stress relief cut-out hole. The next highest alternating stress ratio ($SR-a=3.05$) occurs on the outer hood/cover plate junction. Previous steam dryer stress evaluations indicated the need for reinforcement of the closure plate attachment welds to sustain the stresses induced by closure plate vibrations. With the steam dryer modifications proposed in the current evaluation, these closure plate weld reinforcements are no longer necessary.

These stress ratios are expected to qualify the steam dryer for EPU.

8. References

1. *ASME Boiler and Pressure Vessel Code, Section III, Subsection NG (2007).*
2. Continuum Dynamics, Inc. (2005) *Methodology to Determine Unsteady Pressure Loading on Components in Reactor Steam Domes (Rev. 6).* C.D.I. Report No. 04-09 (Proprietary).
3. Continuum Dynamics, Inc. (2010) *ACM Rev. 4.1: Methodology to Predict Full Scale Steam Dryer Loads from In-Plant Measurements (Rev. 2).* C.D.I. Report No. 10-09P (Proprietary), November.
4. Continuum Dynamics, Inc. (2010) *Acoustic and Low-Frequency Hydrodynamic Loads at CLTP Power Level on Nine Mile Point Unit 2 Steam Dryer to 250 Hz Using ACM Rev. 4.1 (Rev. 2).* C.D.I. Report No. 10-10P (Proprietary), January.
5. Continuum Dynamics, Inc. (2011) *Sub-Modeling in the Nine Mile Point Unit 2 Steam Dryer.* C.D.I. Report No. 11-03P (Proprietary), May.
6. Continuum Dynamics, Inc. (2007) *Methodology to Predict Full Scale Steam Dryer Loads from In-Plant Measurements, with the Inclusion of a Low Frequency Hydrodynamic Contribution.* C.D.I. Report No. 07-09P (Proprietary).
7. Structural Integrity Associates, Inc. (2010) *Nine Mile Point Unit 2 Main Steam Line Strain Gage Data Reduction (Rev. 0).* SIA Calculation Package No. 1000632.301, May.
8. Continuum Dynamics, Inc. (2011) *ACM Rev. 4.1: Methodology to Predict Full Scale Steam Dryer Loads from In-Plant Measurements (Rev. 3).* C.D.I. Report No. 10-09P (Proprietary), November.
9. ANSYS, *Release 10.0 Complete User's Manual Set*, (<http://www.ansys.com>).
10. Continuum Dynamics, Inc. (2007) *Response to NRC Request for Additional Information on the Hope Creek Generating Station, Extended Power Uprate.* RAI No. 14.110.
11. Continuum Dynamics, Inc. (2008) *Stress Assessment of Hope Creek Unit 1 Steam Dryer Based on Revision 4 Loads Model, Rev. 4.* C.D.I. Report No. 07-17P (Proprietary).
12. Press, W.H., et al., *Numerical Recipes*. 2 ed. 1992: Cambridge University Press.
13. Continuum Dynamics, Inc. (2010) *Stress Assessment of Nine Mile Point Unit 2 Steam Dryer Using the Acoustic Circuit Model Rev. 4.1.* C.D.I. Report No. 10-11P (Proprietary), June.
14. Structural Integrity Associates, Inc. (2010) *Flaw Evaluation of Indications in the Nine Mile Point Unit 2 Steam Dryer Vertical Support Plates Considering Extended Power Uprate Flow Induced Vibration Loading (Rev. 0).* SIA Calculation Package No. 1000814.401, July.
15. Continuum Dynamics, Inc. (2009) *Stress Assessment of Nine Mile Point Unit 2 Steam Dryer at CLTP and EPU Conditions, Rev. 1.* C.D.I. Report No. 09-26P (Proprietary), December.
16. Structural Integrity Associates, Inc. (2008) *Flaw Evaluation and Vibration Assessment of the Nine Mile Point Unit 2 Steam Dryer for Extended Power Uprate Operating Conditions.* Report No. 0801273.401.
17. Continuum Dynamics, Inc. (2008) *Stress Assessment of Browns Ferry Nuclear Unit 1 Steam Dryer, Rev. 0.* C.D.I. Report No. 08-06P (Proprietary).
18. O'Donnell, W.J., *Effective Elastic Constants For the Bending of Thin Perforated Plates With Triangular and Square Penetration Patterns.* ASME Journal of Engineering for Industry, 1973. **95**: p. 121-128.

19. de Santo, D.F., *Added Mass and Hydrodynamic Damping of Perforated Plates Vibrating In Water*. Journal of Pressure Vessel Technology, 1981. **103**: p. 175-182.
20. Idel'chik, I E. and E. Fried, *Flow Resistance, a Design Guide for Engineers*. 1989, Washington D.C.: Taylor & Francis. pg. 260.
21. Continuum Dynamics, Inc. (2007) *Dynamics of BWR Steam Dryer Components*. C.D.I. Report No. 07-11P.
22. U.S. Nuclear Regulatory Commission (2007) *Comprehensive Vibration Assessment Program for Reactor Internals During Preoperational and Initial Startup Testing*. Regulatory Guide 1.20, March.
23. Weld Research Council (1998) *Fatigue Strength Reduction and Stress Concentration Factors For Welds In Pressure Vessels and Piping*. WRC Bulletin 432.
24. Pilkey, W.D., *Peterson's Stress Concentration Factors*, 2nd ed. 1997, New York: John Wiley. pg. 139.
25. Lawrence, F.V., N.-J. Ho, and P.K. Mazumdar, *Predicting the Fatigue Resistance of Welds*. Ann. Rev. Mater. Sci., 1981. **11**: p. 401-425.
26. General Electric (GE) Nuclear Energy, *Supplement 1 to Service Information Letter (SIL) 644, "BWR/3 Steam Dryer Failure," September 5. 2003*.
27. Tecplot, Inc. (2004) *Documentation: Tecplot User's Manual Version 10 Tecplot, Inc.*, October.
28. Continuum Dynamics, Inc. (2009) *Compendium of Nine Mile Point Unit 2 Steam Dryer Sub-Models Away From Closure Plates* C.D.I. Technical Note No. 09-16P (Proprietary), August.
29. Continuum Dynamics, Inc. (2010) *Design and Stress Evaluation of Nine Mile Point Unit 2 Steam Dryer Modifications for EPU Operation*. C.D.I. Report No. 10-12P (Proprietary), July.
30. Structural Integrity Associates, Inc. (2009) *Nine Mile Point Unit 2 Steam Dryer Closure Plates Analysis Results*. SIA Letter Report No. 0900895.401 Revision 0, August 21.

ATTACHMENT 4

**AFFIDAVIT FROM
CONTINUUM DYNAMICS, INCORPORATED,
JUSTIFYING WITHHOLDING
PROPRIETARY INFORMATION**



Continuum Dynamics, Inc.

(609) 538-0444 (609) 538-0464 fax

34 Lexington Avenue Ewing, NJ 08618-2302

AFFIDAVIT

Re: (1) Responses to RAIs NMP2-EMCB-SD-RAI-8 S02(d) and NMP2-EMCB-SD-RAI-21 S02;

(2) C.D.I. Report No. 11-03P "Sub-Modeling in the Nine Mile Point Unit 2 Steam Dryer," Revision 1;

(3) C.D.I. Report No. 11-04P "Stress Evaluation of Nine Mile Point Unit 2 Steam Dryer Using ACM Rev. 4.1 Acoustic Loads," Revision 0

I, Alan J. Bilanin, being duly sworn, depose and state as follows:

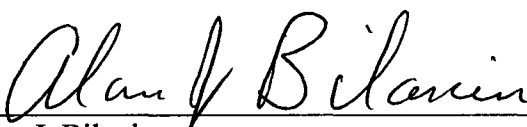
1. I hold the position of President and Senior Associate of Continuum Dynamics, Inc. (hereinafter referred to as C.D.I.), and I am authorized to make the request for withholding from Public Record the Information contained in the documents described in Paragraph 2. This Affidavit is submitted to the Nuclear Regulatory Commission (NRC) pursuant to 10 CFR 2.390(a)(4) based on the fact that the attached information consists of trade secret(s) of C.D.I. and that the NRC will receive the information from C.D.I. under privilege and in confidence.
2. The Information sought to be withheld, as transmitted to Constellation Energy Group as attachment to C.D.I. Letter No. 11067 dated 2 June 2011, (1) Responses to RAIs NMP2-EMCB-SD-RAI-8 S02(d) and NMP2-EMCB-SD-RAI-21 S02; (2) C.D.I. Report No. 11-03P "Sub-Modeling in the Nine Mile Point Unit 2 Steam Dryer," Revision 1; (3) C.D.I. Report No. 11-04P "Stress Evaluation of Nine Mile Point Unit 2 Steam Dryer Using ACM Rev. 4.1 Acoustic Loads," Revision 0
3. The Information summarizes:
 - (a) a process or method, including supporting data and analysis, where prevention of its use by C.D.I.'s competitors without license from C.D.I. constitutes a competitive advantage over other companies;
 - (b) Information which, if used by a competitor, would reduce his expenditure of resources or improve his competitive position in the design, manufacture, shipment, installation, assurance of quality, or licensing of a similar product;
 - (c) Information which discloses patentable subject matter for which it may be desirable to obtain patent protection.

The information sought to be withheld is considered to be proprietary for the reasons set forth in paragraphs 3(a), 3(b) and 3(c) above.

4. The Information has been held in confidence by C.D.I., its owner. The Information has consistently been held in confidence by C.D.I. and no public disclosure has been made and it is not available to the public. All disclosures to third parties, which have been limited, have been made pursuant to the terms and conditions contained in C.D.I.'s Nondisclosure Secrecy Agreement which must be fully executed prior to disclosure.
5. The Information is a type customarily held in confidence by C.D.I. and there is a rational basis therefore. The Information is a type, which C.D.I. considers trade secret and is held in confidence by C.D.I. because it constitutes a source of competitive advantage in the competition and performance of such work in the industry. Public disclosure of the Information is likely to cause substantial harm to C.D.I.'s competitive position and foreclose or reduce the availability of profit-making opportunities.

I declare under penalty of perjury that the foregoing affidavit and the matters stated therein are true and correct to be the best of my knowledge, information and belief.

Executed on this 2nd day of JUNE 2011.


Alan J. Bilanin
Continuum Dynamics, Inc.

Subscribed and sworn before me this day: June 2, 2011


Eileen P. Burmeister, Notary Public

EILEEN P. BURMEISTER
NOTARY PUBLIC OF NEW JERSEY
MY COMM. EXPIRES MAY 6, 2012